Isolated Bimetallic Clusters and Clusters on Surfaces

Dissertation

zur Erlangung des Grades des Doktors der Naturwissenschaften
der Naturwissenschaftlich-Technischen Fakultät III
Chemie, Pharmazie, Bio- und Werkstoffwissenschaften
der Universität des Saarlandes

von

Elisaveta Hristova geb. Kasabova

Saarbrücken, 2009

Acknowledgment

First of all, I would like to thank my doctor-father and supervisor Prof. Dr. Michael Springborg for his scientific guidance and support throughout these years.

I am deeply grateful to Dr. Valeri Grigoryan for the positive and encouraging attitude towards the project and for the many constructive and enriching discussions we have had. Also to Dr. Yi Dong and to Dr. Denitsa Alamanova for nice collaboration.

A special thanks to Michael Bauer for all the technical support during my PhD study.

To my current and past colleagues at the Department of Theoretical Chemistry: Violina Tevekeliyska, Sahar Abdalla, Mohammad Molayem, Karuppuchamy Vishwanathan, Nathalie Atif, Nicolas Louis, Yong Pang, Dr. Habib ur-Rehman, Hanno Kamp, for the pleasant atmosphere and their readiness to help me.

To my teacher in chemistry, who was the one initially woke my interest for research.

I would like to express my gratitude to my mother for her absolute faith in me and to my stepfather for his support in so many ways. Also to my husband for being always by my side and to my sisters for their understanding. Thanks also to my grandparents for encouraging me.

Contents

Abstract

In the past years significant interest in clusters has been developed due to their fundamental importance in both basic and applied science. This increasing interest is amply justified by the unique properties of clusters and by the promise these systems hold as components of optical, magnetic, and electronic sensors and devices. Especially alloy clusters are of increasing interest as the electric, magnetic and catalytic properties of a monometallic cluster can be improved by adding a second component. In order to optimize the materials properties for a given application, it is of paramount importance to have an accurate understanding of the relation between composition/cluster size on the one side and property on the other. Here, computer simulations represent a useful method for predictions of cluster properties and confirming experimental data.

In this work we have performed global optimization on the structures of Ni–Cu, K–Cs and Rb–Cs bimetallic clusters. For Ni_nCu_m bimetallic clusters with $N = n + m$ up to 20 atoms, $N = 23$ and 38 atoms we have demonstrated that most of the bimetallic cluster structures have geometries similar to those of pure Ni clusters. In contrast to the bulk, the ground state structures of Ni–Cu clusters do not experience a smooth transition between the structures of pure copper and pure nickel clusters as the number of Ni atoms changes. Furthermore, an icosahedron, a double icosahedron, and a triple icosahedron with one, two, and three Ni atoms at the centre, respectively, are especially stable (*magic*). In addition, it is found that Ni atoms occupy mainly high-coordination inner (core) sites, while Cu atoms show a tendency to occupy lower-coordination sites at the cluster surface. For K–Cs and Rb–Cs clusters we have found that the introduction of K and Rb substitutions in a Cs cluster for the size range N=34–50 results in new structures, different from those of the pure elements. These are highly symmetric and belong to the same structural family. The last fact leads to a more regular cluster growth in the case of the bimetallic clusters.

Another part of this thesis deals with deposition and global optimization of clusters on surfaces. An understanding of the cluster-surface interaction is important for the development of suitable materials, e.g. thin films, and it plays an important role in nucleation processes and crystal growth. In this thesis we simulate the experimental conditions of the *Low Energy Cluster Beam* experiment to study the influence of the atom type and the impact energy on the structural and energetic properties of the products of deposition of Ni_{13} and Cu_{13} clusters on Ni(111) and Cu(111) surfaces. It is shown that the shape of the nickel clusters deposited on a Cu(111) surface remains well kept, while the copper clusters impacting a Ni(111) surface collapse forming double and triple layered products. In the case of Ag_N clusters with N =2-20 adsorbed on Ag(111) and Ni(111) surfaces, the lowest-energy structures are determined. We have found that from N=18 upwards a reversal of the magic numbers for the Ag/Ni(111) system compared to the Ag/Ag(111) system takes place, which is due to the predominance of the adatom-substrate interactions compared to the adatom-adatom interactions. Finally, due to the large size mismatch it is energetically unfavorable for Ag to form pseudomorphic monolayer structures on Ni(111) and there is considerable strain produced at the interface. The effect of this strain will

give rise to disordered and elongated structures of the adsorbed Ag clusters.

Abstrakt

Cluster spielen, sowohl in der Grundlagenforschung, als auch in Bereichen wie Nanoindustrie, Katalyse, Mikroelektronik, Informationsspeicherung und Medizin, eine wichtige Rolle. Dabei sind besonders bimetallische Cluster von großer Bedeutung, da diese neue Möglichkeiten eröffnen bestehende optische, elektrische oder katalytische Eigenschaften eines monometallischen Clusters durch Zugabe eines zweiten Metalls zu optimieren und bessere Katalysatoren oder elektronische Bauteile zu konstruieren. Aufgrund ihrer geringen Größe und großes Oberflächen- zu Volumen Verhältnis besitzen Cluster Eigenschaften, die von denen eines makroskopischen Festkörpers abweichen und sich von einer Clustergröße zur nächsten drastisch ändern können. Für die erfolgreiche Anwendung und Vorhersage von Clustereigenschaften ist jedoch die richtige Bestimmung der Clusterstruktur entscheidend und hier erweisen sich Computersimulationen als sehr nützlich.

Die vorliegende Arbeit beschäftigt sich mit der globalen Strukturoptimierung von bimetallischen Übergangsmetall- und Alkalimetallclustern folgender Systeme: Ni–Cu, K–Cs und Rb–Cs. Strukturen, Stabilitäten, und Symmetrien der monometallischen Clustern wurden mit denen der bimetallischen Clustern verglichen. Es wurden drastische Strukturumwandlungen mit Änderung der Konzentration der Elemente für bestimmte Clustergrößen beschrieben, sowie überraschendes Auftreten von neuen Strukturen und Wachstumsmotiven durch den Zusatz einer zweiten Komponente im monometallischen Cluster beobachtet. Außerdem wurde das Mischungs- bzw. Segregationsverhalten der Zweikomponenten Clustern mit dem der makroskopischen Zweikomponenten Systeme verglichen.

Ein weiterer Teil dieser Arbeit bezieht sich auf die Deponierung und Strukturoptimierung von Clustern auf metallischen Oberflächen. Das Verständnis der Cluster-Cluster-Wechselwirkungen ist wichtig für die Herstellung von Dünnschicht-Filmen und es spielt eine wichtige Rolle in Kristallwachstumsprozessen. Im Falle der Deponierung von kleinen Ni und Cu Clustern auf Ni(111) und Cu(111) Oberflächen, wurde die experimentelle Prozedur des *Low Energy Cluster Beam*-Experiments simuliert. Man hat untersucht welche Auswirkungen auf die Struktur und Energie der Cluster nach dem Deponierungsprozess zu erwarten sind, wenn Cluster und Substrat aus unterschiedlichen Elementen bestehen. Im Falle der Strukturoptimierung von Ag Clustern auf metallischen Oberflächen, wurden die energetisch niedrigsten Strukturen von kleinen Ag Clustern auf eine Ag(111) Oberfläche mit denen auf eine Ni(111) Oberfläche verglichen und überraschende Umkehr der Stabilitäten für das Ag/Ni(111) System im Vergleich zum Ag/Ag(111) System aufgezeigt.

Zusammenfassung

Während des letzten Jahrzehnts sind Cluster immer mehr in den Mittelpunkt des Interesses von Forschern gerückt, da sie sowohl eine wichtige Rolle in der Grundlagenforschung als auch in Bereichen wie Nanoindustrie, Katalyse, Mikroelektronik, Informationsspeicherung und Medizin spielen. Dabei sind besonders bimetallische Cluster von tragender Bedeutung, da diese neue Möglichkeiten eröffnen bestehende optische, elektrische oder katalytische Eigenschaften eines monometallischen Clusters durch Zugabe eines zweiten Metalls zu optimieren und bessere Katalysatoren oder elektronische Bauteile zu konstruieren.

Unter Cluster versteht man Ansammlungen von Atomen oder Molekülen deren Atomzahl zwischen drei und wenigen Tausenden liegt. Aufgrund ihrer geringen Größe und großes Oberflächen- zu Volumen Verhältnis besitzen Cluster Eigenschaften, die von denen eines makroskopischen Festkörpers und von denen der Moleküle abweichen. Daher ist es ein Hauptziel der Clusterforschung diese neuen Eigenschaften der Cluster herauszufinden und zu verstehen und somit Cluster als neue Materialien nutzen zu können.

Obwohl Cluster schon seit mehr als zwei Jahrzehnten durch eine breite Auswahl an experimentellen Methoden synthetisiert werden, stellt die zweifellose Zuordnung von bestimmten Geometrien zu einem untersuchten Cluster gegenwärtig eine Herausforderung dar. Insbesondere für kleine Cluster ist diese Aufgabe besonders schwierig, da diese aufgrund ihres großen Oberfläche- zu Volumen Verhältnisses Eigenschaften aufweisen, die sich von einer Größe zur nächsten dramatisch ändern können. Für die erfolgreiche Anwendung und Vorhersage von Clustereigenschaften ist aber die richtige Bestimmung der Clusterstruktur entscheidend. Hier erweisen sich Computersimulationen als sehr nützlich, wenn es darum geht experimentelle Ergebnisse zu bestätigen, zu ergänzen, oder Vorhersagen zu treffen. Aufgrund der Riesenanzahl an lokalen Energieminima (und damit auch an möglichen Strukturen), die sogar für Cluster mit weniger als 10 Atomen existieren, sind jedoch first-principles Methoden auf Berechnungen von vordefinierten Konfigurationen und nur auf wenigen Atomen beschränkt. Für bimetallische Cluster ist das Problem der globalen Strukturoptimierung dramatischer, da zusätzlich zu den geometrischen Isomeren auch noch topologische Isomere (*Homotops*) existieren, welche durch Austausch von ungleichen Atomen ohne Änderung der Gesamtstruktur erhalten werden. Um die Grundzustandsstruktur der Zweikomponenten Cluster bestimmen zu können werden in dieser Arbeit semiempirische Potentiale verwendet, wie die Embedded-Atom Methode und das many-body Gupta-Potential. Diese bieten die nötige Einfachheit im Bezug auf die Berechnung von solchen komplizierten Systemen, aber auch eine zufriedenstellende Genauigkeit.

Die vorliegende Arbeit beschäftigt sich mit der globalen Strukturoptimierung von bimetallischen Übergangsmetall- und Alkalimetallclustern, sowie mit Cluster/Oberflächen Systemen mit heteroatomaren Wechselwirkungen, d.h. Wechselwirkungen zwischen zwei chemisch unterschiedlichen Elementen. Die globale Strukturoptimierung von kleinen bimetallischen Ni–Cu Clustern wurde mit Hilfe des Genetischen Algorithmus in Kombina-

tion mit der Embedded-Atom Methode zur Berechnung der Gesamtenergie durchgeführt, während für K–Cs und Rb–Cs Clustern der Basin-Hopping Algorithmus in Kombination mit dem Gupta Potential angewandt wurde. Strukturelle und energetische Eigenschaften, wie z.B. Stabilität, Mischungsenergie, Symmetrie, Radiale Verteilungsfunktion, Ähnlichkeitsfunktion und Wachstum, d.h. inwiefern ein Cluster bestehend aus N Atomen als ein Cluster aus $N-1$ Atomen plus ein zusätzliches Atom betrachtet werden kann, wurden quantifiziert. Strukturen und Stabilitätsfunktionen der monometallischen Clustern wurden mit denen der bimetallischen Clustern verglichen. Außerdem wurde das Mischungs- bzw. Segregationsverhalten der Zweikomponenten Clustern mit dem der makroskopischen Zweikomponenten Systemen verglichen.

Im Fall der Ni_nCu_m Cluster mit $N = n + m$ bis zu 20, N=23 und N=38 Atomen wurden die energetisch niedrigsten Strukturen mit denen der reinen Kupfer und Nickel Cluster verglichen und man fand heraus, dass die meisten der untersuchten bimetallischen Strukturen dieselbe Geometrie aufweisen wie die der reinen Nickel Cluster. Die Clustergröße N=38 stellt dabei einen besonderen Fall dar, da bei dieser Größe eine drastische Strukturumwandlung mit Zunahme des Cu Anteils in den Ni–Cu Clustern vollzogen wird: von einem abgeschnittenen Oktaeder zu einer Struktur mit pentagonaler Symmetrie und dann wider zu Oktaedersymmetrie. Außerdem ist für Cluster mit 15, 16, und 17 Atomen die Auswirkung der Konzentration stärker, als der geometrische Effekt. Als besonders stabile (*magische*) Strukturen wurden der einfache, doppelte und dreifache Ikosaeder mit jeweils eins, zwei und drei Ni Atomen im Zentrum, identifiziert. Im Allgemeinen tendieren die Nickel Atome dazu Plätze im Clusterinneren zu besetzen, welche eine hohe Koordinationszahl ermöglichen, während Cu Atome an die Clusteroberfläche segregieren.

Für $(KCs)_n$ und $(RbCs)_n$ Cluster mit $N = 2n$ bis zu 20 Atomen fanden wir heraus, dass eine Einführung von K oder Rb Verunreinigungen in einem Cs Cluster, für Clustergrößen N=34-50, zur Entstehung von neuen Strukturen führt, welche unterschiedlich sind von denen der reinen K, Rb und Cs Cluster. Diese unterschiedlichen Strukturen sind höchst symmetrisch und gehören der Familie der polyikosaedrischen Strukturen an, welche durch Verkappung des s.g. fünffachen "Pfannkuchens" erhalten werden. Aufgrund dieses dominierenden strukturellen Motivs, weisen die bimetallischen Clustern ein viel regelmäßigeres Wachstumsverhalten auf, verglichen mit dem der monometallischen K, Rb und Cs Cluster. Aufgrund der erhaltenen polyikosaedrischen Strukturen und der Tatsache, dass Cs an die Clusteroberfläche segregiert, können wir schließen, dass Alkalimetall K–Cs und Rb–Cs Cluster ebenfalls *magische Kern-Schalle Strukturen* ausbilden können, wie bereits von bestimmten Übergangsmetallcluster wie Ag–Ni berichtet wurde.

Ein weiterer Teil dieser Arbeit bezieht sich auf die Deponierung und Strukturoptimierung von Clustern auf metallischen Oberflächen. Das Verständnis der Cluster-Cluster-Wechselwirkungen ist wichtig für die Herstellung von geeigneten Materialien, wie z.B. von Dünnschicht-Filmen durch Cluster Deponierung. Weiterhin spielt die Adsorption von Clustern auf Oberflächen eine wichtige Rolle in Kristallwachstumsprozessen. Im Falle der Deponierung von Ni und Cu Clustern auf Ni(111) und Cu(111) Oberflächen, wurde ein *Molekular-Dynamischer* Algorithmus angewandt, der die experimentelle Prozedur des *Low Energy Cluster Beam*-Experiment (LECB) simuliert. Die Cluster-Cluster

und die Cluster-Substrat Wechselwirkungen wurden mit der Embedded Atom Methode nachgeahmt. Das Ziel war, zu untersuchen welche Auswirkungen die heteroatomaren Wechselwirkungen während des Deponierungsprozesses auf die Struktur und Energie der Clustern haben, im Vergleich dazu wenn nur homoatomare Wechselwirkungen herrschen. Man fand heraus, dass im Falle der heteroatomaren Wechselwirkungen die Kohäsionsenergie der Metalle der entscheidende Faktor ist, der die Gestalt der Endstruktur bestimmt. Als Konsequenz davon, führt die Deponierung von Cu_{13} auf Ni(111) Oberfläche zu einer Ausbreitung des Clusters, aufgrund der niedrigen Kohäsionsenergie von Kupfer, während bei der Deponierung von Ni_{13} auf Cu(111) Oberfläche die Anfangsstruktur fast vollständig erhalten bleibt. Die Cluster wurden außeredem mit verschiedenen Anfangsenergien deponiert und man fand heraus, dass die Anwendung von einer Deponierungsenergie von 0.5 eV/Atom im Falle der Cu_{13} Cluster auf Ni(111) Oberfläche bevorzugt für die Herstellung von einschichtigen Filmen verwendet werden könnte.

Im Falle der Strukturoptimierung von Clustern auf metallischen Oberflächen, wurde der Basin-Hopping Algorithmus zur globalen Strukturoptimierung in Kombination mit der Embedded Atom Methode angewandt. Die energetisch niedrigsten und besonders stabilen Strukturen von Ag_N Clustern mit N=2-20 auf Ag(111) wurden mit denen der Ag_N Clustern auf Ni(111) Oberflächen verglichen. Man fand heraus, dass in beiden Fällen kompakte einschichtige Strukturen erhalten werden, in denen die maximale Anzahl an nächsten Nachbarn erreicht wird, mit Ausnahme von Ag_{19} auf Ni(111). Für Silber Cluster, die mehr als 17 Atomen besitzen, findet eine Umordnung der *magischen* Zahlen für das Ag/Ni(111) System im Vergleich zum Ag/Ag(111) System statt. Während Ag_{19} auf Ag(111) besonders stabil ist, wird es auf Ni(111), als Folge der dominierenden Cluster-Substrat Wechselwirkungen, seine kompakte Geometrie verlieren und auch seine besondere Stabilität. Desweiteren ist ein pseudomorphes Schichtwachstum aufgrund der großen Fehlanpassung der Gitterkonstanten und Bindungslängen von Ag und Ni energetisch ungünstig. Dies führt zu einer Spannung an der Grenzschicht Ag/Ni und zur einer Verzerrung der Strukturen der Ag Cluster auf der Ni(111) Oberfläche.

Preface

This thesis consists of the following papers that are referred to in the text by their Roman numerals.

I. E. Hristova, Y. Dong, V. G. Grigoryan, and M. Springborg: "*Structural and energetic properties of Ni–Cu bimetallic clusters*", J. Phys. Chem. A **112** (2008) 7905-7915.

II. E. Hristova, V. G. Grigoryan, and M. Springborg: "*Structure and energetics of equiatomic K–Cs and Rb–Cs binary clusters*", J. Chem. Phys. **128** (2008) 244513. Reprinted with permission from J. Chem. Phys. Copyright 2008, American Institute of Physics.

III. E. Kasabova, D. Alamanova, M. Springborg, and V. G. Grigoryan: "*Deposition of Ni_{13} and Cu_{13} clusters on Ni(111) and Cu(111) surfaces*", Eur. Phys. J. D **45** (2007) 425-431. Reproduced with kind permission of Spinger Science and Business Media.

IV. E. Hristova, V. G. Grigoryan, and M. Springborg: "*Structures and stability of Ag clusters on Ag(111) and Ni(111) surfaces*", in preparation.

The first two papers contain the studies of transition and alkali bimetallic clusters (Ni–Cu, K–Cs and Rb–Cs) and the third and fourth ones deal with deposition and growth of clusters on surfaces. We will describe the background to these studies in an introductory part of the thesis.
The code for the genetic algorithm used in the first paper has been provided by Dr. Yi Dong. The code for the basin-hopping algorithm for the second and fourth paper has been downloaded from the website of Dr. David J. Wales and the molecular dynamics code for the third paper has been provided by Dr. Denitsa Alamanova. The codes for total energy calculation (embedded atom method and the Gupta potential) have been provided by Dr. Valeri G. Grigoryan. All programs for global optimization, total energy calculations, functions for analysing the structures have been changed from the monometallic to the bimetallic case and adapted to the corresponding systems. The embedded atom method of Daw, Baskes and Foiles has been implemented in the genetic algorithm, in the basin-hopping algorithm and in the molecular dynamics simulation code. Further, the basin-hopping algorithm for optimization of free clusters has been modified to optimize clusters on surfaces.

Chapter 1

Introduction

The physics of clusters studies the characteristic properties of aggregates which size is intermediate between the atom and the solid, and thus bridges the gap between atomic and bulk-like behavior. In the past years significant interest in clusters has been developed due to their fundamental importance in both basic and applied science. This increasing interest is amply justified by the unique properties of clusters and by the promise these systems hold as components of optical, magnetic, and electronic sensors and devices. Because of the high proportion of surface atoms in clusters there are some common areas of research between clusters and surface science. Some of these areas, such as the catalytic activity of supported clusters, are clearly of interest in the field of nanotechnology. Beside their importance in nanotechnological applications, clusters also provide a convenient testing ground for many theories in physics. By learning how bulk properties emerge from properties of clusters, as the clusters grow larger and larger, we gain new kinds of understanding of the behavior of bulk matter.

Especially alloy clusters have a major impact in industrial catalysis, as the activity or selectivity of a pure metal catalyst can be improved by adding a second component and by varying the composition and the atomic ordering of the alloy. Used as nanoparticles, alloy clusters are not only important as catalysts in fuel cell electrode reactions, but they are also subject of an increasing interest in optics, magnetism, nanoelectronics and biodiagnostic [1–8]. For example, using $Ag_{core}Au_{shell}$ nanoparticles as biodiagnostic agents the sensitivities for scanometric detection of DNA have been greatly improved, resulting in amplification of the target signal [9].

Although clusters can be synthesized for more than two decades by means of a wide range of methods, their systematic fundamental study is quite recent. Especially for small particles accurate experimental characterization is an arduous task and therefore, computer simulations can be very helpful in confirming and complementing experimental data or in predicting the properties of a cluster.

One of the most important properties of clusters, which is a goal of many experimental and theoretical investigations and an essential input for most calculations, is the geometrical arrangement of the constituents. However, even the most powerful first principles studies have difficulties with the global optimizations already of clusters containing a few

tens of atoms. This is due to the huge number of local minima that already exist at these cluster sizes. For alloy clusters the problem is considerably more challenging, because new structures (topological isomers or *homotops*) exist, in addition to the geometrically different isomers. *Homotops* can be obtained through the interchange of unlike atoms without changing the overall structure. Moreover, in bimetallic clusters the interatomic interactions are much more complicated than in the homoatomic case. To calculate the ground-state structure of the investigated bimetallic clusters, we used semiempirical potentials, the embedded atom method and the Gupta potential, which combine the computational simplicity needed for binary clusters with sufficient accuracy. The global optimization of the structures was performed using the genetic (for Ni–Cu clusters) and the basin-hopping algorithm (for K–Cs and Rb–Cs clusters). Both algorithms possess a high computational efficiency proven in a series of previous studies.

Another part of this thesis deals with deposited and adsorbed clusters on surfaces. Clusters on surfaces constitute a broad subfield of cluster physics. Placing a cluster on a surface significantly modifies its geometry in comparison with equivalent free cluster due to the impact of the interface energy and the surface configuration. Thus, an understanding of the cluster-surface interaction is important for the development of suitable materials, e.g. thin films, through cluster deposition. Further, clusters adsorbed on surfaces play an important role in the nucleation processes and crystal growth. Systematic studies of the changes of the structural properties of clusters on surfaces as a function of cluster size lead to detailed understanding of such processes. In this thesis we employ molecular dynamics simulation to study the deposition of small Ni and Cu clusters on Ni(111) and Cu(111) surfaces and a basin-hopping algorithm to analyse the ground-state structures of adsorbed Ag clusters on Ag(111) and Ni(111) surfaces.

The present work is organized as follows: in Chapter 2 we introduce main terms and concepts related to clusters, as well as important cluster experiments. In Chapter 3, a short introduction to the density functional formalism is given. Here, we also describe the potentials based on it, which are used in this study. The algorithms for the global structure optimization are presented in Chapter 4. The main features of the MD algorithm are described in Chapter 5. Paper I contains the results for Ni–Cu clusters. Paper II presents the structure and energetics of K–Cs and Rb–Cs clusters. Article III deals with the deposition of Ni and Cu clusters on Ni(111) and Cu(111) surfaces and article IV with adsorbed Ag clusters on Ag(111) and Ni(111) surfaces.

Chapter 2

Clusters

Clusters are nanoparticles (aggregates) of between three and a few thousand atoms or molecules. They are intermediates between small molecules and macroscopic solid. Clusters can be placed in the following categories: (1) microclusters (with 3 to 10-13 atoms) for which concepts and methods of molecular physics are applicable (2) small clusters (with 10-13 to about 100 atoms) for which many different geometrical isomers exist for a given cluster size with almost the same energies and molecular concepts lose their applicability (3) large clusters (with 100 to 1000 atoms) for wich a gradual transition is observed to the properties of the solid state (4) small particles or nanocrystals (with at least 1000 atoms) which display some of the properties of the solid state. The special interest in clusters arises because they constitute a new type of material which may have properties distinct from those of individual atoms and molecules or bulk matter. For example, iron and silver are immiscible in the bulk, but readily mix in clusters [10]. Furthermore, gold as bulk hardly reacts with molecular atmospheric oxygen or water, but small gold cluster however do react with oxidation.

According to the types of atoms of which they are composed and the nature of the bonding, clusters can be divided into five different types: metal clusters with delocalized or covalent bonding, semiconductor clusters such as Ga_xAs_y with a strong and directional covalent bonding, ionic clusters such as $[Na_xCl_y]^{(x-y)+}$ with electrostatic bonding, rare gas clusters bound by weak van der Waals dispersion forces and molecular clusters with van der Waals bonding and dipole-dipole interactions. In the present work we will concentrate on metal clusters. Metal clusters are formed by metallic elements from across the periodic table. These include: (1) the simple *s*-block metals (alkali and alkaline earth metals) with delocalized and non-directional bonding involving primarily the *s* orbitals (2) the *sp*-metals (such as aluminium) whith a degree of covalent character where the bonding involves both the *s* and the *p* orbitals and (3) the transition metals (*sd*-metals) with a greater degree of covalency and a higher directionality in bonding.

One of the most popular models which have been developed to describe the bonding in clusters of metallic elements is the so-called jellium model. In this a metal cluster is approximated by a uniform, positive background of density, which binds a delocalized valence electron cloud. The jellium model gives explanation to the observed peaks in the

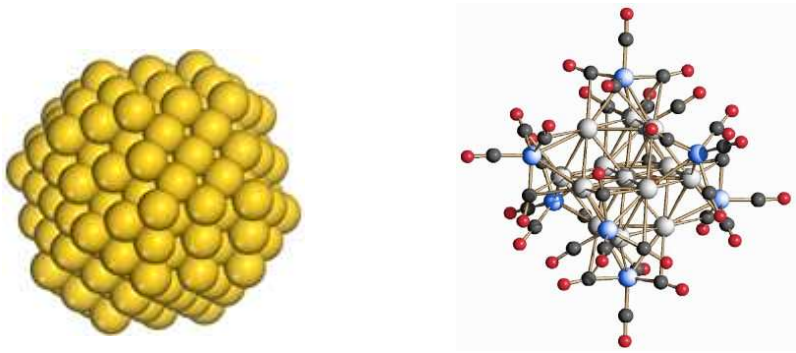

Figure 2.1: Examples for metal clusters: gold clusters (left side, reproduced with permission from Accelrys Inc) and silver clusters stabilized by $Fe(CO)_4$ ligands [11] (right side).

mass spectra of alkali metal clusters, corresponding to the nuclearities N=2, 8, 20, 40, 58, ... The latter were called *magic numbers* and were attributed to the enhanced stability of a cluster (corresponding to an intense peak) compared to its immediate neighbours. These magic numbers are based on the electronic shell closing. Whereas the jellium model is useful for understanding the physical properties of small metal clusters taking into account the internal electronic structure of the cluster, it can not explain the appearance of even-odd numbers observed in the mass spectra of rare gas clusters. The even-odd magic numbers have been ascribed to the filling of concentric polyhedral, or geometric shells of atoms, rather than electrons. Filled geometric shells impart stability to the cluster by maximizing the average coordination number and thereby reducing the cluster surface energy. Geometric shell clusters based on twelve-vertex polyhedra (e.g. icosahedra, decahedra and cuboctahedra) are characterized by the following magic numbers N=13, 55, 147, 309, 561, ... In many cases there is a competition between electron shell and geometric shell (packing) effects.

2.1 Cluster properties

The interesting properties of a cluster are mainly determined by the high ratio of surface atoms to interior (bulk) atoms. Using the SCA (Spherical Cluster Approximation) we can predict this fraction F_s of surface atoms [12]

$$F_s = 4N^{-1/3}. \tag{2.1}$$

In this approximation, an N-atom cluster is modelled by a sphere and the volume of the cluster V_c is assumed to be the volume of an atom V_a multiplied by the number of atoms N in the cluster.

$$V_c = N * V_a. \tag{2.2}$$

Small clusters have more then 86% of their atoms on the surface and large clusters have still 20% on the surface. As surface atoms possess lower coordination numbers and an increased potential energy, large number of atoms in the cluster can be exposed to chemical reactions. Thus, used as very finely dispersed metal, clusters show excellent catalytic properties.

Another important reason for the interest especially in small clusters is the size-dependent evolution of their properties. While in medium-sized or large clusters the properties are smoothly varying functions of the number of atoms, in small clusters properties such as melting point, catalytic activity, magnetic, or structural ones, may drastically change with size [12–14].

With increasing particle size, the surface-to-volume ratio decreases proportionally to the inverse particle size. Thus, all properties which depend on the surface-to-volume ratio extrapolate slowly to bulk values.

The non-metal to metal transition of a cluster depends on the cluster size, too. For small clusters the density of states within a band (the extent of the electronic wave function) is much smaller than that for macroscopic crystallites and it is possible that the full width of a band may not have been developed. Thus, bands which overlap in bulk materials are separated in clusters by a gap, i.e. the band structure for the cluster is not continuous and nanoscopic amounts of a metal may behave as a semiconductor or an insulator. Therefore, especially for small clusters, properties are strongly characterized by *quantum effects*.

2.2 Bimetallic clusters

As the name implies, bimetallic clusters or so called alloy clusters are composed of atoms of two different metallic elements. Such kinds of clusters combine the characteristics of the finite size systems together with those of the alloys.

Whereas, for clusters containing one type of atoms, the properties can be varied simply by changing the size of the clusters, for bimetallic clusters there are three additional parameters to tune the materials properties, namely the composition, the atomic type and the atomic ordering. The last point refers to the fact that compared to the pure clusters with only one type of atoms, binary clusters may show segregation which may result in, e.g., layered structures or core-shell structures, or they may show complete mixing [15–19]. Because of their non-trivial geometric structures [20–26], and complex chemical ordering [27–32], it is difficult to predict the ground state structures of binary clusters from computational point of view. Further, the interatomic interactions in a bimetallic cluster are much more complicated than in a monometallic one. In addition to the interactions between the same types of atoms A-A and B-B we must also consider the interactions between the different types of atoms (A-B/B-A). Moreover, in contrast to monometallic clusters the interatomic interactions in bimetallic clusters depend not only on the atom types, but also on the fractions of the different atom types in the nanoalloy. The problem becomes much more complicated because of the existence of the so-called

homotops [32,33]. Homotops are defined [33] as clusters with the same size, composition and geometric arrangement, differing only in the way in which A and B-type atoms are arranged. The number of *homotops* for an A_nB_m cluster, $P_{n,m}$, is given by

$$P_{n,m} = \frac{(n+m)!}{n!m!}. \tag{2.3}$$

Thus, if we for example consider all possible replacements of 10 K atoms by Cs atoms in an isomer of K_{20}, the number of homotops is as large as 184756. Because of this large number of homotops, that in addition may have only small total-energy differences, a global optimization becomes a very demanding task.

As already mentioned bimetallic clusters combine the characteristics of the finite systems with those of the alloys. In bulk, alloys can be divided in solid solutions and intermetallic compounds. A solid solution is characterized by the lack of a short- and of a long-range order. Compared to an intermetallic compound, where the composition is stochiometric and follows certain distribution 'rules' (e.g. Cu_5Zn_8), a solid solution shows a statistic distribution of the atoms in the lattice (e.g. Ag–Au, Ni–Cu, Rb–Cs, K–Cs) [34,35]. In which case we will obtain a solid solution or an intermetallic compound, respectively, depends on the atom radii of the metal atoms and on the chemical reactivity of the two metals. If the two atom types differ in their atom radii more than 15 % and there are differences in their chemical properties, ordered structures, i.e. intermetallic compounds are preferred. The reason is that the different size of the atoms enables a closer packing of themselves and a better space filling. Furthermore the ordered structure is energetically preferred because of the larger lattice energy set free by building the structure. If the atomic radii are similar, a solid solution is preferred, due to the larger entropy its unordered structure causes. Considering this, one of the basic questions that have to be answered when working with bimetallic clusters is, if they show the same miscibility properties as the corresponding bulk alloys.

2.3 Cluster experiments

2.3.1 Synthesis methods

Mono- and bimetallic clusters can be generated in a variety of ways, in the gas phase, in solution, supported on a substrate, or in a matrix.

Molecular Beams

The development of molecular beam techniques has enabled the study of "free" clusters in an interaction-free environment: the so-called "cluster beam" [36,37]. Clusters are generated in a cluster source with cluster generation consisting of the processes of vaporization (production of atoms or molecules in the gas phase), nucleation (initial condensation of atoms or molecules to form a cluster nucleus), growth (addition of more atoms or molecules to the initially formed nucleus), and coalescence/aggregation (the merging of

small clusters to form larger clusters). Depending on the nature and conditions of the source, different size distributions of clusters may be generated. Most modern day metal cluster sources are of the gas condensation type. These include the following [12,36–40].

(1) Laser vaporization. For bimetallic nanoparticles, a single alloy rod target, mixed metallic powders, or two monometallic targets are vaporized by the incident laser beam.

(2) Pulsed-Arc cluster ion source. Vaporization of the mono- or bimetallic targets is achieved by passing an intense electrical discharge through them.

(3) Ion sputtering. Clusters are produced by bombarding the metal target with high-energy inert gas ions (generally Kr^+ or Xe^-) with bombardment energies in the range 10-30 keV and currents of approximately 10 mA.

(4) Magnetron sputtering. Argon plasma is ignited over a target by applying either a potential and confined by a magnetic field. Ar^+ ions in the plasma are then accelerated onto the target, resulting in sputtering.

After vaporization, condensation of clusters can be achieved by letting the metallic vapors collide with a cold inert carrier gas and expansion through a nozzle. Once clusters have been made and are in the form of gaseous particles, it is frequently desirable to make them into some kind of controllable beam or stream that can be studied or captured. To observe clusters in a beam, one can probe them while they are free or trap them in a matrix, liquid, glassy or crystalline.

Fig. 2.2 shows an example of the production of a cluster beam by magnetron sputtering in the group of Palmer *et al.* [41]. Here Ar+ ions are accelerated by a high voltage supplied to the Ag target, which results in sputtering of the target atoms and the creation of a dense vapour of energetic Ag atoms and small Ag clusters. Cold He gas is used to remove excess energy from these particles, leading to condensation of clusters. To form a cluster beam, charged clusters of various sizes are extracted electrostatically from the production chamber through a series of small apertures, and subsequently focused by a series of electrostatic lenses. By mass selection in a mass filter a size-selected cluster beam is generated.

Chemical Reduction

One problem with studying naked metal clusters, such as those created in cluster molecular beams, is that they cannot be isolated and handled on a preparative scale like conventional molecules. To enable the investigation of clusters and to exploit their properties in device applications, it is necessary to protect ("passivate") them with a ligand shell, as this avoids coalescence at high cluster densities. Such systems are realized as dispersion of particles of one material in another. Each particle in these so-called 'colloids' consists of a metallic core surrounded by a ligand shell.

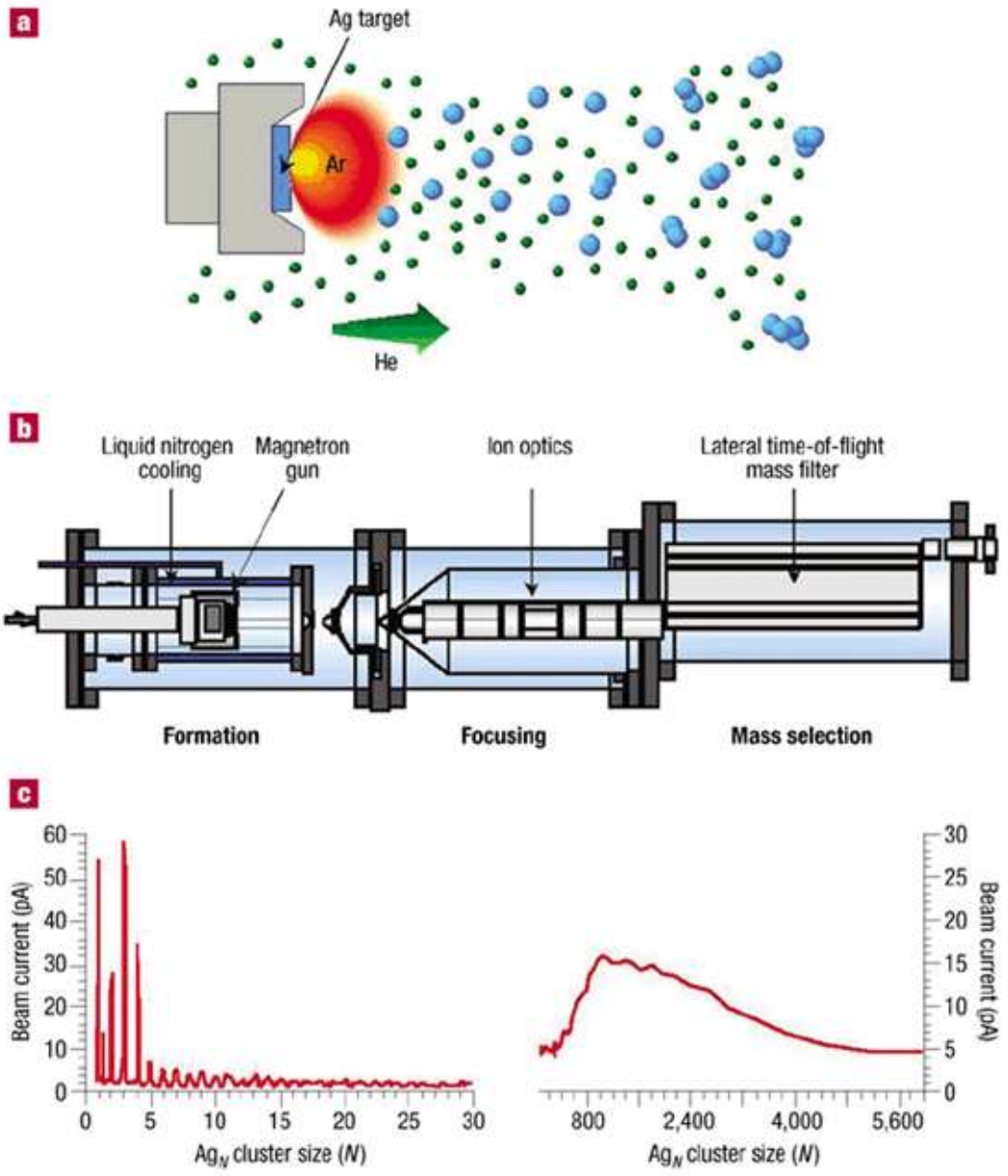

Figure 2.2: Production of size-selected cluster beams. (a) Cluster formation by plasma sputtering and gas aggregation. (b) Overview of the complete cluster beam source. (c) Mass spectra of Ag clusters produced by the source by two different sets of source parameters such as the Ar and He pressures [41].

Colloidal metallic particles can be produced by chemical reduction of metal salts dissolved in an appropriate solvent in the presence of surfactant (e.g., citrate, alkylthiols, or thioethers) or polymeric ligands, which passivate the cluster surface [42, 43]. Bimetallic colloids can readily be prepared by chemical reduction of the appropriate mixture of salts in the solution phase using reduction agents such as $NaBH_4$, N_2H_4 and H_2 gas [42–45]. During the reduction process, the metal species with the highest redox potential precipitates first, forming a core on which the second component is deposited as a shell [45]. As an example, co-reduction of Ag and Pd generally leads to $Pd_{core}Ag_{shell}$ clusters due to the higher redox potential of Pd.

Another way of making bimetallic particles is to reduce complexes which contain both of the metal species [45]. This approach has been used, for example, to generate Pd–Ag and Pd–Pt nanoparticles [46].

Thermal Decomposition of Transition-Metals

Bare nanoalloys (e.g., Ni-Cu, Ag-Au, and Cu-Pd) have been generated by thermal evaporation of the metals in a vacuum. XPS measurements of core-level binding energies show that shifts (relative to the bulk metals) have contributions due to size-effects as well as mixing [47].

Electrochemical Synthesis

Bimetallic Pd-Ni and Fe-Co nanocolloids have been prepared using two sacrificial bulk metallic anodes in a single electrolysis cell [48]. Core-shell layered bimetallic nanoparticles, as e.g. $Pt_{core}Pd_{shell}$ can also be produced electrochemically, where, the Pt core can be regarded as a "living metal polymer" on which the Pd atoms are deposited [42, 49].

2.3.2 Investigation of Clusters

Mass Spectrometry

Traditional mass spectrometers use homogeneous electric or magnetic field sectors to deflect charged clusters by an extent depending on their charge-to-mass ratio and their velocities. If there is an inherent stability associated with a given number of atoms in a neutral cluster then this will give rise to a greater abundance of this clusters and a large peak in intensity (magic numbers), relative to similarly sized clusters. Neutral clusters can be mass selected by deflection using an intersecting beam of inert gas atoms, or by reneutralising ions that have previously been mass selected.

X-ray Spectroscopy

High-energy X-ray radiation is particularly useful for studying metallic nanoparticles because the binding energies and hence the spectral lines of the atomic core electrons are very sensitive to the atomic number of the element, allowing metals which are adjacent in

the periodic table to be distinguished. X-ray absorption spectroscopy techniques are used to determine the geometrical arrangement, atomic number, distance and the coordination number of the atoms in the cluster.

Ion mobility studies

In these experiments, cluster ions, produced in laser vaporization source, are mass selected and injected into a long drift tube which is filled with an inert buffer gas. The cluster mobilities (which are inversely related to the time taken to pass through the drift tube) depend on the number of collisions with the buffer gas and these in turn depend on the collisional cross sectional area, and hence the shape of the cluster. For a given number of atoms, spherical clusters have the smallest collision cross sections and therefore travel fastest though the drift tube. Prolate spheroidal clusters carve out a large sphere, and thus have high collisions cross sectional areas and slower drift times. In this way clusters with different shapes are temporally separated and appear at different times at the detector.

Electron Microscopy

In the electron microscopy the atomic structure of clusters is imaged using electron beams, that can be accelerated to an appropriate energy and can be focused by electrostatic lenses. High resolution transmission electron microscopy (HRTEM) offers resolution down to the Angstrom level and enables information to be obtained on the structure rather than just the morphology of the nanoparticles.

Photoelectron Spectroscopy

Electronic and dynamic properties of metal clusters can be investigated by photoelectron spectroscopy using lower energy radiation.

Scanning Probe Microscopy

In scanning probe microscopy (SPM) a surface is imaged at high resolution by rastering an atomically sharp tip across the surface. Measurement of the strength of the interaction is used to map out the topography and electronic structure of the surface. In scanning tunneling microscopy (STM), a potential bias is applied between the needle tip and the substrate, causing electrons to tunnel from the surface to the needle. One can either measure the varying tunneling current in constant height mode or keep the tunneling current constant and vary the height of the tip above the substrate. In the atomic force microscopy (AFM) a fine tip is brought into close contact (without touching) with the sample and senses the small repulsive force between the probe tip and the surface. Using SPM we can examine the morphology of clusters adsorbed or deposited onto a surface. The last processes are topic of the next section.

2.4 Clusters on Surfaces

Through the deposition of size-selected clusters onto a suitable substrate it is possible to produce novel materials, such as thin films or nanostructured surfaces, in a well-controlled way. A way to size-select clusters is to use electrostatic or magnetic deflection of a beam of charged clusters as described in Sec. 2.3.1. Various techniques such as sputtering, Pulsed Laser Deposition, Ionized Cluster Beam Deposition etc., have been employed to obtain layers on surfaces. The use of moderate impact energies (10-100 eV) generally leads to flattening of the cluster and little surface damage, while by use of high impact energies (keV), a crater hollow is formed on the surface. If one wishes to deposit clusters on substrate without the clusters themselves breaking up or the surface morphology of the substrate being disrupted, the clusters must be deposited with a low impact energy (0.1-1 eV). Low-energy cluster deposition experiments have been carried out with the aim of producing novel materials which have a memory of the free cluster structure. Such an effect, where the clusters remain distinct and identifiable upon film formation, was observed for films of fullerenes, but not for metallic cluster depositions, yet. However, independently of the nature of the incident clusters, the low-energy cluster beam deposition technique (LECBD) allows to produce nanostructured materials with a morphology consisting of a nearly random stacking of clusters. Fig. 2.3 shows an example of a setup of the Konstanz Cluster Deposition Experiment in the group of Prof. Dr. G. Gantefoer [50]. In this experiment, clusters are produced by a magnetron sputter source, which allows coverages up to several monolayers cluster material within a few hours. The clusters are first produced as ions in the gas phase, accelerated by an electric potential, mass separated by means of a sector magnet and soft landed on a given substrate. These surfaces can be examined with various methods used in surface analysis, for instance STM (Scanning Tunneling Microscopy), LEED (Low Energy Electron Diffraction) and FIM (Field Ion Microscopy).

To understand the deposition process and thin film formation, first one has to understand the mechanisms governing the cluster-cluster and cluster-substrate interaction, which also can result in new effects. The impact of a single cluster onto a surface should be considered as the basic process in cluster impact thin film formation. Therefore, a simulation of this process gives valuable information pertaining to the growth characteristics of energetic cluster impact films. It may predict, for example, if the structure of the nanoparticle will be kept unchanged when deposited, and on which kind of substrate this is most likely to happen. To simulate theoretically the experimental process of deposition we performed Molecular Dynamics (MD) simulations (see Chapter 5), as they explicitly describe the molecular system as a function of time, and can directly calculate time-dependent phenomena. The impact cluster energies used in this work are in the range of the experimental Low Energy Cluster Beam Deposition (see paper III). Another approach we chose to investigate the cluster growth on surface, was to extend the basin-hopping algorithm in order to generate and optimize clusters onto substrates (see paper IV).

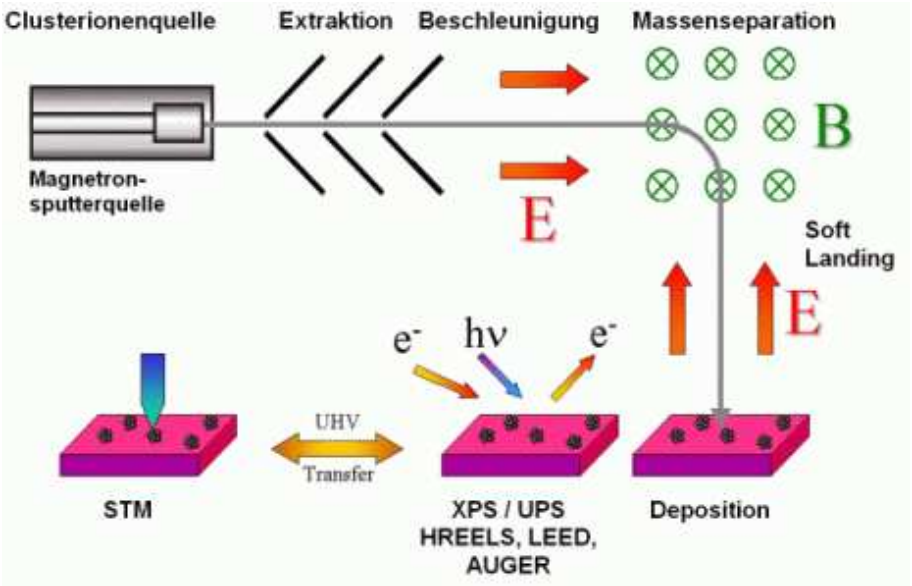

Figure 2.3: Setup of the Konstanz Cluster Deposition Experiment [50].

Chapter 3

Energy Potentials

In order to predict a cluster structure, first a mathematical model of the total potential energy E of the cluster has to be chosen. The accuracy of the model for the interatomic forces is a key factor in calculating the real properties of a system. In this Chapter we will give an overview of some of the most popular energy potentials and present those ones used to model the interactions between the atoms in the bimetallic clusters and in the 'cluster+surface' systems in the present thesis.

A simple and widely used energy potential is the Lennard-Jones (LJ) one. In this potential the binding forces are represented by pairwise interactions

$$V(r) = 4\epsilon \left[\left(\frac{\sigma}{r}\right)^n - \left(\frac{\sigma}{r}\right)^m \right]. \tag{3.1}$$

Here r is the interatomic distance and σ is the interatomic distance where the potential curve crosses zero. Most commonly n=12 and m=6 are assumed. This potential approximates van der Waals interactions and gives good representations of some rare gas and molecular clusters.

However, for truly representations of real clusters we need potentials which are not pairwise additive and more accurate. In metal clusters the many-body nature of the metallic cohesion (a consequence of the characteristic delocalization of the electrons) makes an adequate description of even the homointeractions a challenging task. Reproduction of the heteroatomic interactions is only a more complex problem. Searching for the right potential for describing an intermetallic system one can choose between *ab initio*, density-functional, or semiempirical methods such as the embedded atom method or tight-binding potentials like the Gupta potential. Both first methods give highly accurate results, but they are much more time consuming. Even for clusters with only one type of atoms, it is overwhelmingly demanding to identify the structure for clusters with just around 10–20 atoms using these methods. In contrast, the last two methods are fast potentials with high computational efficiency. Their parameters are fitted to experimental properties of bulk metals and alloys. Moreover, both of them are many-body potentials and thus based on the concept of density, or coordination. Such potentials give shorter and stronger bonds for low-coordination atoms. This many-body character of the interaction potential is very important for a reasonably accurate modelling of metallic systems.

In the present thesis the interactions between the atoms in the Ni–Cu bimetallic clusters as well as in the "cluster+surface" systems are described through the embedded atom method in the version of Daw, Baskes and Foiles, whereas for K–Cs and Rb–Cs bimetallic clusters we used the Gupta tight-binding method. In the following we will give a short overview of the density functional theory formalism before describing the semiempirical potentials based on it.

3.1 Density-Functional Theory (DFT)

The main problem in theoretical chemistry remains the solution of the Schrödinger equation

$$\widehat{H}\Psi = E\Psi, \tag{3.2}$$

which enables the calculation of the electronic and structural properties of a given material [51]. Unfortunately, it is possible to calculate the Schrödinger equation without any approximation only for rather small molecular systems. In order to obtain a solution of this equation for multielectron systems we use the Born-Oppenheimer approximation. Within this approximation the electronic and nuclear motion are separated within the Hamiltonian because the nuclei are much heavier than the electrons and from the point of view of the electrons they can be seen as fixed particles. Focusing only on time-independent properties within this approximation we can solve Schrodinger's equation for the electrons [52]:

$$\left\{ \sum_{i=1}^{N} \left[-\frac{\hbar^2}{2m}\nabla_i^2 + V_{ext}(\mathbf{r}_i) \right] + \frac{1}{2} \sum_{i \neq j=1}^{N} \frac{e^2}{\mid \mathbf{r}_i - \mathbf{r}_j \mid} \right\} \Psi(\mathbf{r}_1, \ldots, \mathbf{r}_N) = E \cdot \Psi(\mathbf{r}_1, \ldots, \mathbf{r}_N) \tag{3.3}$$

where $\mathbf{r}_i$ is the position of the ith electron, N is the total number of electrons, V_{ext} is the external field in which the electrons move, E is the total electronic energy, and Ψ is the electron wavefunction. $V_{ext}(\mathbf{r})$ is the electrostatic potential generated by the atomic nuclei, but it may also contain contributions from surrounding media or other perturbations on the system.

For the calculation of experimental observables we need to know the complete N-electron wavefunction $\Psi(\mathbf{r}_1, \ldots, \mathbf{r}_N)$. However, calculating $\Psi(\mathbf{r}_1, \ldots, \mathbf{r}_N)$ does give much more detailed information than is actually needed in any practical application, and it would be a very great computational simplification if one could avoid the extra unused information contained in the electron wavefunction. The main ansatz in the density-functional theory itself [53, 54] is that we don't need to calculate the whole N-particle wavefunction of the system, but simply the electron density in order to obtain any ground state property of the system. This theorem has been published by Hohenberg and Kohn in 1964 [55]. They have proved that the electron density $\rho(\mathbf{r})$ of the ground state determines uniquely the external potential $V_{ext}(\mathbf{r})$. This means that the electron density in three-dimensional position space is sufficient in constructing the full Hamilton operator of Eq. 3.3 and once that is known it is possible to solve the Schrödinger equation 3.3 and thus

obtain any ground state property. Thus, the total electronic energy, which is a ground state property of a given system, becomes a functional of the electron density

$$E = E[\rho(\mathbf{r})]. \tag{3.4}$$

However, the Hohenberg-Kohn theorem proves the existence of the functionals but do not provide any instruction on how to derive them. Due to this lack of exact functionals, the electron density $\rho(\mathbf{r})$ and the total electronic energy E are calculated by using certain approximations. A very useful approach for the calculation of the electron density was presented by Kohn and Sham in 1965 [56]. The approximation begins with the step of writing the total electronic energy $E[\rho]$ of the system as

$$E[\rho] = T[\rho] + \int \rho(\mathbf{r}) \left[V_{ext}(\mathbf{r}) + \frac{1}{2} V_C(\mathbf{r}) \right] d\mathbf{r} + E_{xc}[\rho]. \tag{3.5}$$

Here, T is the total kinetic energy, V_C the electrostatic Coulomb potential seen by the electron, V_{ext} the external potential, and E_{xc} is the exchange-correlation energy, which contains all terms that are not included in the other three addends. After exertion of the variational principle using the Lagrange multiplier μ we obtain

$$\frac{\delta T}{\delta \rho} + V_{ext}(\mathbf{r}) + V_C(\mathbf{r}) + \frac{\delta E_{xc}}{\delta \rho} = \mu. \tag{3.6}$$

The Lagrange multiplier is per construction the chemical potential for the electrons. Kohn and Sham compared this result with that obtained for N non-interacting particles (fermions) moving in another external potential V_{eff} defined in such a way that the electron density of this system is the same as that for the real system. The equivalent of equation 3.6 is in this case

$$\frac{\delta \tilde{T}}{\delta \rho} + V_{eff}(\mathbf{r}) = \mu \tag{3.7}$$

where $\tilde{T}$ is the kinetic energy of the non-interacting particles and not these of the physical system. For these non-interacting particles we can solve the Schrödinger equation. The last is significantly simplified and can be written as the sum of N single-particle equations of the form

$$\left[-\frac{\hbar^2}{2m} \nabla^2 + V_{eff}(\mathbf{r}) \right] \psi_i(\mathbf{r}) = \epsilon_i \psi_i(\mathbf{r}). \tag{3.8}$$

By solving this Schrödinger equation we can compute the electron density, which is the sum over the N orbitals with the lowest single-particle energies ϵ_i:

$$\rho(\mathbf{r}) = \sum_{i=1}^{N} \mid \psi_i(\mathbf{r}) \mid^2 . \tag{3.9}$$

Given the density, one determines the exchange energy and hence its variation with density. One can now recompute the effective potential, solve again the one-electron

Schrödinger equation, and recompute the density. The procedure is repeated until the process converges in a self-consistent manner.

Thus, Kohn and Sham reformulated the problem of calculating the total electronic energy E as a functional of the electron density $\rho(\mathbf{r})$ as that of solving a set of single-particle Schrödinger-like equations, and this approach has formed the basis for almost all practical applications of the densty-functional theory.

3.2 The Embedded Atom Method (EAM)

The EAM presents a semiempirical approximation for extended systems with largely delocalized electrons (mainly for early and late transition metals). It is based on the density functional formalism.

3.2.1 The EAM in the version of Daw, Baskes and Foiles (DBF)

The conceptual platform for the development of the EAM was provided in 1980 by the approach of Stott and Zaremba, named the quasi-atom method [57]. This approach has its roots in the DFT. Accordingly, the energy change associated with placing an atom into a host system of atoms is a functional of the electronic density of the host system before the new atom is embedded. The energy of the host with impurity is then a functional of the unperturbed host electron density and a function of the impurity charge and position. By analogy with the approach of Stott and Zaremba, Daw and Baskes [58–60] consider each atom of a metal as an impurity embedded in a host provided by all other atoms. According to this view the total energy E_{tot} has the following form

$$E_{\rm tot} = \sum_{i=1}^{N} [F_i(\rho_i^h) + \frac{1}{2} \sum_{j=1(j\neq i)}^{N} \phi_{ij}(r_{ij})]. \tag{3.10}$$

In Eq. 3.10, ρ_i^h is the local electron density at site i and F_i is the embedding energy required to embed an atom into this density. The local density at site i is assumed being a superposition of atomic electron densities,

$$\rho_i^h = \sum_{j=1(j\neq i)}^{N} \rho_j^a(r_{ij}), \tag{3.11}$$

where $\rho_j^a(r_{ij})$ is the spherically averaged atomic electron density provided by atom j at the distance r_{ij}. Further, in Eq. 3.10 ϕ_{ij} is the short-range pair repulsive interaction between atoms i and j

$$\phi_{ij}(r_{ij}) = \frac{Z_i(r_{ij}) Z_j(r_{ij})}{r_{ij}}, \tag{3.12}$$

separated by the distance r_{ij}.

The detailed analysis made in Ref. [60] have shown that the main Ansatz of the EAM, Eq. (3.10), also holds good in the case of the binary alloys. In accord with Ref. [60] the pair interaction between two different species (A-B/B-A heterointeraction) can be approximated by the geometric mean of the pair interaction for the individual species: $\phi_{AB}(R) = \sqrt{\phi_{AA}(R) \cdot \phi_{BB}(R)}$. Further, the embedding functions for the Ni–Cu and Ag–Ni systems have been determined by Daw, Baskes and Foiles empirically by fitting to experimental data of bulk sublimation energy, elastic constant and the heat of solution of binary alloys [60]. The values for ρ_i^a, F_i and ϕ_{ij} are available in numerical form for Ni, Cu and Ag [61]. The validity of the embedding functions for the Ni–Cu and Ag–Ni systems has been tested by computing a wide range of properties as e.g. the segregation energy of substitutional impurities to the (100) surface [60].

The EAM of DBF has been successfully applied to many bulk and low-symmetric problems in transition metals such as defects, surface structures and surface segregation/mixing effects in alloys [62]. Furthermore, in our previous works [63–68] (those include also the discussions with the available experiments) we have found that this approach provides accurate information on pure Cu_N, Ni_N and Ag_N clusters, which is our main reason for choosing this potential for studying Ni–Cu and Ag–Ni heteroatomic systems.

3.2.2 The EAM version of Voter and Chen

There is another well-accepted version of the EAM developed by Voter and Chen [69, 70]. This version of the EAM distinguishes from the version of DBF mainly by means of the parametrization and by the form of the pair potential. Furthermore, the version of Voter and Chen takes into account properties of the dimer as well as bulk properties in the fitting procedure, whereas Daw and Baskes use only bulk properties of the metals in their parametrization.

In the fitting procedure of Voter and Chen the pairwise interaction is taken to be a Morse potential,

$$\phi(r) = D_M[1 - e^{(-\alpha_M(r-R_M))}]^2 - D_M \tag{3.13}$$

where the three parameters D_M, R_M and α_M, define the depth, position of the minimum, and a measure of the curvature near the minimum, respectively. The density function, $\rho(r)$, is taken as

$$\rho(r) = r^6[e^{-\beta r} + 2^9 e^{-2\beta r}] \tag{3.14}$$

where β is an adjustable parameter.

To be suitable for use in molecular dynamics, the interatomic potential $\phi(r)$ as well as the electron density $\rho(r)$ should be continuous. This is accomplished by forcing $\phi(r)$ and $\rho(r)$ to go smoothly to zero at a cutoff distance, r_{cut}, which is used as a fitting parameter. The five parameters defining $\phi(r)$ and $\rho(r)$ (D_M, R_M, α_M, β and r_{cut}) are optimized by minimizing the root-mean-square deviation (χ_{rms}) between the calculated and experimental values for the three cubic elastic constants, the vacancy formation energy, the bond length and the bond strength of the diatomic molecule.

Although the two versions of EAM have completely different parametrizations, they yield clusters that are structurally and energetically almost identical, as previous studies of Grigoryan *et al.* have shown [64, 67].

3.3 The Gupta Potential

The Gupta potential [71] has been successfully applied to study the structure, energetics, free energy, surface energy and melting point of alkali metal clusters [72, 73]. It has been derived from Gupta's expression for the cohesive energy of a bulk material. According to this, the total energy of a system with N atoms is written in terms of repulsive and attractive many-body terms,

$$V_{clus} = \sum_{i=1}^{N} \Big[V^r(i) - V^m(i) \Big] \tag{3.15}$$

where

$$V^r(i) = \sum_{j=1\,(\neq i)}^{N} A(a,b) \exp\left[-p(a,b) \left(\frac{r_{ij}}{r_0(a,b)} - 1 \right) \right] \tag{3.16}$$

and

$$V^m(i) = \left\{ \sum_{j=1\,(\neq i)}^{N} \zeta^2(a,b) \exp\left[-2q(a,b) \left(\frac{r_{ij}}{r_0(a,b)} - 1 \right) \right] \right\}^{\frac{1}{2}}. \tag{3.17}$$

In these equations, r_{ij} is the distance between atoms i and j, and A, r_0, ζ, p, and q are parameters whose values are fitted to experimental values such as cohesive energy, lattice parameters and independent elastic constants for the reference crystal structure at 0 K. Finally, a and b refer to atom type of atom i and j.

The parameters for inhomogeneous K–Cs (Rb–Cs) interactions are taken as the average of the K–K and Cs–Cs (Rb–Rb and Cs–Cs) parameters obtained by Li *et al.* [73]. The reasoning for this is that bulk K–Cs and Rb–Cs alloys are solid solutions, rather than ordered intermetallics, and mixture energies and mixture parameters of molten K–Cs and Rb–Cs alloys computed in a study of Christman [74] are very close to the averages of the corresponding single constituent values. Furthermore, also for other alloy systems it has been found that the parameters are close to the average values and in general lie between the limits of the homonuclear interaction parameters [75].

Chapter 4

Optimization Algorithms

Optimization is a common problem in science, engineerings, business, politics and every day life. Engineers try to construct machines with an energy or material consumption as efficient as possible. Managers try to maximise the profit and minimise the loss of their companies. Also the rays of light in a medium follow a path which minimises the travel time. Finally in biology Darwin's paradigm of the survival of the fittest (Darwin, 1859) interprets the origin of species as an optimization process. In this work we concentrate our attention on the problem of structure prediction of clusters, where the most stable structure corresponds to a global minimum in the potential energy surface (PES). Hereby, the PES represents the potential energy of the cluster as a function of its atomic coordinates. Each local minimum in the PES corresponds to a possible mechanically stable configuration of the atomic coordinates where the gradient of the potential vanishes.

But, even for the simpler case of monoatomic cluster, we are faced with the problem of complexity, i.e., the number of local minima in the PES increases exponentially with cluster size. Bimetallic clusters possess much more complex PES due to the inequivalence of homotops (as mentioned in Chapt. 2)). Therefore, to obtain a precise information on the structure of the lowest total energy and thus to calculate the properties of interest, an unbiased and accurate exploration of the potential energy surface is required.

4.1 Local Optimization

For the calculation of the closest local total-energy minima we use two different methods: the Broyden-Fletcher-Goldfarb-Shanno method, which belongs to the variable metric/ quasi-Newton methods, and the conjugate gradient method.

Both variable metric and conjugate gradient methods require that you are able to compute the function's gradient, or first partial derivatives, at arbitrary points. The goal of both methods is to accumulate information from successive line minimizations so that N such line minimizations lead to the exact minimum of a quadratic form in N dimensions. The variable metric approach differs from the conjugate gradient in the way that it stores and updates the information that is accumulated.

4.1.1 The Variable Metric/Quasi-Newton Method

The basic idea of the method is the application of the Newton method for solving nonlinear systems of equations in order to find a zero point of the gradient of the function *f(x)* [76,77]. The Newton step is then

$$x_{i+1} = x_i - \mathbf{H}^{-1}\nabla f(x_i) \tag{4.1}$$

where $\mathbf{H}^{-1}$ is the inversed Hessian matrix, i.e. the matrix of the second derivative of f at point x_i. A major drawback of using the Newton step is the necessity to evaluate the Hessian matrix $\mathbf{H}$, which might be computationally expensive and error-prone. Furthermore one has to invert this matrix, which is computational demanding too. The method presented in this section alleviates this difficulty by approximating the inverse of the Hessian using solely the gradient of the function. Thus, the 'quasi' in the quasi-Newton method is that we don't use the actual Hessian matrix $\mathbf{H}$, but instead construct a sequence of matrices $\mathbf{H}_\mathrm{i}$, which approximates the Hessian matrix

$$\lim_{i\to\infty} \mathbf{H}_\mathrm{i} = \mathbf{H}^{-1}. \tag{4.2}$$

The search direction d_i at the i-th step, i.e. the directions along which f decreases is defined as following

$$d_i = -\mathbf{A}_i \nabla f(x_i). \tag{4.3}$$

Hereby, $\mathbf{A}_i$ is a symmetric and positive definite matrix, which approximates the inverse Hessian matrix. The different quasi-Newton methods differ in the update formula for the inverse Hessian matrix. Such methods, with step wise approximation of the Newton direction, exhibit a fast rate of convergence. In the neighbourhood of the minimum they converge within few iterations yielding a high accuracy of the solution.

4.1.2 The Broyden-Fletcher-Goldfarb-Shanno Method (BFGS)

The Broyden-Fletcher-Goldfarb-Shanno algorithm [76] belongs to the family of quasi-Newton methods. Here the inverse Hessian matrix $\mathbf{A}_i$ is updated as follows:

$$\mathbf{A}_{i+1} = \mathbf{A}_i + \frac{s_i s_i^T}{s_i^T v_i} - \frac{\mathbf{A}_i v_i v_i^T \mathbf{A}_i}{v_i^T \mathbf{A}_i v_i} + (v_i^T \mathbf{A}_i v_i) \cdot u_i \tag{4.4}$$

with

$$u_i = \frac{s_i}{s_i^T v_i} - \frac{\mathbf{A}_i v_i}{v_i^T \mathbf{A}_i v_i} \tag{4.5}$$

where

$$s_i = x_{i+1} - x_i \tag{4.6}$$

and

$$v_i = \nabla f(x_{i+1}) - \nabla f(x_i). \tag{4.7}$$

Since quasi-Newton methods require the storage of the Hessian matrix (or its inverse), their memory requirement is high, which in most cases prevent their application to large scale optimization problems like minimizing the potential energy of a cluster with more than 3000 atoms. A method to reduce the memory requirement, is to choose a compact, implicit representation of the Hessian matrix. The most widely used method, the limited-memory BFGS, or L-BFGS algorithm for short, was introduced by Nocedal (1980) [78]. It is almost identical in its implementation to the BFGS method. The only difference is in the matrix update: at every step the oldest information contained in the quasi-Newton matrix is discarded and replaced by new one. In this way a more up to date model of the functions is achieved. In this thesis a slightly modified implementation of the L-BFGS algorithm developed by Liu & Nocedal (1989) [79] was used for the local optimization of the "surface+cluster" systems as well as of the K–Cs and Rb–Cs cluster structures, and a simple BFGS algorithm was employed for the optimization of Ni–Cu cluster geometries.

4.1.3 The Conjugate Gradient Method

In the conjugate gradient method the new search direction is conjugate to the previous search directions [76]. Starting with an arbitrary initial vector $\mathbf{g}_0$ and letting $\mathbf{h}_0 = \mathbf{g}_0$, the conjugate gradient method constructs two sequences of vectors from the recurrence

$$\mathbf{g}_{i+1} = \mathbf{g}_i - \lambda_i \mathbf{A} \cdot \mathbf{h}_i \qquad \mathbf{h}_{i+1} = \mathbf{g}_{i+1} + \gamma_i \mathbf{h}_i \qquad i = 0, 1, 2, ... \tag{4.8}$$

The vectors satisfy the orthogonality and conjugacy conditions with respect to a symmetric, positive definite matrix $\mathbf{A}$ if

$$\mathbf{g}_i \cdot \mathbf{g}_j = 0 \qquad \mathbf{h}_i \cdot A \cdot \mathbf{h}_j = 0 \qquad \mathbf{g}_i \cdot \mathbf{h}_j = 0 \qquad j < i. \tag{4.9}$$

The scalars λ_i and γ_i are given by

$$\lambda_i = \frac{\mathbf{g}_i \cdot \mathbf{g}_i}{\mathbf{h}_i \cdot A \cdot \mathbf{h}_i} = \frac{\mathbf{g}_i \cdot \mathbf{h}_i}{\mathbf{h}_i \cdot A \cdot \mathbf{h}_i} \tag{4.10}$$

$$\gamma_i = \frac{\mathbf{g}_{i+1} \cdot \mathbf{g}_{i+1}}{\mathbf{g}_i \cdot \mathbf{g}_i}. \tag{4.11}$$

Suppose that we have $\mathbf{g}_i = -\nabla f(\mathbf{P}_i)$, for some point $\mathbf{P}_i$. We proceed from $\mathbf{P}_i$ along the direction $\mathbf{h}_i$ to the local minimum of f located at some point $\mathbf{P}_{i+1}$ and then set $\mathbf{g}_{i+1} = -\nabla f(\mathbf{P}_{i+1})$. Then, this $\mathbf{g}_{i+1}$ is the same vector as would have been constructed by Eq. 4.8. We have, then, the basis of an algorithm that requires neither knowledge of the Hessian matrix $\mathbf{A}$, nor even the storage necessary to store such a matrix. A sequence of directions $\mathbf{h}_i$ is constructed, using only line minimizations, evaluations of the gradient vector, and an auxiliary vector to store the latest in the sequence of $\mathbf{g}$'s.

The algorithm described so far is the original Fletcher-Reeves version of the conjugate gradient algorithm. Later, Polak and Ribiere introduced one significant change. They proposed using the form

$$\gamma_i = \frac{(\mathbf{g}_{i+1} - \mathbf{g}_i) \cdot \mathbf{g}_{i+1}}{\mathbf{g}_i \cdot \mathbf{g}_i} \tag{4.12}$$

instead of Eq. 4.11. The Polak-Ribiere formula accomplishes the transition to further iterations, after you have arrived at the minimum of the quadratic form, more gracefully. It tends to reset $\mathbf{h}$ to be down the local gradient, which is equivalent to beginning the conjugate-gradient procedure anew.

4.2 Global Optimization

In this work the genetic algorithm has been used to determine the global minima of the total energy of the Ni–Cu binary clusters, and the basin-hopping algorithm was applied to K–Cs and Rb–Cs clusters, as well as to Ag clusters adsorbed on Ag(111) and Ni(111) surfaces.

4.2.1 The Genetic Algorithm (GA)

Genetic algorithms are based on Darwins theory of evolution, i.e. on the mechanisms of natural selection ("survival of the fittest"). The GA employs operators that are analogues of the evolutionary processes of genetic crossover and mutation to explore multidimensional parameter space. It can be applied to any problem where the variables to be optimized ("genes") can be encoded to form a string ("chromosome"), each string representing a trial solution to the problem. The use of GAs for optimizing cluster geometries was pioneered in the early 1990s by Hartke (for small silicon clusters) and Xiao and Williams (for molecular clusters). Since then, genetic algorithms have been increasingly used in a variety of global optimization problems in chemistry, physics, materials science and biology. Notable applications of GAs in the chemistry/biochemistry field include the simulation of protein folding, structural studies of RNA and DNA, the design and docking of drug molecules, the prediction of crystal structures and the solution from single crystal, powder and thin film diffraction data. In the case when the GA is applied on atomic clusters the more fit individuals in a generation are selected and mated to produce the next generation of offsprings. Here the fitness is a measure of the energetic stability for a certain cluster structure.

Our version of the genetic algorithms has been applied to clusters with one, two, and three types of atoms, for example Au, Na, AlO and HAlO clusters [80–82], and we have found that this optimization method is reliable when studying the structural and energetic properties of one-component as well as of multi-component clusters.

For the study on a given Ni_nCu_m cluster, a number of randomly generated structures are optimized locally with the quasi-Newton method. The three lowest-total-energy structures are then used as the initial population. Subsequently, a new set of clusters is constructed by cutting each of the three original ones randomly into two parts, that are interchanged and randomly rotated relative to each other, and afterwards allowed to

relax. Out of the total set of six structures, the three ones with the lowest total energy are kept as the next generation. This procedure is repeated until the lowest total energy is unchanged for a large number of generations.

4.2.2 The Basin-Hopping Algorithm (BH)

In the following we will give a short overview of the Monte Carlo method before describing the BH algorithm based on it.

The Monte Carlo Method (MC)

The Monte Carlo method was developed by von Neumann, Ulam, and Metropolis at the end of the Second World War to study the diffusion of neutrons in fissionable material. The name 'Monte Carlo', chosen because of the extensive use of random numbers in the calculation, was coined by Metropolis in 1947. The method represents a random walk through phase space, where the new particle positions are either accepted or rejected by the energy criterion of Metropolis. According to the Metropolis criterion, if the energy of the new minimum, E_{new} is lower than the energy calculated in the last step E_{old}, then the probability to realize the new state is greater than those to realize the old state and the step is accepted. If E_{new} is greater than E_{old}, then the step is accepted if exp[-$(E_{old} - E_{new})/k_B T$] is greater than a random number drawn from the interval [0,1]. If the move uphill in energy is rejected, the system remains in the old state. In this case the atom is retained at its old position and the old configuration is recounted as a new state in the chain.

In comparison to molecular dynamics simulations, which is described in Chapter 5, time does not enter in the MC scheme, i.e. the temporal progression is lost.

The BH Method

The BH method is based upon Li and Scheraga's Monte Carlo minimization [83–87]. In this method perturbations in the algorithm are introduced by changing slightly the latest set of coordinates and carrying out a gradient-based optimization from the resulting geometry. Moves are accepted or rejected based on the Metropolis criterion. Thus, the difference from the standard MC algorithm is that the energy should be minimized with respect to the local minimum before the Metropolis acceptance rule is applied. The use of a minimization procedure before the application of the acceptance criterion is equivalent to searching for a transformed potential energy surface defined by

$$\tilde{E}(\vec{X}) = \min\{E(\vec{X})\}, \tag{4.13}$$

where min{...} represents a local energy minimization process with $\vec{X}$ as initial structure. The topography of the transformed surface is that of a multidimensional staircase. Each step corresponds to the basin of attraction (plateau) surrounding a particular minimum.

The Monte Carlo part of the BH algorithm is introduced in order to allow the system to hop from one plateau to another at a thermal energy $k_B T^*$ measured in units of the binding energy of the cluster dimer. The hopping probability depends highly on the choice of the "temperature" T^* and on the reduced-energy difference between the plateaus of the two consecutive steps. In the present work the Monte Carlo simulation has been performed at a *constant* reduced "temperature" of 0.8.

The maximum allowed displacement of atoms is given by the parameters *STEP* and *ASTEP*. The first one specifies the maximum change of any Cartesian coordinate and the second one the tolerance on the binding energy of individual atoms below which an angular step is taken for that atom. In this thesis we have used a combination of 0.36 and 0.4 for *STEP* and *ASTEP*, respectively, to explore the PES of binary clusters and a combination of 1.3 and 0.4 to optimize clusters on surfaces.

A further parameter is the *ACCEPTRATIO* which governs the size of the trial move. If this parameter is too large then a large fraction of moves are accepted but the phase space of the cluster is explored slowly, i.e. consecutive states are highly correlated. If it is too small then nearly all the trial moves are rejected and again there is little movement through phase space. An acceptance ratio of 0.5 (which means that half of the moves are accepted) is most common and used also in this work.

The BH algorithm has successfully located all the lowest known minima for Lennard-Jones clusters with up to 110 atoms, including all the nonicosahedral structures (sizes 38, 75-77, 102-104), for the first time in unbiased searches [86]. In a recent study, Doye *et al.* have found the particularly stable structures for binary Lennard-Jones clusters with up to 100 atoms [88].

The BH code we used in this work has been downloaded from the website of Dr. David J. Wales [89]. For the present study, the EAM of DBF and the Gupta potential, both written for the case of bimetallic systems, have been implemented in the algorithm. To optimize a cluster structure on a surface, the code has been modified as follows. We disturb randomly the coordinates of the cluster separately from those of the surface and then carry out a gradient-based optimization on the "cluster+surface" system. Afterwards the Metropolis acceptance rule is applied using the old and new local minima of the "cluster+surface". For the next step the cluster atoms that belong to the latest set "cluster+surface" coordinates are disturbed randomly again. This procedure is repeated until the lowest total energy of the "cluster+surface" system is found.

Chapter 5

Molecular Dynamics Simulation (MD)

MD is a widely used method to compute the motions of individual molecules or atoms in models of solids, liquids, and gases. It can be viewed as a simulation of the system as it develops over a period of time. The molecular dynamics method was first introduced by Alder and Wainwright in the late 1950's [90,91] to study the interactions of hard spheres. The first molecular dynamics simulation of a realistic system was done by Rahman and Stillinger in their simulation of liquid water in 1971 [92]. A molecular dynamics simulation generates a sequence of points in phase space as a function of time. These points belong to the same ensemble, and they correspond to the different conformations of the system and their respective momenta. There exist different ensembles with different characteristics.

1. Microcanonical ensemble (NVE) : The thermodynamic state characterized by a fixed number of atoms, N, a fixed volume, V, and a fixed energy, E. This corresponds to an isolated system.

2. Canonical Ensemble (NVT): This is a collection of all systems whose thermodynamic state is characterized by a fixed number of atoms, N, a fixed volume, V, and a fixed temperature, T.

3. Isobaric-Isothermal Ensemble (NPT): This ensemble is characterized by a fixed number of atoms, N, a fixed pressure, P, and a fixed temperature, T.

4. Grand canonical Ensemble (μVT): The thermodynamic state for this ensemble is characterized by a fixed chemical potential, μ, a fixed volume, V, and a fixed temperature, T.

In this thesis we use a microcanonical NVE ensemble, where kinetic and potential energy are transformed into each other all the time keeping the total energy of the system constant. In contrast to the Monte Carlo method (see Chapter 4), which follows a random walk, in MD the system moves in phase space along its physical trajectory as determined by Newton's equations of motion. These are integrated numerically.

In Newton's second low the mass m_i of atom i and its acceleration are related to the force $\mathbf{f}_i$ on that atom

$$m_i \ddot{\mathbf{x}}_i = \mathbf{f}_i \tag{5.1}$$

with

$$\mathbf{f}_i = \nabla_{x_i} \mathbf{V}. \tag{5.2}$$

Here $\mathbf{x}_i$ are the coordinates of atom i and $\mathbf{V}$ is the gradient of the potential energy field. In a classical MD code the starting conditions are the positions of the atoms. Following Newton's prescription, from the initial positions, velocities and forces, it is possible to calculate the positions and velocities of the atoms at a small time interval (a time step) later. From the new positions the forces are recalculated and another step in time made. The cycle has to be repeated many times in the course of a full simulation, usually for many thousands of time steps. It is worth noting that a single time step is usually of the order of 1 femtosecond, and thus significantly smaller than the typical time taken for a molecule to travel its own length.

At the end of the simulation event, a certain number of steps is dedicated to the simulated annealing of the system, in which the temperature is gradually reduced. As on the one hand the potential energy of the system decreases as a result of the interaction between the particles and on the other hand our program uses an *NVE* ensemble, i.e. the total energy is kept constant, there will be an increase in the kinetic energies of the cluster atoms. Thus, in order to obtain reasonable final structures, we have to cool down the structures at the end of the simulation and give the system the opportunity to surmount energetic barriers, and find non-local minima.

5.1 The Verlet algorithm

The Verlet algorithm [93,94] is a direct solution of the second-order Newtonian equations. In this method the positions at the next time step are calculated from the positions at the previous and current time steps, without using the velocity. The equations are solved on a step-by-step basis. To use such a finite time-step method of solution, it is essential that the particle positions vary smoothly with time. Whenever the potential varies sharply, impulsive collisions between particles occur at which the velocities change discontinuously. The particle dynamics at the moment of each collision must be treated explicitly, and separately from the smooth inter-collisional motion. Thus, a Taylor expansion of $\mathbf{x}(t)$ about time t is necessary to obtain a potential energy which is a continuous function of particle positions. In this sense the Verlet algorithm is a combination of two Taylor expansions. First the Taylor series for position from time t forward to $t + \Delta t$ is written as

$$\mathbf{x}(t + \Delta t) = \mathbf{x}(t) + \frac{d\mathbf{x}(t)}{dt}\Delta t + \frac{1}{2}\frac{d^2\mathbf{x}(t)}{dt^2}\Delta t^2 + \frac{1}{3!}\frac{d^3\mathbf{x}(t)}{dt^3}\Delta t^3 + ... \tag{5.3}$$

Then the Taylor series from t backward to $t - \Delta t$ is written as follows

$$\mathbf{x}(t - \Delta t) = \mathbf{x}(t) - \frac{d\mathbf{x}(t)}{dt}\Delta t + \frac{1}{2}\frac{d^2\mathbf{x}(t)}{dt^2}\Delta t^2 - \frac{1}{3!}\frac{d^3\mathbf{x}(t)}{dt^3}\Delta t^3 + ... \tag{5.4}$$

Adding these two expansions gives the basic Verlet formula

$$\mathbf{x}(t+\Delta t) = 2\mathbf{x}(t) - \mathbf{x}(t-\Delta t) + \frac{d^2\mathbf{x}(t)}{dt^2}\Delta t^2 + ... \tag{5.5}$$

This offers the advantage that the first and third-order term from the Taylor expansion cancels out, thus making the Verlet integrator an order more accurate than integration by simple Taylor expansion alone. As it can be seen in the basic Verlet formula, the velocities are not explicitly given in the basic Verlet equation, but often they are necessary for the calculation of certain physical quantities as the kinetic energy. The velocities may be obtained from the formula

$$\mathbf{v}(t) = \frac{\mathbf{x}(t+\Delta t) - \mathbf{x}(t-\Delta t)}{2\Delta t}. \tag{5.6}$$

5.2 The Velocity Verlet algorithm

A similar, but more commonly used algorithm is the Velocity Verlet algorithm [94]. This method explicitly incorporates velocity. Positions and velocities are calculated at the same time

$$\mathbf{x}(t+\Delta t) = \mathbf{x}(t) + \mathbf{v}(t)\Delta t + \frac{1}{2}\mathbf{a}(t)\Delta t^2 \tag{5.7}$$

$$\mathbf{v}(t+\Delta t) = \mathbf{v}(t) + \frac{1}{2}\Delta t[\mathbf{a}(t) + \mathbf{a}(t+\Delta t)]. \tag{5.8}$$

At the time $t+\Delta t$, the kinetic energy is available and the potential energy will have been evaluated in the force loop. The most time consuming part of the MD method is the force calculation and not the integration algorithm. Thus, it is important to be able to employ a long time step Δt. In this way, a given period of simulation time can be covered in a modest number of integration steps, i.e. in an acceptable amount of computer time. In contrast to other methods of numerical integration, such as the predictor-corrector algorithm, the Velocity Verlet method is fast, requires little memory and allows the use of a long time step. Its numerical stability, convenience, and simplicity make it perhaps the most attractive proposed to date. In this thesis molecular dynamics simulation combined with the Velocity Verlet algorithm was performed to study the deposition process of small Ni and Cu clusters on Ni(111) and Cu(111) surfaces.

Bibliography

[1] S. Koutsopoulos, K. M. Eriksen, and R. Fehrman, J. Catal. **238**, 270 (2006).

[2] S. Devarajan, P. Bera, and S. Sampath, J. Colloid Interface Sci. **290**, 117 (2005).

[3] J. V. Barth, G. Costantini, and K. Kern, Nature **437**, 671 (2005).

[4] C. N. R. Rao, G. U. Kulkarni, and P. J. Thomas, Chem. Soc. Rev. **29**, 27 (2000).

[5] M. Gaudry, E. Cottancin, M. Pellarin, J. Lerme, L. Arnaud, J. R. Huntzinger, J. L. Vialle, M. Broyer, J. L. Rousset, M. Treilleux, and P. Melinon, Phys. Rev. B **67**, 155409 (2003).

[6] S. Xiao, W. Hu, W. Luo, Y. Wu, X. Li, and H. Deng, Eur. Phys. J. **54**, 479 (2006).

[7] A. Aguado, L. E. Gonzalez, and J. M. Lopez, J. Phys. Chem. B **108**, 11722 (2004).

[8] C. Mottet, G. Rossi, F. Balleto, and R. Ferrando, Phys. Rev. Lett. **95**, 035501 (2005).

[9] N. L. Rosi and C. A. Mirkin, Chem. Rev. **105**, 1547 (2005).

[10] M. P. Andrews and S. C. O'Brien, J. Phys. Chem. **96**, 8233 (1992).

[11] http://www2.fci.unibo.it/ longoni/image/

[12] R. L. Johnston, *Atomic and Molecular Clusters* (Taylor and Francis, London, 2002).

[13] R. L. Johnston, Philos. Trans. R. Soc. London A **356**, 211 (1998).

[14] E. Roduner, *Nanoscopic Materials: Size Dependent Phenomena* (The Royal Society of Chemistry, UK, 2006).

[15] A. Christensen, P. Stoltze, and J. K. Nørskov, J. Phys.: Condens. Matter **7**, 1047 (1995).

[16] Y. Shimizu, K. S. Ikeda, and S. Sawada, Phys. Rev. B **64**, 075412 (2001).

[17] H. B. Liu, U. Pal, R. Perez, and J. A. Ascencio, J. Phys. Chem. **110**, 5191 (2006).

[18] Z. Li, J. P. Wilcoxon, F. Yin, Y. Chen, R. E. Palmer, and R. L. Johnston, Faraday Discuss. **138**, 363 (2008).

[19] M. Polak and L. Rubinovich, Phys. Rev. B **75**, 045415 (2007).

[20] S. Darby, T. V. Mortimer-Jones, R. L. Johnston, and C. Roberts, J. Chem. Phys. **116**, 1536 (2002).

[21] G. Rossi, A. Rapallo, C. Mottet, A. Fortunelli, F.Baletto, and R. Ferrando, Phys. Rev. Lett. **93**, 105503 (2004).

[22] A. Rapallo, G. Rossi, R. Ferrando, A. Fortunelli, B. C. Curley, L. D. Lloyd, G. M. Tarbuck, and R. L. Johnston, J. Chem. Phys. **122**, 194308 (2005).

[23] G. Rossi, R. Ferrando, A. Rapallo, A. Fortunelli, B. C. Curley, L. D. Lloyd, and R. L. Johnston, J. Chem. Phys. **122**, 194309 (2005).

[24] T. Van Hoof and M. Hou, Phys. Rev. B **72**, 115434 (2005).

[25] G. Barcaro, A. Fortunelli, G. Rossi, F. Nita, and R. Ferrando, J. Phys. Chem. B **110**, 23197 (2006).

[26] L. O. Paz-Borbón, R. L. Johnston, G. Barcaro, and A. Fortunelli, J. Phys. Chem. C **111**, 2936 (2007).

[27] D. Ferrer, A. Torres-Castro, X. Gao, S. Sepulveda-Guzman, U. Ortiz-Mendez, and M. José-Yacamán, Nano Lett. **7**, 1701 (2007).

[28] M. C. Fromen, J. Morrilo, M. J. Casanove, and P. Lecante, Europhys. Lett. **73**, 885 (2006).

[29] T. Van Hoof and M. Hou, Eur. Phys. J. D. **29**, 33 (2004).

[30] D. Cheng, W. Wang, and S. Huang, J. Phys. Chem. B **11**, 16193 (2006).

[31] F. Baletto, C. Mottet, and R. Ferrando, Phys. Rev. Lett. **90**, 135504 (2003).

[32] L. D. Lloyd, R. L. Johnston, S. Salhi, and N. T. Wilson, J. Mater. Chem. **14**, 1691 (2004).

[33] J. Jellinek and E. B. Krissinel, Chem. Phys. Lett. **258**, 283 (1996).

[34] U. Müller, *Anorganische Strukturchemie* (TeubnerStudienbücher, Stuttgart, 1996).

[35] Holleman-Wiberg, *Lehrbuch der Anorganischen Chemie* (Walter de Gruyter, Berlin, New York, **101**, 1995).

[36] C. Binns, Surf. Sci. Rep. **44**, 1 (2001).

[37] P. Milani and I. Iannotta, *Cluster Beam Synthesis of Nanostructured Materials* (Springer, Berlin, 1999).

[38] H. Haberland, *Clusters of Atoms and Molecules* (Springer, Berlin, 1994).

[39] F. Baletto and R. Ferrando, Rev. Mod. Phys. **77**, 371 (2005).

[40] W. A. De Heer, Rev. Mod. Phys. **65**, 611 (1993).

[41] R. E. Palmer, S. Pratontep and H. -G. Boyen, Nat. Mater. **2**, 443 (2003).

[42] H. Bönnemann and R. M. Richards, Eur. J. Inorg. Chem. **10**, 2455 (2001).

[43] N. Toshima and T. Yonezawa, New J. Chem. **22**, 1179 (1998).

[44] C. Burda, X.-B. Chen, R. Narayanan, and M. A. El-Sayed, Chem. Rev. **105**, 1025 (2005).

[45] D. V. Goia and E. Matijevic, New J. Chem. **22**, 1203 (1998).

[46] K. Torigoe and K. Esumi, Langmuir **9**, 1664 (1993).

[47] K. R. Harikumar, S. Ghosh, and C. N. R. Rao, J. Phys. Chem. A **101**, 536 (1997).

[48] M. T. Reetz, W. Helbig, and S. A. Quaiser, Chem. Mater. **7**, 2227 (1995).

[49] U. Kolb, S. A. Quaiser, M. Winter, and M. T. Reetz, Chem. Mater. **8**, 1889 (1996).

[50] http://www.uni-konstanz.de/sfb513/abstracts/

[51] M. Springborg, *Methods of Electronic-Structure Calculations* (John Wiley & Sons Ltd, 2000).

[52] M. Springborg, *Density-Functional Methods in Chemistry and Materials Science* (John Wiley & Sons Ltd, 1997).

[53] P. Geerlings, F. De Proft, and W.Langenaecker, *Density Functional Theory* (VUBPRESS-Brussels, 1999).

[54] R. M. Dreizler and E. K. U. Gross, *Density Functional Theory* (Springer Verlag Berlin Heidelberg, 1990).

[55] P. Hohenberg and W. Kohn, Phys. Rev. **136**, B864 (1964).

[56] W. Kohn and L. J. Sham, Phys. Rev. **140**, A1133 (1965).

[57] M. J. Stott and E. Zaremba, Phys. Rev. B **22**, 1564 (1980).

[58] M. S. Daw and M. I. Baskes, Phys. Rev. Lett. **50**, 1285 (1983).

[59] M. S. Daw and M. I. Baskes, Phys. Rev. B **29**, 6443 (1984).

[60] S. M. Foiles, M. I. Baskes, and M. S. Daw, Phys. Rev. B **33**, 7983 (1986).

[61] http://enpub.fulton.asu.edu/cms/potentials/main/main.htm

[62] M. S. Daw, S. M. Foiles, and M. I. Baskes, Mat. Sci. Rep. **9**, 251 (1993).

[63] V. G. Grigoryan and M. Springborg, Chem. Phys. Lett. **375**, 219 (2003).

[64] V. G. Grigoryan, D. Alamanova, and M. Springborg, Eur. Phys. J. D **34**, 187 (2005).

[65] D. Alamanova, V. G. Grigoryan, and M. Springborg, Z. Phys. Chem. **220**, 811 (2006).

[66] V. G. Grigoryan and M. Springborg, Phys. Rev. B **70**, 205415 (2004).

[67] V. G. Grigoryan, D. Alamanova, and M. Springborg, Phys. Rev. B **73**, 115415 (2006).

[68] D. Alamanova, V. G. Grigoryan, and M. Springborg, J. Phys. Chem. C **111**, 12577 (2007).

[69] A. Voter, *Intermetallic Compounds: Principles and Practice* (John Wiley and Sons, Ltd, 1994, p. 77).

[70] A. Voter and S. Chen, Mat. Res. Soc. Symp. Proc. **82**, 175 (1987).

[71] R. P. Gupta, Phys. Rev. B **23**, 6265 (1981).

[72] S. K. Lai, P. J. Hsu, K. L. Wu, W. K. Liu, and M. Iwamatsu, J. Chem. Phys. **117**, 10715 (2002).

[73] Y. Li, E. Blaisten-Barojas, and D. A. Papaconstantopoulos, Phys. Rev. B **57**, 15519 (1998).

[74] J. R. Christman, Phys. Rev. **153**, 225 (1967).

[75] F. Cleri and V. Rosato, Phys. Rev. B **48**, 22 (1993).

[76] W. Press and S. Teukolsky, *Numerical Recipes in Fortran 77* (Cambridge University Press, 1986).

[77] I. Bronstein, K. Semendjajew, G. Musiol, and H. Mühlig, *Taschenbuch der Mathematik* (Verlag Harri Deutsch, Thun, Frankfurt am Main, 2000).

[78] J. Nocedal, Mathematics of Computation **35**, 773 (1980).

[79] D. Liu and J. Nocedal, Mathematical Programming B **45**, 503 (1989).

[80] Y. Dong, M. Springborg, M. Burkhart, and M. Veith, *Advances in Computational Methods in Science and Engineering* **4A**, 1010 (2005).

[81] Y. Dong, M. Burkhart, M. Veith, and M. Springborg, J. Phys. Chem. B **109**, 22820, (2005).

Structural and energetic properties of Ni–Cu bimetallic clusters

Elisaveta Kasabova,* Yi Dong,† Valeri G. Grigoryan,‡ and Michael Springborg§

Physical and Theoretical Chemistry,

University of Saarland, 66123 Saarbrücken, Germany

Abstract

The lowest-energy structures for all compositions of Ni_nCu_m bimetallic clusters with $N = n + m$ up to 20 atoms, $N = 23$, and $N = 38$ atoms have been determined using a genetic algorithm for unbiased structure optimization in combination with an embedded-atom method for the calculation of the total energy for a given structure. Comparing bimetallic clusters with homoatomic clusters of the same size, it is shown that the most stable structures for each cluster size are composed entirely of Ni atoms. Among the bimetallic clusters in the size range $N = 2 - 20$ the $Ni_{N-1}Cu_1$ clusters possess the highest stability. Further, it has been established that most of the bimetallic cluster structures have geometries similar to those of pure Ni clusters. The size $N = 38$ presents a special case, as the bimetallic clusters undergo a dramatic structural change with increasing atom fraction of Cu. Moreover, we have identified an icosahedron, a double and a triple icosahedron with one, two, and three Ni atoms at the centers, respectively, as particularly stable structures. We show that in all global-minimum structures Ni atoms tend to occupy mainly high-coordination inner sites and we confirm the segregation of Cu on the surface of Ni–Cu bimetallic clusters predicted in previous studies. Finally, it is observed that, in contrast to the bulk, the ground state structures of the 15-, 16-, and 17-atom bimetallic clusters do not experience a smooth transition between the structures of the pure copper and the pure nickel clusters as a function of the relative number of the two types of atoms. For these sizes the concentration effect on energy is more important than the geometric one.

PACS numbers: (2008) 61.46.Bc, 61.46.Df, 36.40.-c, 36.40.Mr, 68.65.-k, 61.43.Dq

* e-mail: elli@springborg.pc.uni-sb.de

† e-mail: y.dong@springborg.pc.uni-sb.de

‡ e-mail: vg.grigoryan@mx.uni-saarland.de

§ Corresponding author.e-mail:m.springborg@mx.uni-saarland.de

I. INTRODUCTION

During the last few decades, clusters have attracted considerable interest both from basic science and for applications. Their partly controllable, unique physical and chemical properties can be related to the large surface-to-volume ratio as well as to finite-size or quantum-confinement effects.[1–3] Thus, for clusters containing one type of atoms, the properties can be varied simply by varying the size of the clusters.

An additional degree of freedom for tuning the materials properties is provided by clusters containing not one but two different types of atoms. Such bimetallic clusters have received considerable attention because of their special chemical and physical properties.[4–7] A change in the concentration under the conditions of quantum-confinement effects may result in new types of structures,[8–11] including, for example, core-shell structures[12–14]. Moreover, these materials possess, for chemical applications, interesting enhanced bifunctional catalytic properties that have made them attractive candidates for various chemical applications.[15,16] Thus, considering, e.g., the case of a nickel-copper alloy, the substitution of nickel atoms by copper atoms adds extra electrons to the system. The degree to which the d band is filled can affect the catalytic activity. Thus, by varying the composition of such alloy clusters it is possible to influence the selectivity of a catalyst and improve the catalytic properties of the heteroatomic clusters compared to their monometallic counterparts. Furthermore, bimetallic clusters are also interesting candidates for use in nanoelectronics.[17,18]

In order to optimize the materials properties for a given application, it is of paramount importance to have an accurate understanding of the relation between composition/cluster size on the one side and property on the other. Although experimental studies can provide much of this information, a full characterization of the experimentally studied systems is often lacking, suggesting that additional, theoretical studies can be helpful. However, only through precise information on the structure of the lowest total energy one may be able to calculate the properties of interest. And even for clusters with only one type of atoms, it is overwhelmingly demanding to identify this structure for clusters with just around 10–20 atoms when no assumption is made on the structure.

A nanoalloy cluster distinguishes drastically from a homoatomic cluster in the number of different structures resulting by the permutation of the unlike atoms. For a one-component cluster different isomers differ by the geometrical arrangement of the atoms. For a two-

component cluster, however, different isomers may be obtained by interchanging atoms of the different types without changing the geometrical arrangement of the atoms. Jellinek and co-workers introduced in 1996 the term *homotops*[19,20] for such structures. The number of *homotops* (topological isomers) for a A_nB_m cluster, $P_{n,m}$, is given through

$$P_{n,m} = \frac{(n+m)!}{n!m!}. \tag{1}$$

If we consider all possible replacements of 10 Cu atoms by Ni atoms in an isomer of Cu_{20}, for example, the number of combinations is 184756. Because of this large number of homotops, that, in addition may have only small total-energy differences, a global optimization becomes a very demanding task.

Studies of the properties of a larger series of A_nB_m clusters have to rely on simplified descriptions of the interatomic interactions. In this case, an extra complication may show up, i.e., it is necessary to consider not only A–A and B–B interactions, but also A–B interactions, and all of those may depend indirectly on the local and global concentrations of the two types of atoms.

Most earlier theoretical studies have assumed that a structure that is particularly stable for the pure A_N and/or B_N clusters, also will be so for the A_nB_m ($n+m=N$). This is, e.g., the case for the study of Montejano-Carrizales *et al.*[21] who studied the structure and stability of Cu_nNi_m and Cu_nPd_m, $N = 55$ and 147, and in particular explored whether segregation or mixing would be found. In similar studies, Rey *et al.*[22] considered Ni_nAl_m with $N = 13$, 19, and 55, and López *et al.*[23] studied Cu_nAu_m with $N = 13$ and 14, whereby molecular-dynamics simulations were used in identifying the structures of the lowest total energy. Hsu and Lai[24] used a genetic algorithm and the basin-hopping approach in optimizing the structures of Cu_nAu_m, $N = 38$. Cheng *et al.*[25] used Monte-Carlo simulations in studying the temporal behavior of the structural properties of Cu_nAu_m, $N = 55$. Only in two studies, by Lordeiro *et al.*[8] and by Bailey *et al.*,[26] a systematic study of the structural properties of a whole class of bimetallic clusters, Cu_nAu_m with $N \leq 30$ in the first case, and Ni–Al with up to 55 atoms in the second case, has been presented. Finally, the results of a number of studies on the structural and thermodynamic properties (often with special emphasis on segregation and/or the occurrence of core-shell structures) of selected larger bimetallic clusters have been presented, too (see, e.g., [27–32]).

In this study we will concentrate on the Ni–Cu system. In the past, a long time this

system has been considered to be a classical example for a substitutional solid solution since it seemed to exhibit complete miscibility over the whole range of concentrations. However, experiments[33–35] have shown that bulk Ni–Cu alloys in fact tend to phase separate. The latest phase diagram of the bulk alloy presents a miscibility gap at a critical point of 65.6% Ni and 627.5 K.[36] To the best of our knowledge experiments on Ni–Cu clusters have not been performed so far. Furthermore there are only few theoretical studies on Ni–Cu clusters, that are neither systematic nor unbiased. Mainardi and Balbuena[37,38] have predicted the surface segregation of Cu for some Ni–Cu clusters containing 64, 125, 216, 343, 512, 729, 1000 and 8000 atoms using Monte Carlo Simulations, and hence without a fully geometry optimization. Ni–Cu clusters with $N = 55$ and 147 atoms have been studied by Montejano-Carrizales *et al.*[21] but also without a systematic determination of the lowest-energy structures, i.e. the energies of random generated structures are simply compared to each other to find the global minimum.

Derosa *et al.*[39] optimized the geometry of Ni–Cu clusters, but restricting to cluster sizes containing up to five atoms and geometries with planar configurations.

The purpose of the present work is to study systematically and unbiased both the size and the composition dependence of the total energy and the structure of a whole class of binary clusters, i.e., of Ni_nCu_m clusters with N up to 20, N=23 and N=38 atoms. The size N=23 has been chosen because of the particular stability in both cases of pure Cu and Ni clusters.[40,41]For N=38 Hsu and Lai[24] found that this specific nuclearity has the consequence of driving the Cu atoms in Cu_nAu_m clusters to change dramatically the structure of the bimetallic clusters in dependence of the Cu content.

In particular we will study whether those values of N that for the pure clusters correspond to particularly stable structures also do so for in the present case. Moreover, by using various descriptors we shall quantify to which extent the structures resemble those of the pure clusters.

Our approach is based on the embedded-atom method (EAM) for calculating the total energy of a given structure and we use a genetic algorithm in determining the structures of the lowest total energies. The paper is organized as follows. In Sec. II we briefly outline the embedded-atom method and the genetic algorithm. The main results are presented in Sec. III, and a brief summary is offered in Sec. IV.

II. COMPUTATIONAL METHOD

A. The Embedded-Atom Method

The interactions between the atoms in the bimetallic clusters are described through the EAM in the version of Daw, Baskes and Foiles (DBF).[42–44] The main idea of the EAM is to consider each atom as an impurity embedded in a host provided by the rest of the atoms. In addition, an electrostatic interaction between the atoms is included. Accordingly, the total energy (relative to that of the isolated atoms) has the following form

$$E_{\rm tot} = \sum_{i=1}^{N} [F_i(\rho_i^h) + \frac{1}{2} \sum_{j=1(j\neq i)}^{N} \phi_{ij}(r_{ij})]. \tag{2}$$

In Eq. (2), ρ_i^h is the local electron density at site i, F_i is the embedding energy required to embed an atom into this density, and ϕ_{ij} is a short-range potential between atoms i and j separated by distance r_{ij}. The local density at site i is assumed being a superposition of atomic electron densities,

$$\rho_i^h = \sum_{j=1(j\neq i)}^{N} \rho_j^a(r_{ij}), \tag{3}$$

where $\rho_j^a(r_{ij})$ is the spherically averaged atomic electron density provided by atom j at the distance r_{ij}.

The detailed analysis made in Ref. 44 have shown that the main Ansatz of the EAM, Eq. (2), also holds good in the case of the binary alloys. In accord with Ref. 44 the pair interaction between two different species (A-B/B-A heterointeraction) can be approximated by the geometric mean of the pair interaction for the individual species: $\phi_{AB}(R) = \sqrt{\phi_{AA}(R) \cdot \phi_{BB}(R)}$. Daw, Baskes and Foiles determined the embedding functions for the Ni–Cu system empirically by fitting to experimental data of bulk sublimation energy, elastic constant and the heat of solution of binary alloys.[44] The values for ρ_i^a, F_i and ϕ_{ij} are available in numerical form for Ni and Cu.[45] The validity of the embedding functions for the Ni–Cu system has been tested by computing a wide range of properties as e.g. the segregation energy of substitutional impurities to the (100) surface.[44]

The EAM has been successfully applied to many bulk and low-symmetric problems in transition metals such as defects, surface structures and surface segregation/mixing effects in alloys.[46] Furthermore, in our previous works[40,41,47–49] (those include also the discussions with the available experiments) found that this approach provides accurate information on

pure Cu_N and Ni_N clusters, which is our main reason for choosing this potential for studying Ni_nCu_m clusters.

Considering two types of atoms A (Ni) and B (Cu), we have adopted for the case of computational convenience that all the A-atoms have in Eq. (2) the numbers between 1 and N^A and the B-atoms – between $N^A + 1$ and $N = N^A + N^B$. Further there are two different cutting distances at which three different types of short-range interactions: A-A, B-B (homointeractions) and A-B/B-A (heterointeractions) vanish (s. Ref. 45): $r_{cut}^{Ni} = 4.80\,\text{Å}$ for A-A interaction and $r_{cut}^{Cu} = 4.95\,\text{Å}$ for B-B interaction. The cutting distance for the A-B/B-A heterointeractions is the minimum from these two distances or 4.80 Å. Correspondingly, the neighbour analysis in the case of bimetallic clusters is more complicated as that for monoatomic ones. For each pair of atoms i, j the following situations are possible: (i) $r_{ij} \geq r_{cut}^{Cu}$: no interactions and no contributions of electron density at sites i and j; (ii) $r_{ij} \leq r_{cut}^{Ni}$: the atoms interact with each other, i contributes electron density at site j and j – at site i; (iii) $r_{cut}^{Ni} < r_{ij} < r_{cut}^{Cu}$, i = Ni, j = Ni: as in case (i); (iv) $r_{cut}^{Ni} < r_{ij} < r_{cut}^{Cu}$, i = Cu, j = Cu: as in case (ii); (v) $r_{cut}^{Ni} < r_{ij} < r_{cut}^{Cu}$, i = Ni, j = Cu: no interactions between atoms, atom j contributes electron density at site i – contribution to the total energy [Eq. (2)] via the embedding function $F_i(\rho_i^h)$; (vi) $r_{cut}^{Ni} < r_{ij} < r_{cut}^{Cu}$, i = Cu, j = Ni: no interactions between atoms, atom i contributes electron density at site j – contribution to the total energy [Eq. (2)] via the embedding function $F_j(\rho_j^h)$.

B. The Genetic Algorithm

The global minima of the total energy of the binary clusters has been determined using the *variable metric/quasi-Newton* method in combination with a genetic algorithm.

Genetic algorithms[50,51] are optimization techniques based on the mechanisms of natural selection. Our version of the genetic algorithms has been applied to clusters with one, two, and three types of atoms, for example Au, Na, AlO and HAlO clusters,[52–55] and we have found that this optimization method is reliable when studying the structural and energetic properties of one-component as well as of multi-component clusters.

In the present study on a given Ni_nCu_m cluster, a number of randomly generated structures are optimized locally with the quasi-Newton method. The three lowest-total-energy structures are then used as the initial population. Subsequently, a new set of clusters is

constructed by cutting each of the three original ones randomly into two parts, that are interchanged and randomly rotated relative to each other, and afterwards allowed to relax. Out of the total set of six structures, the three ones with the lowest total energy are kept as the next generation. This procedure is repeated until the lowest total energy is unchanged for a large number of generations.

III. RESULTS

A. Structural Properties

Whereas macroscopic, crystalline Cu and Ni have the same crystal structures (fcc), pure copper and nickel clusters, Cu_N and Ni_N, have different structures for certain values of N. For $2 \leq N \leq 14$, $18 \leq N \leq 20$ and $N = 23$ the clusters have the same lowest-energy-minimum structures, whereas for $15 \leq N \leq 17$ they possess different ground-state structures. For instance, for N =3, 4, 5, 6 the optimized structures correspond to an equilateral triangle, a tetrahedron, a trigonal bipyramid and an octahedron, respectively, whereas for $N = 15$ a centered bicapped hexagonal antiprism (D_{6d}) is found for Cu, but a bicapped icosahedron (C_{2v}) for Ni.[40,41] Thus, an important issue is whether these structures will be recovered for the bimetallic clusters, and, for $15 \leq N \leq 17$, which (if any) of the two structures for the pure clusters will be found.

In Figs. 1 and 2 we show the global-minimum structures of monometallic and bimetallic clusters for $N = 13$ and $N = 23$ for different values of (n, m). The results are typical for most of the clusters we have examined, i.e., the geometry of the clusters is the same as found for both pure clusters. Moreover, Ni atoms (dark atoms) tend to occupy the central parts of the clusters, whereas Cu atoms are often found on the surface.

A different scenario concerning the evolution of the structure with composition is observed when looking at alloy clusters of $N = 38$ (see Fig. 3). Up to $n = 4$ the lowest-energy structure of the pure clusters, the truncated octahedron, is also found for the bimetallic clusters. But from $n = 5$ upwards there is a dramatic change to a structure with pentagonal symmetry (C_{5v}), presenting an icosahedral fragment. In this structure the nearest Ni–Ni distance is 3 % shorter than that in the octahedral structure with 4 Ni atoms. Thus, for the Ni atoms which possess the higher cohesive energy (E_{coh}^{Ni}=4.44 eV, E_{coh}^{Cu}=3.49 eV)[56] the possibility is

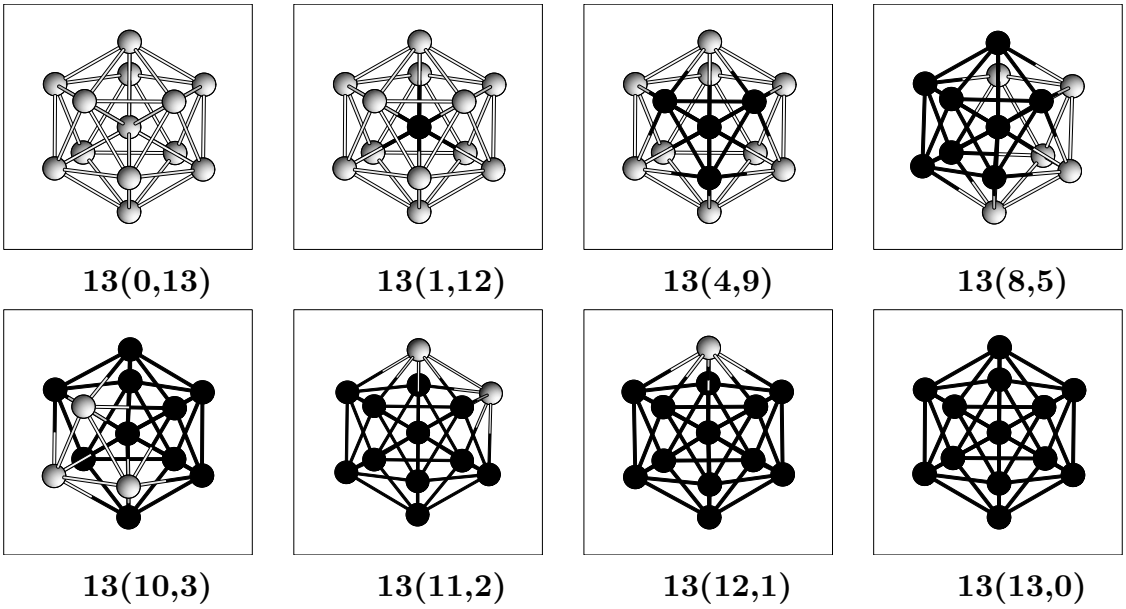

FIG. 1: The energetically lowest isomers of Ni_nCu_m clusters for a fixed value of $N = 13$. The dark atoms mark the Ni atoms.

given to form stronger bonds with the corresponding lowering of the cluster total energy. In the composition range $n = 26 - 37$ we find again the octahedral symmetry. The structural evolution with declining atom fraction of Cu described above is quite different from the structural change of the Cu_nAu_m clusters (with $n + m$=38) in a study of Hsu and Lai.[24] In the mentioned study the authors classify four categories of the lowest-energy structures: octahedral, pentagonal, hexagonal, and amorphous.

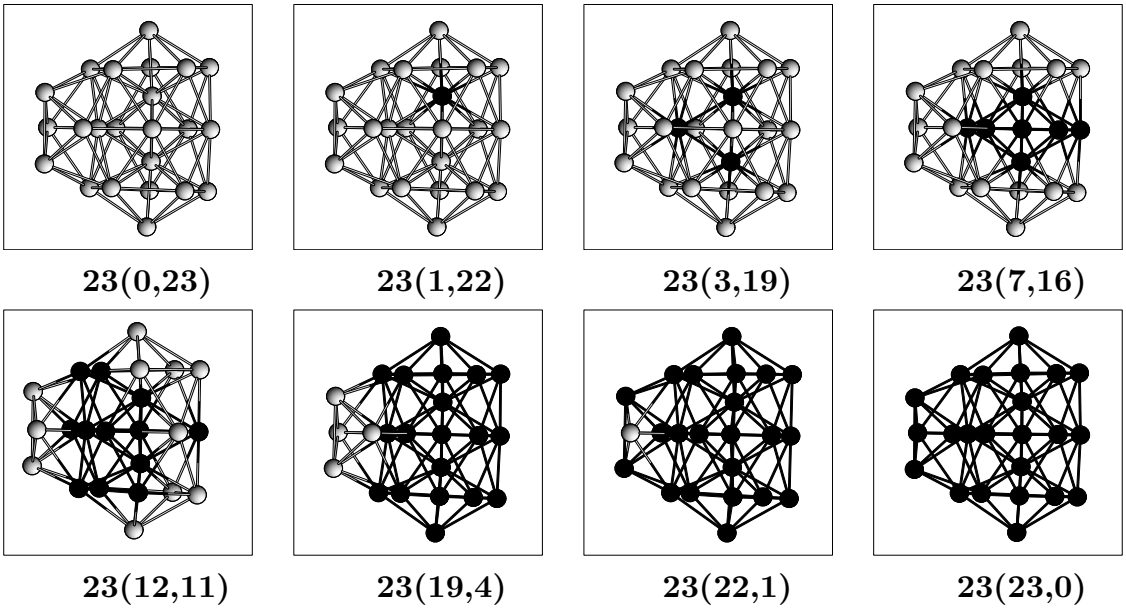

FIG. 2: The energetically lowest isomers of Ni_nCu_m clusters for a fixed value of $N = 23$.

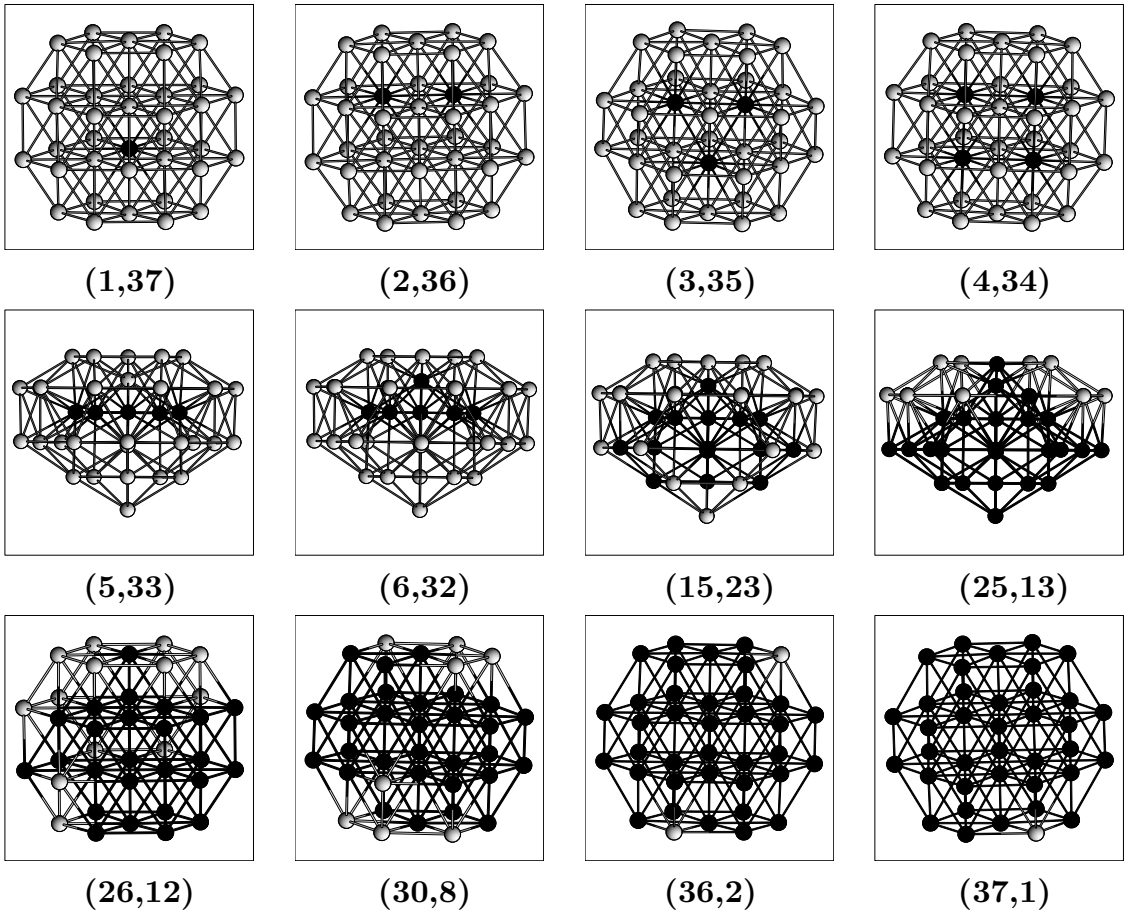

FIG. 3: The energetically lowest isomers of Ni_nCu_m clusters for a fixed value of $N = 38$.

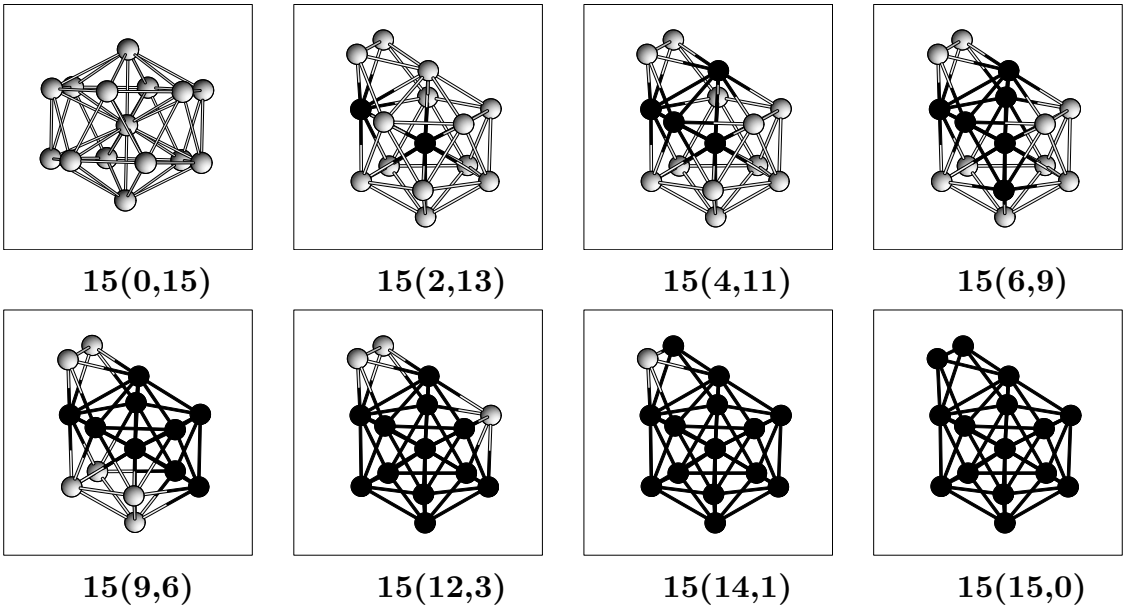

FIG. 4: The energetically lowest isomers of Ni_nCu_m clusters for a fixed value of $N = 15$.

Next we consider the case of $N = 15$ for which the pure clusters have different ground-state structures. Here, one may expect that the bimetallic clusters of this size would have Cu-like or Ni-like ground state structures for low nickel and low copper concentrations, respectively. However, as Fig. 4 shows, all structures of these Ni_nCu_m clusters with $n \neq 0$ prefer the structure of the pure Ni cluster (C_{2v}) over that of the pure Cu cluster (D_{6d}). The same trend is found for the 16-atom bimetallic clusters, which are not shown here. These two examples suggest that the structural properties of the Ni–Cu alloy clusters can not be obtained by interpolating (as a function of concentration) between the properties of the corresponding pure clusters.

In order to obtain a quantitative comparison of the structures of the bimetallic clusters

with those of the pure Cu and Ni clusters of the same sizes we use the so-called similarity functions that we have used in previous studies, too.[40,41] For each atom we define its radial distance

$$r_n = |\vec{R}_n - \vec{R}_0| \tag{4}$$

with

$$\vec{R}_0 = \frac{1}{N}\sum_{i=1}^{N}\vec{R}_i. \tag{5}$$

These are sorted in increasing order. Simultaneously, for each of the pure clusters we calculate and sort the radial distances, $\{r'_n\}$, for this, too. Subsequently, from

$$q = \left[\frac{1}{N}\sum_{n=1}^{N}(r_n - r'_n)^2\right]^{1/2}, \tag{6}$$

the similarity function is given as

$$S = \frac{1}{1 + q/u_l} \tag{7}$$

(u_l = 1 Å), which approaches 1 (0) if the A_nB_m cluster is very similar to (different from) the pure cluster. The results are shown in Fig. 5 for N = 15, 17 and 23 and in Fig. 6 for N = 38 as a function of the number of Ni atoms, n. The results for N = 23 are typical for most values of N, i.e., the structure is very similar to that of the pure clusters. The main difference can be related to the differences in Ni–Ni, Cu–Cu, and Ni–Cu bond-lengths.

Different results are found for N = 15 and N = 17. For these cluster sizes the calculated functions show a higher similarity of the bimetallic clusters to the structure of the pure Ni_N cluster than to that of the pure Cu_N cluster. For N = 17 an additional discontinuity in the similarity functions at n = 5 indicates the formation of new structures, different from those of the pure Ni and Cu clusters. The similarity function for N = 38 in Fig. 6 shows the structural change in the composition range $n = 5 - 25$, discussed for Fig. 3. Up to n = 4 and from n = 26 upwards the lowest-energy structure for the bimetallic clusters is found to be the truncated octahedron (the same as for the pure clusters). But from n = 5 to n = 25 there is a change to a structure with pentagonal symmetry C_{5v}, very different from the pure Ni and Cu clusters.

As mentioned above we found that for $9 \leq N \leq 20$ the central position of the global-minimum structures, which are icosahedral, is always occupied by a Ni atom (see for example Figs. 1 and 4). There are three possible reasons for that. First, it is well-known that there is strong internal strain in an icosahedron. Replacing the inner atom with smaller atoms

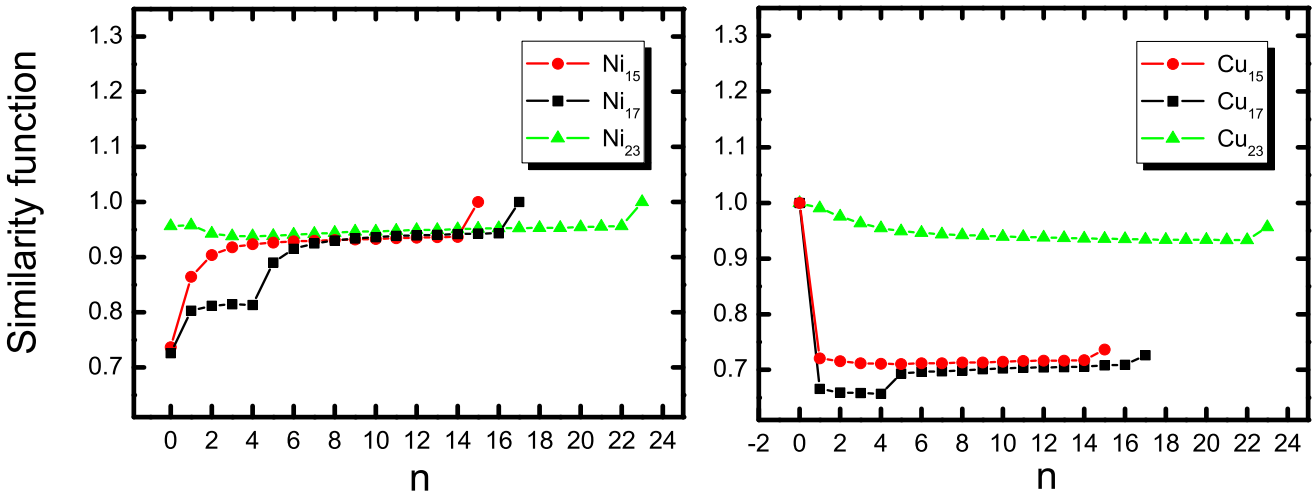

FIG. 5: The similarity function vs the number of Ni atoms n. In the left panel the structures of the bimetallic clusters of the sizes N=15, 17 and 23 are compared with those of the pure Ni_{15}, Ni_{17}, and Ni_{23} clusters, respectively. The panel to the right shows the same comparison with the corresponding pure Cu clusters.

(in our case Cu atoms with smaller Ni ones) may decrease this strain significantly. Second, Ni–Ni bonds are stronger, making structures with large Ni coordinations energetic favorable. Third, Cu possesses a smaller surface energy [$\sigma(111) = 69.5$ kJ/mol], compared with that of Ni [$\sigma(111) = 80$ kJ/mol] (see, e.g. [57]), once again suggesting that Ni atoms prefer to occupy positions with the highest coordination numbers (e.g. the center of an icosahedron).

In agreement with our findings Montejano-Carrizales *et al.*[21] explained the surface segregation of Cu by the smaller surface energy of Cu compared to Ni. Also Bailey *et al.*[26] observed a correlation between cohesive energy, surface energy and the atomic size on the one side and the structure of bimetallic Ni–Al clusters with up to 55 atoms on the other side. He found that the central site of the cluster is favoured by the Ni atom because of its smaller size, higher cohesive and higher surface energy. The results of Lordeiro *et al.*,[8] López *et al.*,[23] Hsu and Lai,[24] and Cheng *et al.*[25] on Cu–Au clusters, who observed the tendency

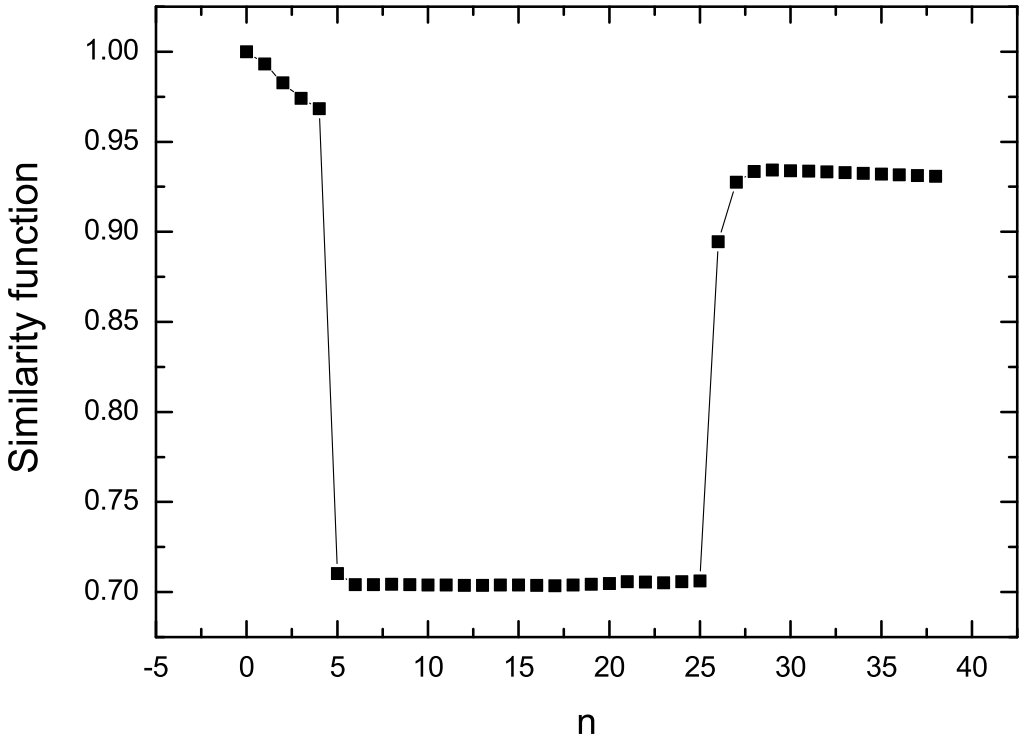

FIG. 6: The similarity function vs the number of Ni atoms n. The bimetallic clusters of the size N=38 are compared with those of the pure Cu_{38} clusters.

of the smaller atom (Cu) to occupy the central site of the icosahedron and of the larger atom (Au) to locate at surface sites are similar to our findings, too. Thus, our results are in agreement with those of the earlier studies on other systems.

On the other hand, the icosahedral structures with only one Au atom found by Lordeiro *et al.*[8] is markedly different from those with one Cu atom found by us. Whereas in all global-minimum structures determined in our study the central position of the icosahedron is always occupied by the atom with the higher surface energy and the slightly smaller size (Ni), the central atom in the work of Lordeiro *et al.*[8] can be replaced by a Au atom. Obviously, the fact that Au atoms posses a lower surface energy and larger size than Cu atoms does not necessarily drive them to locate at the surface. The crucial factor for the atomic arrangement in Cu–Au clusters is that Au–Cu bonds are stronger than Cu–Cu bonds (Au–Au>Au–Cu > Cu–Cu),[58] which drives the single Au atom to maximize the interactions with atoms of the different type. This competition between maximizing the strongest atomic interactions and minimizing the bulk strain which exists in a Cu–Au icosahedron is not to

be found in a Ni–Cu cluster, resulting in different homotops of the icosahedral structures of both cluster types.

Besides, the fact that the central atom of a Cu–Au icosahedron prefers to be surrounded by atoms of different type can be explained by the negative heats of solution[58] for solid Cu–Au alloys favoring mixing of atoms of a different type, whereas the positive heats of solution of Ni–Cu alloys leads to a segregation of copper to the surface. This segregation tendency combined with the role of the relative cohesive energies results in different structures compared to Cu–Au clusters in spite of the relative similar behavior in size and surface energy of the atoms.

In Tables I and II we list the point groups of the three energetically lowest isomers for the clusters investigated in this work. One can identify a symmetry reduction from I_h to C_{5v} when going from the first to the second isomer in the case of Ni_1Cu_{12}, whereas for $Ni_{12}Cu_1$ there is an increase in symmetry from C_{5v} to I_h. The reason is that in contrast to the first isomers of these bimetallic clusters, the second isomers have a Cu atom and not a Ni atom at the center. The energy difference between the first and the second isomers for these clusters is rather large, i.e., 0.51 eV for Ni_1Cu_{12} and 0.62 eV for $Ni_{12}Cu_1$. Thus, also this finding demonstrates that when Ni atom is occupying the center a strong stabilization of the icosahedral structure results.

When comparing with the energy difference between the first and the second isomers of the pure copper (1.06 eV) and the pure nickel (1.16 eV) cluster, the energy differences mentioned above are smaller. The reason is that for bimetallic clusters these isomers are homotops and the existence of homotops leads to a much richer total-energy surface.

B. Energetic Properties

Next we shall turn our attention to the energetic properties and stability of the Ni–Cu bimetallic clusters as a function of cluster size and composition. In Fig. 7 we show the binding energy per atom

$$E_{n,m} = -E_{\rm tot}(n,m)/N \tag{8}$$

as a function of cluster size for $n = 1 - 16$. Here, $E_{\rm tot}(n,m)$ is the total energy of the energetically lowest Ni_nCu_m cluster.

A kink at $N = 13$ and a smaller one at $N = 19$ indicates a stabilization of the structures at

TABLE I: Point groups of the first three isomers.

N	n,m	I	II	III	N	n,m	I	II	III	N	n,m	I	II	III	N	n,m	I	II	III
2	0,2	$D_{\infty h}$			8	7,1	C_s	C_s	C_s	12	5,7	C_s	C_s	C_s	15	3,12	C_{2v}	C_1	C_s
2	1,1	$C_{\infty h}$			8	8,0	D_{2d}	C_s	D_{3d}	12	6,6	C_s	C_{5v}	C_1	15	4,11	C_s	C_s	C_1
2	2,0	$D_{\infty h}$			9	0,9	C_{2v}	D_{3h}	C_{2v}	12	7,5	C_{5v}	C_1	C_s	15	5,10	C_{2v}	C_1	C_s
3	0,3	D_{3h}			9	1,8	C_{2v}	C_s	C_s	12	8,4	C_s	C_1	C_s	15	6,9	C_s	C_1	C_s
3	1,2	C_{2v}			9	2,7	C_s	C_s	C_1	12	9,3	C_s	C_s	C_s	15	7,8	C_1	C_s	C_1
3	2,1	C_{2v}			9	3,6	C_{2v}	C_1	C_1	12	10,2	C_s	C_s	C_s	15	8,7	C_1	C_s	C_s
3	3,0	D_{3h}			9	4,5	C_s	C_1	C_1	12	11,1	C_s	C_{5v}	C_s	15	9,6	C_1	C_{2v}	C_1
4	0,4	T_d			9	5,4	C_{2v}	C_1	C_s	12	12,0	C_{5v}	C_1	D_{3h}	15	10,5	C_s	C_1	C_s
4	1,3	C_s			9	6,3	C_1	C_s	C_1	13	0,13	I_h	C_s	C_s	15	11,4	C_s	C_2	C_1
4	2,2	C_{2v}			9	7,2	C_s	C_2	C_s	13	1,12	I_h	C_{5v}	C_s	15	12,3	C_1	C_s	C_s
4	3,1	C_{3v}			9	8,1	C_1	C_s	C_s	13	2,11	C_{5v}	D_2	C_{2v}	15	13,2	C_{2v}	C_1	C_1
4	4,0	T_d			9	9,0	C_{2v}	D_{3h}	C_{2v}	13	3,10	C_{2v}	D_{6d}	C_{2v}	15	14,1	C_s	C_1	C_s
5	0,5	D_{3h}			10	0,10	C_{3v}	D_{2h}	C_2	13	4,9	C_{3v}	C_s	C_s	15	15,0	C_{2v}	D_{6d}	C_{2v}
5	1,4	C_{2v}	C_{3v}		10	1,9	C_{3v}	C_s	C_s	13	5,8	C_{2v}	C_s	C_2	16	0,16	D_{3h}	C_s	C_s
5	2,3	C_{2v}	C_s	D_{3h}	10	2,8	C_s	C_s	C_s	13	6,7	C_s	C_s	C_1	16	1,15	C_s	C_s	D_{3h}
5	3,2	D_{3h}	C_s	C_{2v}	10	3,7	C_s	C_1	C_s	13	7,6	C_{5v}	C_2	C_{3v}	16	2,14	C_s	C_1	C_1
5	4,1	C_{3v}	C_{2v}		10	4,6	C_{3v}	C_s	C_1	13	8,5	C_s	C_s	C_s	16	3,13	C_1	C_1	C_s
5	5,0	D_{3h}			10	5,5	C_s	C_s	C_1	13	9,4	C_{2v}	C_s	C_s	16	4,12	C_1	C_1	C_1
6	0,6	O_h	C_{2v}	C_{2v}	10	6,4	C_s	C_1	C_s	13	10,3	C_{3v}	C_s	C_s	16	5,11	C_1	C_s	C_s
6	1,5	C_{4v}	C_s	C_s	10	7,3	C_{3v}	C_s	C_1	13	11,2	C_{2v}	C_{2v}	D_{5d}	16	6,10	C_1	C_1	C_1
6	2,4	C_{2v}	D_{4h}	C_{2v}	10	8,2	C_s	C_1	C_s	13	12,1	C_{5v}	I_h	C_s	16	7,9	C_1	C_1	C_s
6	3,3	C_{3v}	C_{2v}	C_s	10	9,1	C_s	C_s	C_s	13	13,0	I_h	C_s	C_s	16	8,8	C_1	C_1	C_s
6	4,2	C_{2v}	C_{2v}	D_{4h}	10	10,0	C_{3v}	D_{2h}	C_2	14	0,14	C_{3v}	C_{2v}	C_{6v}	16	9,7	C_1	C_s	C_1
6	5,1	C_{4v}	C_s	C_s	11	0,11	C_{2v}	C_2	C_{2v}	14	1,13	C_{3v}	C_{2v}	C_s	16	10,6	C_1	C_s	C_1
6	6,0	O_h	C_{2v}	C_{2v}	11	1,10	C_{2v}	C_s	C_{3v}	14	2,12	C_s	C_s	C_s	16	11,5	C_s	C_s	C_1
7	0,7	D_{5h}	C_{3v}	C_2	11	2,9	C_s	C_s	C_1	14	3,11	C_s	C_s	C_s	16	12,4	C_s	C_1	C_1
7	1,6	C_{5v}	C_{2v}	C_s	11	3,8	C_{2v}	C_1	C_{2v}	14	4,10	C_{3v}	C_s	C_1	16	13,3	C_1	C_1	C_1
7	2,5	D_{5h}	C_s	C_{2v}	11	4,7	C_s	C_s	C_1	14	5,9	C_s	C_s	C_s	16	14,2	C_s	C_1	C_1
7	3,4	C_{2v}	C_s	C_s	11	5,6	C_{2v}	C_1	C_1	14	6,8	C_1	C_s	C_1	16	15,1	C_1	C_s	C_s
7	4,3	C_{2v}	C_{2v}	C_s	11	6,5	C_1	C_s	C_s	14	7,7	C_1	C_s	C_s	16	16,0	C_s	C_s	C_2
7	5,2	C_{2v}	C_{2v}	C_s	11	7,4	C_s	C_2	C_s	14	8,6	C_s	C_1	C_1	17	0,17	T_d	C_2	C_2
7	6,1	C_{2v}	C_{5v}	C_{3v}	11	8,3	C_1	C_1	C_1	14	9,5	C_s	C_1	C_1	17	1,16	C_s	C_2	C_s
7	7,0	D_{5h}	C_{3v}	C_2	11	9,2	C_{2v}	C_1	C_s	14	10,4	C_s	C_1	C_1	17	2,15	C_s	C_s	C_1
8	0,8	D_{2d}	C_s	D_{3d}	11	10,1	C_s	C_1	C_s	14	11,3	C_1	C_s	C_s	17	3,14	C_1	C_s	C_2
8	1,7	C_s	C_s	C_s	11	11,0	C_{2v}	C_2	C_{2v}	14	12,2	C_s	C_s	C_s	17	4,13	C_s	C_1	C_s
8	2,6	C_{2v}	C_2	C_s	12	0,12	C_{5v}	C_1	D_{3h}	14	13,1	C_{3v}	C_s	C_s	17	5,12	C_2	C_s	C_s
8	3,5	C_s	C_s	C_s	12	1,11	C_{5v}	C_s	C_{5v}	14	14,0	C_{3v}	C_{2v}	C_1	17	6,11	C_1	C_1	C_1
8	4,4	D_{2d}	C_1	C_s	12	2,10	C_s	C_{5v}	C_s	15	0,15	D_{6d}	C_{2v}	D_2	17	7,10	C_2	C_1	C_1
8	5,3	C_s	C_s	C_1	12	3,9	C_s	C_s	C_s	15	1,14	C_{2v}	D_{6d}	C_s	17	8,9	C_1	C_1	C_1
8	6,2	C_{2v}	C_2	C_s	12	4,8	C_s	C_s	C_s	15	2,13	C_s	C_s	C_s	17	9,8	C_1	C_2	C_1

TABLE II: Point groups of the first three isomers.

N	n,m	I	II	III	N	n,m	I	II	III	N	n,m	I	II	III	N	n,m	I	II	III
17	10,7	C_1	C_1	C_1	19	13,6	C_{5v}	C_s	C_1	23	12,11	C_1	C_1	C_1	38	28,10	C_1	C_1	C_1
17	11,6	C_2	C_1	C_1	19	14,5	C_s	C_1	C_1	23	13,10	C_1	C_1	C_1	38	29,9	C_1	C_1	C_1
17	12,5	C_1	C_1	C_1	19	15,4	C_s	C_2	C_2	23	14,9	C_s	C_s	C_1	38	30,8	C_1	C_1	C_1
17	13,4	C_2	C_2	C_s	19	16,3	C_s	C_s	C_s	23	15,8	C_1	C_1	C_1	38	31,7	C_1	C_1	C_1
17	14,3	C_1	C_{3v}	C_1	19	17,2	C_s	C_2	C_{2v}	23	16,7	C_1	C_1	C_1	38	32,6	C_s	C_1	C_1
17	15,2	C_2	C_1	C_1	19	18,1	C_s	C_{5v}	C_{2v}	23	17,6	C_s	C_s	C_1	38	33,5	C_1	C_1	C_1
17	16,1	C_1	C_s	C_1	19	19,0	D_{5h}	C_1	C_s	23	18,5	C_1	C_1	C_1	38	34,4	C_2	C_1	C_1
17	17,0	C_2	C_s	C_s	20	0,20	C_{2v}	D_{3d}	D_2	23	19,4	C_{2v}	C_1	C_1	38	35,3	C_1	C_1	C_1
18	0,18	C_s	C_{5v}	C_{2v}	20	1,19	C_s	C_{3v}	C_2	23	20,3	C_s	C_1	C_1	38	36,2	D_2	C_1	C_s
18	1,17	C_s	C_s	C_s	20	2,18	C_{2v}	D_{3d}	D_2	23	21,2	C_1	C_{2v}	C_s	38	37,1	C_s	C_s	C_1
18	2,16	C_s	C_{5v}	C_1	20	3,17	C_s	C_{2v}	C_s	23	22,1	C_s	C_s	C_1	38	38,0	O_h	C_{5v}	C_{5v}
18	3,15	C_1	C_1	C_1	20	4,16	C_{2v}	C_s	C_s	23	23,0	D_{3h}	D_{3h}	D_2					
18	4,14	C_1	C_s	C_s	20	5,15	C_s	C_{2v}	C_s	38	0,38	O_h	C_5	C_5					
18	5,13	C_s	C_s	C_1	20	6,14	C_s	C_{2v}	C_1	38	1,37	C_{4v}	C_1	C_5					
18	6,12	C_1	C_s	C_s	20	7,13	C_{2v}	C_s	C_s	38	2,36	C_{2v}	C_1	C_1					
18	7,11	C_s	C_1	C_s	20	8,12	C_s	C_s	C_2	38	3,35	C_{3v}	D_2	C_1					
18	8,10	C_1	C_1	C_1	20	9,11	C_{2v}	C_1	C_1	38	4,34	D_{4h}	C_1	C_1					
18	9,9	C_s	C_s	C_s	20	10,10	C_1	C_1	C_s	38	5,33	C_{5v}	C_1	C_1					
18	10,8	C_s	C_s	C_s	20	11,9	C_1	C_s	C_2	38	6,32	C_{5v}	C_5	C_5					
18	11,7	C_s	C_s	C_s	20	12,8	C_1	C_1	C_s	38	7,31	C_{5v}	C_1	C_3					
18	12,6	C_1	C_s	C_1	20	13,7	C_1	C_1	C_1	38	8,30	C_s	C_3	C_1					
18	13,5	C_s	C_1	C_1	20	14,6	C_1	C_1	C_1	38	9,29	C_s	C_s	C_s					
18	14,4	C_s	C_1	C_1	20	15,5	C_1	C_1	C_1	38	10,28	C_s	C_1	C_s					
18	15,3	C_s	C_s	C_1	20	16,4	C_1	C_s	C_1	38	11,27	C_s	C_1	C_1					
18	16,2	C_s	C_1	C_1	20	17,3	C_2	C_s	C_1	38	12,26	C_{5v}	C_1	C_1					
18	17,1	C_1	C_s	C_1	20	18,2	C_1	C_1	C_s	38	13,25	C_s	C_1	C_1					
18	18,0	C_s	C_{5v}	C_s	20	19,1	D_2	C_1	C_1	38	14,24	C_s	C_s	C_s					
19	0,19	D_{5h}	C_1	C_1	20	20,0	C_{2v}	D_{3d}	D_2	38	15,23	C_s	C_1	C_1					
19	1,18	C_{5v}	C_{2v}	C_{5v}	23	0,23	D_{3h}	D_2	D_{3h}	38	16,22	C_s	C_s	C_1					
19	2,17	D_{5h}	C_s	C_{5v}	23	1,22	C_{2v}	C_{3v}	C_1	38	17,21	C_{5v}	C_1	C_1					
19	3,16	C_{2v}	C_{5v}	C_s	23	2,21	C_{2v}	C_1	C_s	38	18,20	C_s	C_1	C_1					
19	4,15	C_{2v}	C_{2v}	C_s	23	3,20	D_{3h}	C_s	C_s	38	19,19	C_s	C_1	C_1					
19	5,14	C_{2v}	C_{2v}	C_s	23	4,19	C_{3v}	C_s	C_{2v}	38	20,18	C_s	C_1	C_1					
19	6,13	C_{2v}	C_1	C_1	23	5,18	C_s	C_s	C_{2v}	38	21,17	C_1	C_1	C_1					
19	7,12	D_{5h}	C_1	C_s	23	6,17	C_s	C_s	C_s	38	22,16	C_{5v}	C_1	C_1					
19	8,11	C_s	C_1	C_2	23	7,16	C_{2v}	C_2	C_1	38	23,15	C_{5v}	C_s	C_1					
19	9,10	C_s	C_2	C_2	23	8,15	C_1	C_s	C_1	38	24,14	C_1	C_1	C_1					
19	10,9	C_s	C_s	C_s	23	9,14	C_2	C_1	C_1	38	25,13	C_1	C_1	C_1					
19	11,8	C_s	C_2	C_2	23	10,13	C_s	C_1	C_1	38	26,12	C_1	C_1	C_1					
19	12,7	C_s	C_1	C_1	23	11,12	C_1	C_1	C_1	38	27,11	C_1	C_1	C_1					

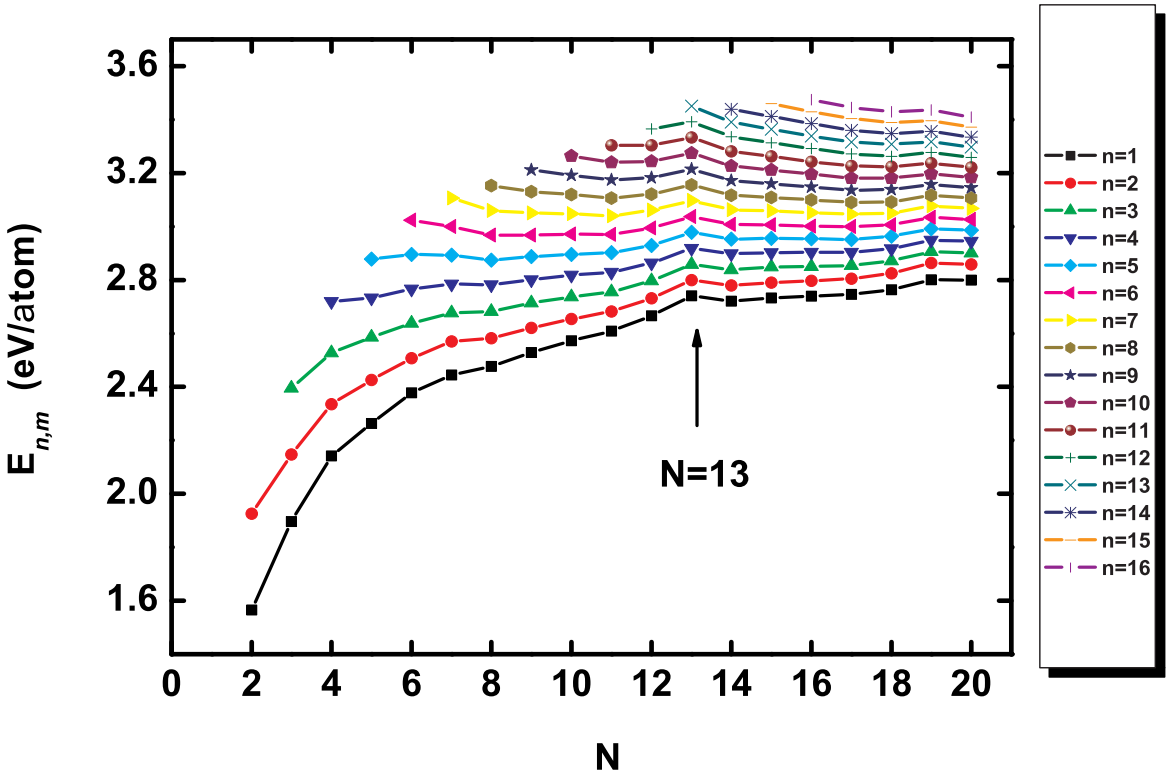

FIG. 7: The binding energy per atom as a function of cluster size for different number of Ni atoms n.

these cluster sizes for all Ni concentrations due to the icosahedral geometry. Thus, structures that are particularly stable for the monatomic clusters due to geometric effects, may also be so for bimetallic clusters. Another relevant observation is that for $N = 15$, 16 and 17 the binding energy increases for clusters containing up to $n = 4$ Ni atoms and decreases for clusters containing $n = 6$ Ni atoms upwards. The same result, namely that the concentration effect on the binding energy is more important than the geometrical one is also found for $N = 10$ and $N = 11$. Further we could find the nonmonotonic dependence of the binding energy $E_{n,m}$ with increasing N in the range $n \leq N \leq 13$ for $n = 4 - 10$. Those regions are

especially pronounced for $n = 6,\ 7$ and 8 (see Fig. 7). Next we use

$$E_{\rm stab}(n,m) = E_{\rm tot}(n+1,m-1) + E_{\rm tot}(n-1,m+1) - 2E_{\rm tot}(n,m) \tag{9}$$

to check the relative stability of a cluster compared to clusters of the same size containing one more and one less Ni atom. As a function of n for given N $E_{\rm stab}$ has peaks at particularly stable clusters, so-called *magic* clusters. We notice that if the substitution of a Ni atom by a Cu atom was accompanied by a concentration- and size-independent total-energy difference, $E_{\rm stab}$ would vanish.

In Fig. 8 we show this function together with the binding energy, for four different values of N, i.e., N=13, 19, 23 and 38. We observe that the pure Ni clusters possess the most stable structures (if compared to bimetallic clusters of the same size) for all investigated cluster sizes. Further, among the bimetallic Ni–Cu clusters the $Ni_{N-1}Cu_1$ clusters have the lowest total energy and hence are the most stable ones in the size range N=2-20. This is not surprising as the binding energy is expected to increase with Ni content due to its higher cohesion.

The plots show special features, i.e., a kink in the binding energy function and a maximum in the stability function $E_{\rm stab}(n,m)$, for n=1, 2, 3 and 7. The corresponding *magic* clusters for a larger set of values of N are presented in Fig. 9. The maximum in the stability function at n=1 for N=13 refers to the icosahedron with only one Ni atom at the center whereas for $n = 2$ and $N = 19$ the double icosahedron with two Ni atoms centered in each icosahedron is found. These two structures turn out to be especially stable because they are obtained both from the size dependence of the binding energy as well as from the concentration dependence of the stability function (see also Figs. 8). In our study the magic cluster for the size N=38 refers to the structure with Ni atoms forming a pentagonal bipyramid in the cluster core. For comparison we want to mention that in a study of Hsu and Lai[24] of Cu–Au clusters the peak in the stability function for $N = 38$ is found to be at $n = 6$. In the corresponding *magic* cluster the Cu atoms form a plane hexagon at the center of the cluster.

Further, Fig. 9 shows that all of the *magic* clusters in the size range $10 \leq N \leq 20$ have icosahedron-based structures with a Ni atom at the center of each icosahedron. The magic cluster for $N = 23$ is a triple icosahedron and it shows a perfect core-shell structure. The Ni atoms centered in each icosahedron form the core while the copper atoms, which possess the lower surface energy, form the shell of the cluster. That there is a tendency towards

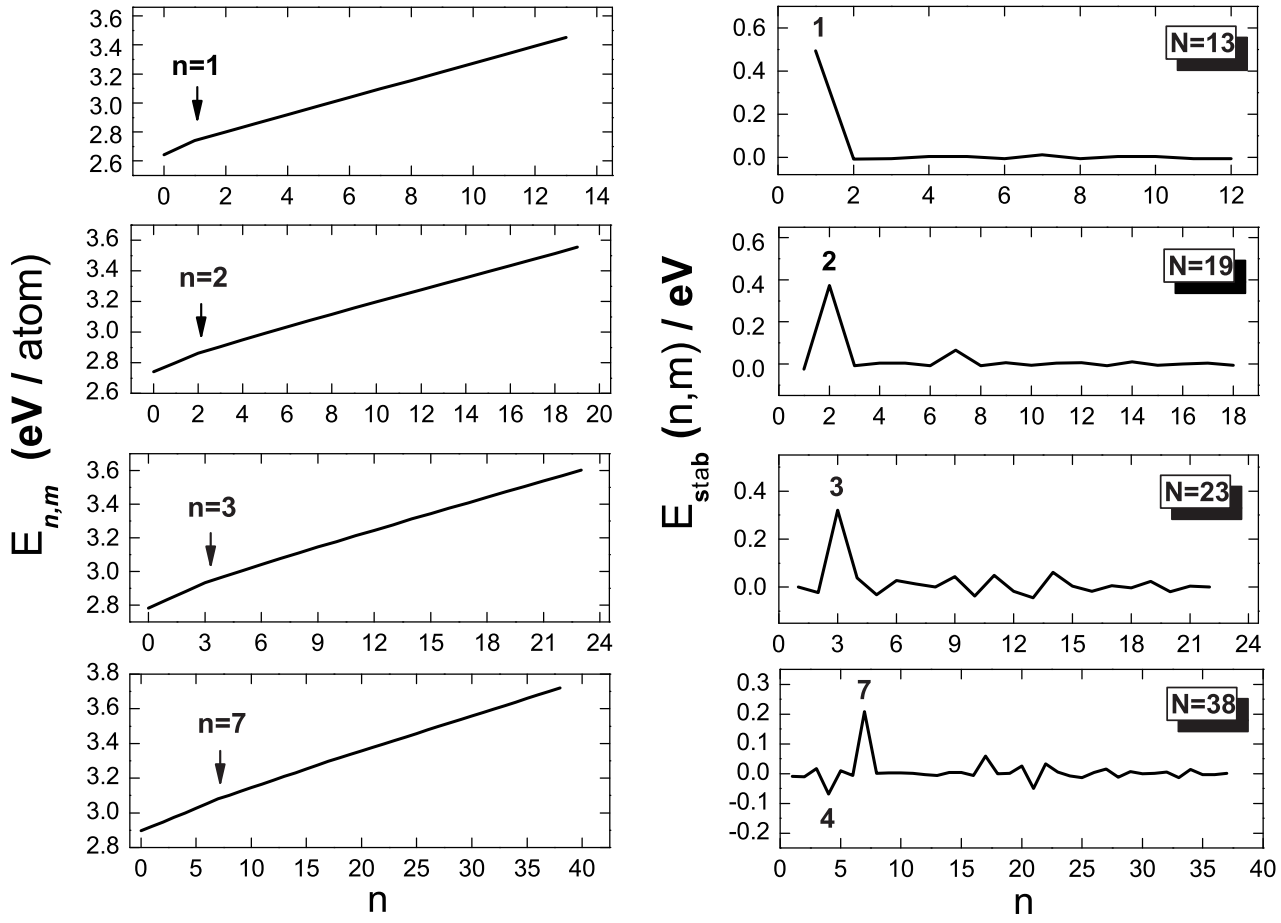

FIG. 8: The left panels show the binding energy per atom and the right panels the stability energy $E_{\rm stab}(n,m)$ as a function of n for $N = n + m$ being 13 (top panels), 19 and 23 (middle panels), and 38 (bottom panels).

the formation of core-shell structures can be further demonstrated by plotting the radial distances of the Ni and Cu atoms separately. This is done in Fig. 10 for N=23. For a small concentration of nickel (until $n = 3$), the Ni atoms prefer to occupy the inner positions, whereas with increasing concentration of nickel, they have to occupy positions further away from the center, but first for $n = 11$ also surface positions are occupied by Ni. The Cu atoms display the opposite behavior: for a small copper concentration they are located to the surface region and with increasing concentration of Cu, also the inner positions of the

cluster are occupied.

The quantity

$$E_{\mathrm{subst}}(n,m) = E_{\mathrm{tot}}(n-1,m+1) - E_{\mathrm{tot}}(n,m) \tag{10}$$

describes the relative stability of a cluster with n Ni atoms with respect to clusters with one less Ni and one more Cu atom. Thus, the function represents the energy gain (or loss) when a Cu atom is replaced by a Ni atom. In Fig. 11 this function is presented in dependence of the number of n for different cluster sizes, $N = n + m$. For $n = 1$ and N up to 8 the function has relatively low values because the pure Cu clusters of these sizes do not form strained icosahedral structures which can be stabilized by the replacement of a centered Cu atom by a smaller Ni atom. From $N = 9$ upwards the stabilization effect begins to increase corresponding to the icosahedral growth of the clusters (cf. Fig. 9). In agreement with the discussion above, the most pronounced peak is found for $N = 13$ and $n = 1$, describing the strong tendency of a Ni atom to replace one Cu atom in the center of the icosahedron. The peaks for the other two magic clusters at $n = 2$ for $N = 19$ and at $n = 3$ for $N = 23$ posses slightly lower values. Obviously a replacement of a Cu atom centered in the second icosahedron of a double icosahedron leads to a lower stabilization of the structure compared to the replacement of a Cu atom centered in a single icosahedron. The reason is that by the replacement of the Cu atom by the smaller Ni atom in the center of the first icosahedron a major part of the strain is released. Thus when the second Ni atom is added it will occupy a position at the center of a less strained icosahedron.

Another criterion that we use for comparing the relative stability of alloy clusters of the same size but with a different composition is the change in cluster binding energy on mixing defined by[59]

$$\Delta E_{\mathrm{mix}} = E_{\mathrm{n,m}}^{Ni-Cu} - \frac{m}{N} E_{\mathrm{N}}^{Cu} - \frac{n}{N} E_{\mathrm{N}}^{Ni} \tag{11}$$

where $E_{\mathrm{n,m}}^{Ni-Cu}$ is the binding energy of the alloy cluster containing n Ni atoms, m the number of the Cu atoms in the cluster and E_{N}^{Cu} (E_{N}^{Ni}) is the cohesive energy of the pure $\mathrm{Cu_N}$ ($\mathrm{Ni_N}$) cluster. The function represents the energy gain (or loss) for a mixed cluster with respect to pure clusters of the same size. Here we want to emphisize that in our study positive values for the mixing energies refer to exothermic process. Thus, a positive value of ΔE_{mix} corresponds to a nanoalloy cluster which is thermodynamically stable with

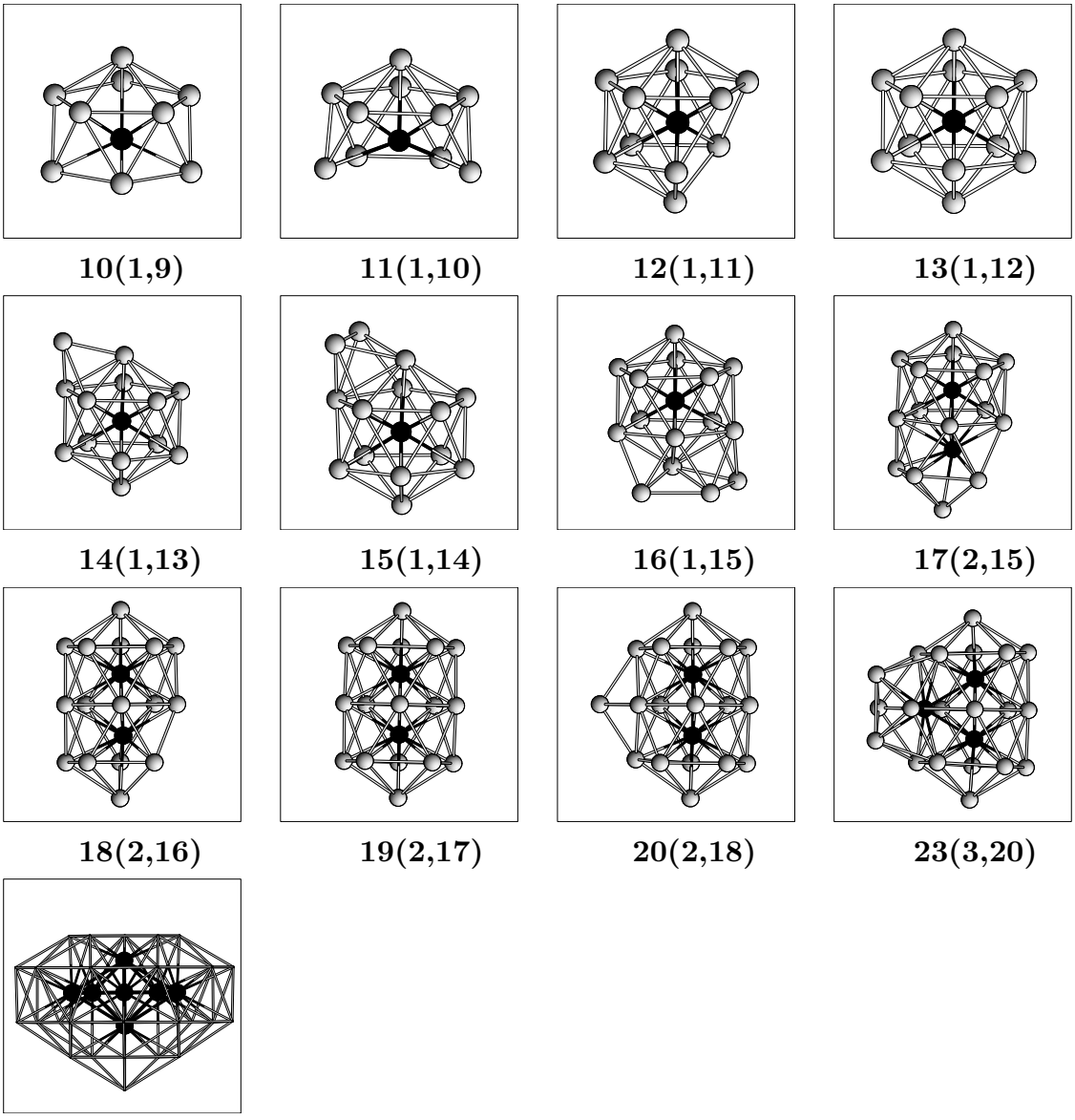

FIG. 9: The structures of the magic Ni_nCu_m clusters for $10 \leq N \leq 20$, $N = 23$ and $N = 38$ atoms. The labels are given as $N(n, m)$ with N being the total number of atoms, n the number of Ni atoms, and m the number of Cu atoms.

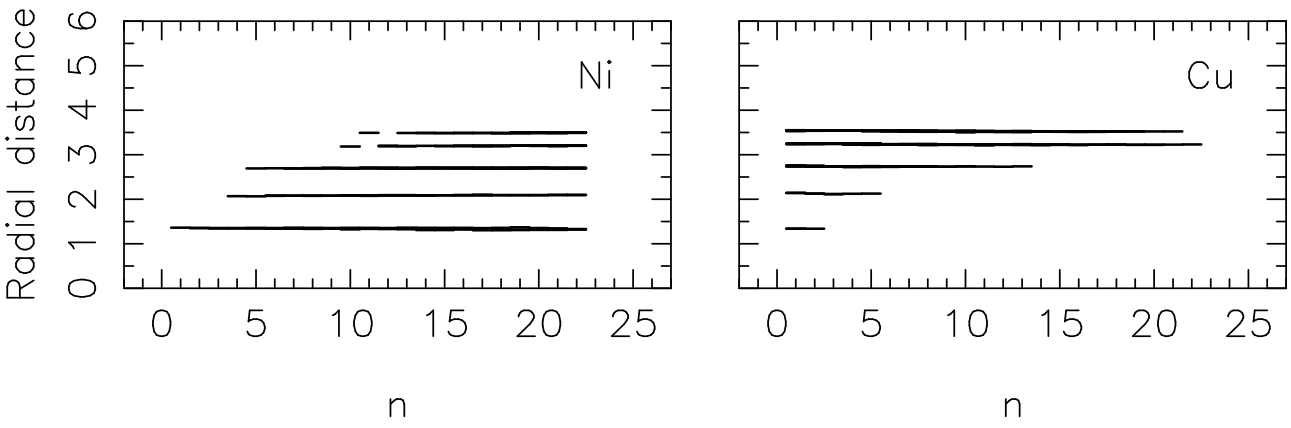

FIG. 10: The radial distances (in Å) for Ni and Cu atoms, separately, as a function of the number of Ni atoms, n. In each panel a small horizontal line shows that at least one atom of the corresponding type has that distance to the center of the cluster for a given value of $N = 23$.

respect to corresponding pure elemental clusters. The energies of mixing of the energetically lowest isomers for each composition are shown in Fig. 12 for the nuclearities $N = 13$, 19, 23 and 38. The mixing energy for all bimetallic clusters investigated here is found to be positive, corresponding to energy-favoured mixing. These results are not consistent with the endothermic experimental enthalpie of mixing in solid Ni–Cu alloys[58] which favours ensembles with neighbours of the same type. We deduce: in contrast to bulk Ni–Cu alloys the formation of Ni–Cu nanoalloy clusters is energetically favoured.

It is also interesting to obsreve that for $N = 19$ and 38 there is well defined composition range: from $n = 2$ to 7 and from $n = 7$ to 17 (with a maximum value at $n = 9$) where the structures possess a remarkable stability. This result suggests that beside the perfect core-shell structures with all Cu atoms on the surface and all Ni atoms inside, there is a range of very stable bimetallic structures with Ni atoms occupying both the core and the surface. For $N = 23$ this range begins from $n = 3$ and it is less pronounced, whereas for $N = 13$ there is only one structure at $n = 1$ with special stability relative to the corresponding pure clusters.

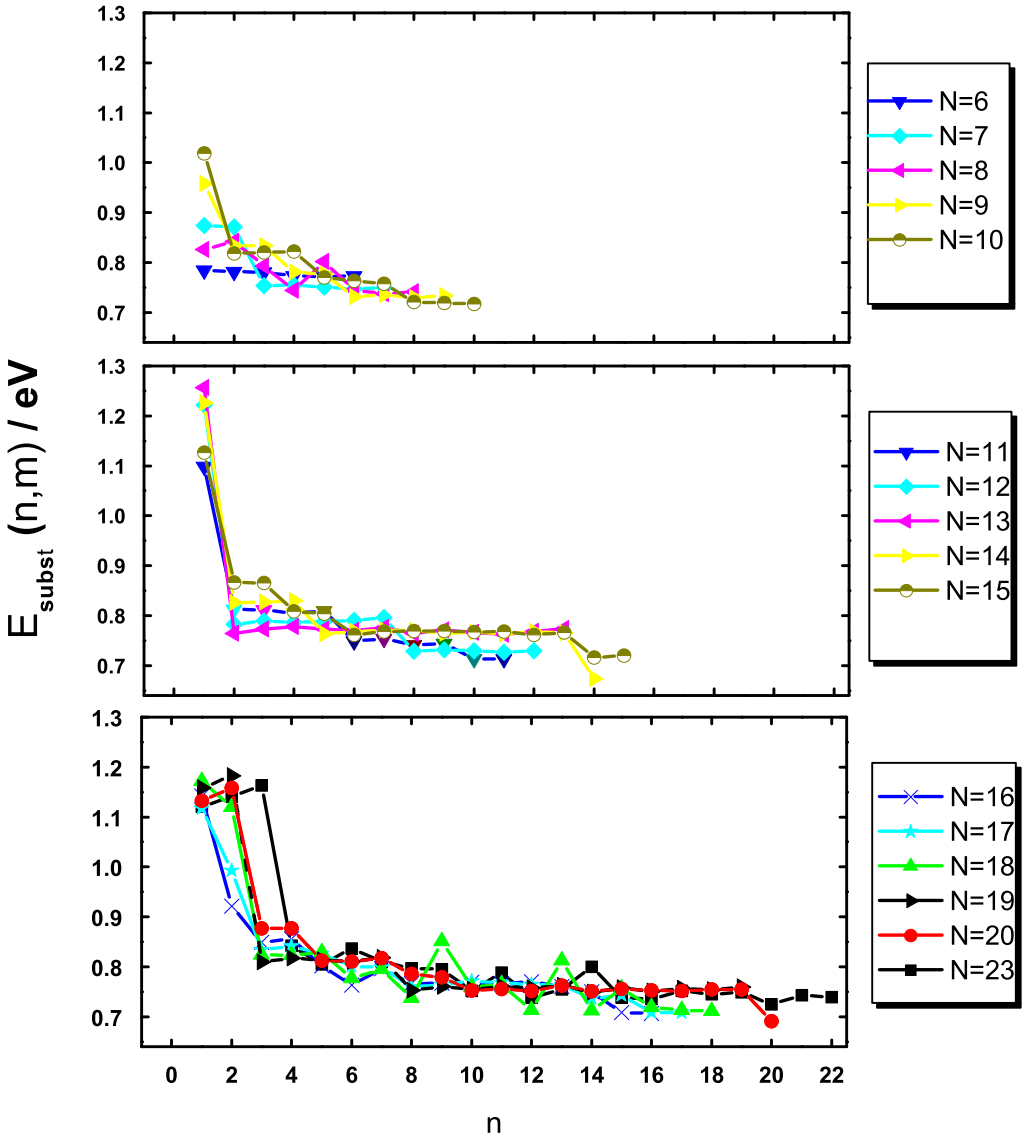

FIG. 11: The total-energy difference between a cluster with n Ni atoms and a cluster with one less Ni atom and one more Cu atom as a function of n for different cluster sizes N.

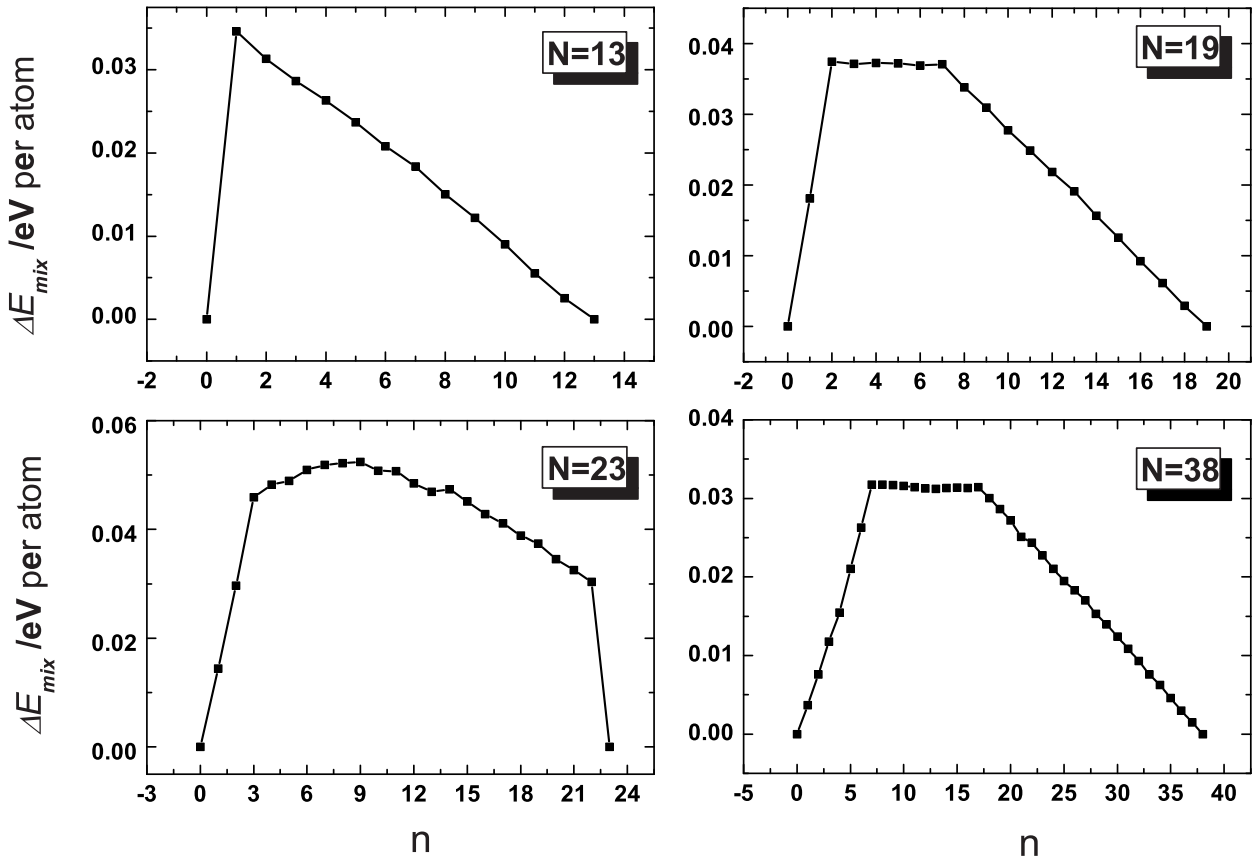

FIG. 12: $\Delta E_{\rm mix}$ as a function of n for $N = 13$, 19, 23 and 38.

To sum up, our calculations on small Ni–Cu clusters confirm the tendency for segregation of Cu to the surface, predicted by experiments[33–35] and theoretical[60,61] calculations for Ni–Cu macroscopic alloys as well as by Monte Carlo Simulations[37,38] for larger Ni–Cu clusters (64-8000 atoms). This effect is explained by the difference in the cohesive and surface energies of Cu and Ni, by the bond enthalpy of the Ni–Cu bond, which is smaller than the average of those of Ni–Ni and Cu–Cu bonds[58] and by the positive heats of mixing of solid Ni–Cu alloys.[58]

IV. CONCLUSIONS

In this work we have studied the structural and energetic properties of Ni_nCu_m bimetallic clusters with $N = n+m$ up to 20 atoms and additionally for $N = 23$ and 38 atoms. We have investigated systematically and unbiased both the size and the composition dependence of the total energy and the structure of the clusters. The total energy of the bimetallic clusters was computed with the embedded-atom method in the version of Daw, Baskes and Foiles. The global geometry optimization was performed using a genetic algorithm.

We have determined the lowest-energy structures as well as the *magic* clusters for all considered cluster sizes and concentrations of the components. It is demonstrated that all Ni–Cu clusters investigated in this work are energetically stable. Comparing bimetallic clusters with homoatomic clusters of the same size, we found that the most stable clusters for each cluster size are those composed of Ni atoms, due to their higher cohesive energy. Among the bimetallic clusters in the size range $N = 2 - 20$ the $Ni_{N-1}Cu_1$ clusters possess the highest stability.

Furthermore, our results show that an icosahedron, a double icosahedron, and a triple icosahedron with one, two, and three Ni atoms, respectively, are especially stable (*magic*). Thus, structures that for the pure clusters are particularly stable are also so for the bimetallic clusters. In addition, it is found that for all global-minimum structures of the Ni–Cu bimetallic clusters Ni atoms occupy mainly high-coordination inner (core) sites. In contrast, Cu atoms show a tendency to occupy lower-coordination sites on the cluster surface.

Moreover, we found that most of the bimetallic cluster structures have geometries similar to those of pure Ni clusters. The size $N = 38$ presents a special case: from $n = 5$ upwards the bimetallic clusters undergo a dramatic structural change from the truncated octahedron

to a structure with pentagonal symmetry and return at $n = 25$ again to the octahedral symmetry.

Finally, in contrast to the bulk, the ground state structures of Ni_nCu_{15-n}, Ni_nCu_{16-n}, and Ni_nCu_{17-n} clusters do not experience a smooth transition between the structures of pure copper and pure nickel clusters as the number of Ni atoms changes. For these sizes the concentration effect on energy turned out to be more important than the geometric one.

Acknowledgments

This work was supported by the DFG through the project Sp 439/24-1.

---

[1] W. H. Qi, M. P. Wang, J. Mater. Sci. Lett. **21**, 1743 (2002).

[2] F. Balleto, R. Ferrando, Rev. Mod. Phys. **77**, 371 (2005).

[3] B. Balamurugan, T. Maruyama, Appl. Phys. Lett. **87**, 143105 (2005).

[4] M. Gaudry, E. Cottancin, M. Pellarin, J. Lerme, L. Arnaud, J. R. Huntzinger, J. L. Vialle, M. Broyer, J. L. Rousset, M. Treilleux and P. Melinon, Phys. Rev. B **67**, 155409 (2003).

[5] S. Xiao, W. Hu, W. Luo, Y. Wu, X. Li, and H. Deng, Eur. Phys. J. **54**, 479 (2006).

[6] A. Aguado, L. E. Gonzalez, and J. M. Lopez, J. Phys. Chem. B **108**, 11722 (2004).

[7] C. Mottet, G. Rossi, F. Balleto, and R. Ferrando, Phys. Rev. Lett. **95**, 035501 (2005).

[8] R. A. Lordeiro, F. F. Guimares, J. C. Belchoir, R. L. Johnston, Int. J. Quant. Chem. **95**, 112 (2003).

[9] L. D. Lloyd, R. L. Johnston, S. Salhi, and N. T. Wilson, J. Mater. Chem. **14**, 1691 (2004).

[10] J. Wang, G. Wang, X. Chen, W. Lu, and J. Zhao, Phys. Rev. B **66**, 014419 (2002).

[11] X. Sun, J. A. Toledo, Z. L. Cui, and Z. K. Zhang, J. Nanoparticle Research **3**, 325 (2001).

[12] F. Baletto, C. Mottet, and R. Ferrando, Phys. Rev. Lett. **90**, 135504 (2003).

[13] G. Rossi, A. Rapallo, C. Mottet, A. Fortunelli, F. Baletto, and R. Ferrando, Phys. Rev. Lett. **93**, 105503 (2004).

[14] D. Cheng, S. Huang, and W. Wang, Phys. Rev. B **74**, 064117 (2006).

[15] S. Koutsopoulos, K. M. Eriksen, R. Fehrman, J. Catal. **238**, 270 (2006).

[16] S. Devarajan, P. Bera, S. Sampath, J. Colloid Interface Sci. **290**, 117 (2005).

[17] J. V. Barth, G. Costantini, and K. Kern, Nature **437**, 671 (2005).

[18] C. N. R. Rao, G. U. Kulkarni, P. J. Thomas, Chem. Soc. Rev. **29**, 27 (2000).

[19] J. Jellinek, E. B. Krissinel, Chem. Phys. Lett. **258**, 283 (1996).

[20] L. D. Lloyd, R. L. Johnston, S. Salhi, and N. T. Wilson, J. Mater. Chem. **14**, 1691 (2004).

[21] J. M. Montejano-Carrizales, M. P. Iñiguez, and J. A. Alonso, Phys. Rev. B **49**, 16649 (1994).

[22] C. Rey, J. García-Rodeja, and L. J. Gallego, Phys. Rev. B **54**, 2942 (1996).

[23] M. J. López, P. A. Marcos, and J. A. Alonso, J. Chem. Phys. **104**, 1056 (1996).

[24] P. J. Hsu and S. K. Lai, J. Chem. Phys. **124**, 044711 (2006).

[25] D. Cheng, S. Huang, and W. Wang, Eur. Phys. J. D **39**, 41 (2006).

[26] M. S. Bailey, N. T. Wilson, C. Roberts, and R. L. Johnston, Eur. Phys. J. D **25**, 41 (2003).

[27] A. Christensen, P. Stolze, and J. K. Nørskov, J. Phys. Cond. Matt. **7**, 1047 (1995).

[28] Y. Shimizu, K. S. Ikeda, and S. Sawada, Phys. Rev. B **64**, 075412 (2001).

[29] S.-P. Huang and P. B. Balbuena, J. Phys. Chem. B **106**, 7225 (2002).

[30] Y. H. Chui and K.-Y. Chan, Chem. Phys. Lett. **408**, 49 (2005).

[31] H. B. Liu, U. Pal, R. Perez, and J. A. Ascencio, J. Phys. Chem. B **110**, 5191 (2006).

[32] L. Rubinovich, M. I. Haftel, N. Bernstein, and M. Polak, Phys. Rev. B **74**, 035405 (2006).

[33] T. Sakurai, T. Hashizume, A. Jimbo, A. Sakai, and S. Hyodo, Phys. Rev. Lett. **55**, 514 (1985).

[34] H. Shimizu, M. Ono, and K. Nakayama, Surf. Sci. **36**, 817 (1973).

[35] L. E. Rehn, H. A. Hoff, and N. Q. Lam, Phys. Rev. Lett **57**, 780 (1986).

[36] T. B. Massalski, *Binary Alloy Phase Diagrams* (ASM International, Metals Park, Ohio, 1990).

[37] D. S. Mainardi, P. B. Balbuena, Langmuir **17**, 2047 (2001).

[38] D. S. Mainardi, P. B. Balbuena, Int. J. Quant. Chem. **85**, 580 (2001).

[39] P. A. Derosa, J. M. Seminario, and P. B. Balbuena, J. Phys. Chem. A, **105**, 7917 (2001).

[40] V. G. Grigoryan and M. Springborg, Phys. Rev. B **70**, 205415 (2004).

[41] V. G. Grigoryan, D. Alamanova, and M. Springborg, Phys. Rev. B **73**, 115415 (2006).

[42] M. S. Daw and M. I. Baskes, Phys. Rev. Lett. **50**, 1285 (1983).

[43] M. S. Daw and M. I. Baskes, Phys. Rev. B **29**, 6443 (1984).

[44] S. M. Foiles, M. I. Baskes, and M. S. Daw, Phys. Rev. B **33**, 7983 (1986).

[45] Internet address: 146.246.250.1

[46] M. S. Daw, S. M. Foiles, and M. I. Baskes, Mat. Sci. Rep. **9**, 251 (1993).

[47] V. G. Grigoryan and M. Springborg, Chem. Phys. Lett. **375**, 219 (2003).

[48] V. G. Grigoryan, D. Alamanova, and M. Springborg, Eur. Phys. J. D **34**, 187 (2005).

[49] D. Alamanova, V. G. Grigoryan, and M. Springborg, Z. Phys. Chem. **220**, 811 (2006).

[50] J. Holland, *Adaptation in Natural and Artificial Systems*; University of Michigan Press: Ann Arbor **MI**, 1975.

[51] D. E. Goldberg, *Genetic Algorithms in search, Optimization and Machine Learning*; Addison-Wesley: Reading **MA**, 1989.

[52] Y. Dong, M. Springborg, M. Burkhart, and M. Veith, *Advances in Computational Methods in Science and Engineering* **4A**, 1010 (2005).

[53] Y. Dong, M. Burkhart, M. Veith, and M. Springborg, J. Phys. Chem. B **109**, 22820, (2005).

[54] Y. Dong and M. Springborg, submitted.

[55] V. Tevekeliyska, Y. Dong, M. Springborg, and V.G. Grigoryan, Eur. Phys. J. D **43**, 19 (2007)

[56] C. Kittel, *Introduction to Solid State Physics, 8th ed.* (Wiley, New York, 2005).

[57] L. Zhu, A. E. DePristo, J. Catal. **167**, 400 (1997).

[58] R. Hultgren, P. D. Desai, D. T. Hawkins, M. Gleiser, and K. K. Kelley, *Selected Values of the Thermodynamic Properties of Binary Alloys* (American Society for Metals, Metals Park, Ohio, 1973).

[59] N. T. Wilson and R. L. Johnston, J. Matter. Chem. **12**, 2913 (2002).

[60] S. M. Foiles, Phys. Rev. B **32**, 7685 (1985).

[61] A. Pasturel, V. Drchal, J. Kudrnovsky, and P. Weinberger, Phys. Rev. B **48**, 2704 (1993).

Structure and energetics of equiatomic K–Cs and Rb–Cs binary clusters

Elisaveta Hristova,[a] Valeri G. Grigoryan,[b] and Michael Springborg[c]
Physical and Theoretical Chemistry, University of Saarland, 66123 Saarbrücken, Germany

(Received 22 April 2008; accepted 21 May 2008; published online 25 June 2008)

The basin-hopping algorithm combined with the Gupta many-body potential is used to study the structural and energetic properties of $(KCs)_n$ and $(RbCs)_n$ bimetallic clusters with $N=2n$ up to 50 atoms. Each binary structure is compared to those of the pure clusters of the same size. For the cluster size $N=28$ and for the size range of $N=34-50$, the introduction of K and Rb atoms in the Cs alkali metal cluster results in new ground state structures different from those of the pure elements. In the size range $N\geqslant 38$ the binary and pure clusters show not only structural differences, but they also display different magic numbers. Most of the magic Rb–Cs and K–Cs clusters possess highly symmetric structures. They belong to a family of pIh structures, where a fivefold pancake is a dominant structural motif. Such geometries have not been reported for alkali binary clusters so far, but have been found for series of binary transition metal clusters with large size mismatch. Moreover, tendency to phase separation (shell-like segregation) is predicted for both K–Cs and Rb–Cs clusters with up to 1000 atoms. Our finding of a surface segregation in Rb–Cs clusters is different from that of theoretical and experimental studies on bulk Rb–Cs alloys where phase separation does not occur. © *2008 American Institute of Physics*. [DOI: 10.1063/1.2944244]

I. INTRODUCTION

Bimetallic clusters have attracted considerable interest both from basic science and for practical applications. Due to their special chemical and physical properties, e.g., enhanced bifunctional catalytic activity, they are subject of an increasing interest in the fields of catalysis, optics, magnetism, and nanoelectronics.[1–8] Compared to the pure clusters with only one type of atoms, binary clusters may show segregation which may result in, e.g., layered structures or core-shell structures. Alternatively, the clusters may show complete mixing.[9–13]

In order to optimize the materials properties for a given application, it is of paramount importance to have an accurate understanding of the relation between cluster size on the one side and property on the other. Although experimental studies can provide much of this information, a full characterization of the experimentally studied systems is often lacking, suggesting that additional, theoretical studies can be helpful.

Even for clusters consisting of just one elements, it is difficult to make theoretical predictions about their structure (see, e.g., Ref. 14). Because of their nontrivial geometric structures,[15–21] as well as their complex chemical ordering,[22–27] it becomes much more difficult to predict the ground state structures of binary clusters. Therefore, to obtain a precise information on the structure of the lowest total energy and thus to calculate the properties of interest, an unbiased and accurate exploration of the potential energy surface (PES) is required. But, even for the simpler case of monoatomic cluster, we are faced with the problem of complexity, i.e., the number of local minima in the PES increases exponentially with cluster size. Bimetallic clusters possess even more complex PES due to the inequivalence of so-called homotops.[27,28] Homotops are defined[28] as clusters with the same size, composition, and geometric arrangement, differing only in the way in which A- and B-type atoms are arranged. The number of *homotops* for an A_nB_m cluster, $P_{n,m}$, is given by $P_{n,m}=(n+m)!/n!m!$. Thus, if we, for example, consider all possible replacements of 10 K atoms by Cs atoms in an isomer of K_{20}, the number of homotops is as large as 184 756. Because of this large number of homotops, that in addition may have only small total-energy differences, a global optimization becomes a very demanding task.

Whereas a large number of studies have been carried out for binary transition metal clusters,[29–34] only few reports are available for mixed alkali metal clusters. López *et al.*[35–37] studied the structural and segregation properties of Na–Cs, Na–Li, and Na–K nanoalloys using the density functional theory method. *Ab initio* calculations, such as those of Deshpande *et al.*[38,39] on Na–Li clusters, are restricted to small sizes up to $N=12$. To our knowledge, there are no theoretical and experimental studies on the structure and energetics of K–Cs and Rb–Cs clusters so far. Therefore, these systems will be in the focus of the present work.

Both bulk alloy systems form random substitutional solid solutions over the whole concentration range. Theoretical and experimental studies on surface properties of bulk K–Cs and Rb–Cs alloys suggest that while surface segregation is present for K–Cs alloys, it does not occur in Rb–Cs alloys.[40] Moreover, whereas for K–Cs the heats of formation are positive indicating segregation behavior, for Rb–Cs they are negative, suggesting perfect mixing.[41] Considering this,

[a]Electronic mail: elli@springborg.pc.uni-sb.de.
[b]Electronic mail: vg.grigoryan@mx.uni-saarland.de.
[c]Author to whom correspondence should be addressed. Electronic mail: m.springborg@mx.uni-saarland.de.

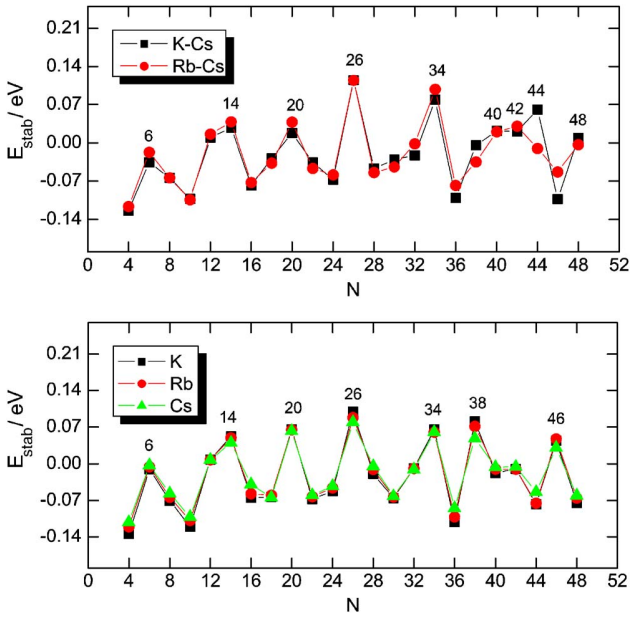

FIG. 1. (Color online) The stability function for (top part) bimetallic K–Cs and Rb–Cs and (bottom part) pure K, Rb, and Cs clusters as a function of N.

we found it interesting to study if and how the miscibility properties change in these alloy clusters compared to those of bulk alloys.

The purpose of the present work is, accordingly, to determine and analyze the ground state structures of binary K–Cs and Rb–Cs clusters with N up to 50 atoms in an unbiased study. The dominant structural motif of the particularly stable clusters will be found and compared to those of the magic binary clusters build up by transition metals. Further, we shall explore whether those values of N that for the pure clusters correspond to particularly stable structures also do so for in the present case. Moreover, by using various descriptors, we shall quantify to which extent the structures resemble those of the pure clusters.

We have determined the lowest-energy structures of K–Cs and Rb–Cs binary clusters using a basin-hopping (BH) algorithm combined with a Gupta many-body potential.

The paper is organized as follows. In Sec. II we briefly outline the Gupta potential and the BH algorithm. The main results are presented in Sec. III, and a brief summary is offered in Sec. IV.

II. COMPUTATIONAL METHOD

A. The Gupta potential

The Gupta potential[42] has been successfully applied to study the structure, energetics, free energy, surface energy, and melting point of alkali metal clusters.[43,44] It has been derived from Gupta's expression for the cohesive energy of a bulk material. According to this, the total energy of a system with N atoms is written in terms of repulsive and attractive many-body terms,

$$V_{\mathrm{clus}} = \sum_{i=1}^{N} [V^r(i) - V^m(i)], \tag{1}$$

where

$$V^r(i) = \sum_{j=1(\neq i)}^{N} A(a,b)\exp\left[-p(a,b)\left(\frac{r_{ij}}{r_0(a,b)} - 1\right)\right], \tag{2}$$

and

$$V^m(i) = \left\{\sum_{j=1(\neq i)}^{N} \zeta^2(a,b) \times \exp\left[-2q(a,b)\left(\frac{r_{ij}}{r_0(a,b)} - 1\right)\right]\right\}^{1/2}. \tag{3}$$

In these equations, r_{ij} is the distance between atoms i and j, and A, r_0, ζ, p, and q are parameters whose values are fitted to experimental values such as cohesive energy, lattice parameters, and independent elastic constants for the reference crystal structure at 0 K. Finally, a and b refer to atom type of atom i and j.

The parameters for inhomogeneous K–Cs (Rb–Cs) interactions are taken as the average of the K–K and Cs–Cs (Rb–Rb and Cs–Cs) parameters obtained by Li *et al.*[44] The reasoning for this is that bulk K–Cs and Rb–Cs alloys are solid solutions, rather than ordered intermetallics, and mixture energies and mixture parameters of molten K–Cs and Rb–Cs alloys computed in a study of Christman[45] are very close to the averages of the corresponding single constituent values. Furthermore, also for other alloy systems it has been found that the parameters are close to the average values and in general lie between the limits of the homonuclear interaction parameters.[46]

B. The basin-hopping algorithm

The basic idea of the BH method[47–50] is to transform the complex energy landscape as a function of $\mathbf{X} \equiv (\mathbf{R}_1, \mathbf{R}_2, \ldots, \mathbf{R}_N)$ (with $\mathbf{R}_i$ being the position of the ith atom) to a new reduced-energy landscape, which consists of plateaus of energy minima only,

$$\tilde{E}(\mathbf{X}) = \min\{E(\mathbf{X})\}, \tag{4}$$

where $\min\{\cdots\}$ represents a local energy minimization process with $\mathbf{X}$ as initial structure. Perturbations in the algorithm are introduced by changing slightly the latest set of coordinates and carrying out a gradient-based optimization from the resulting geometry. Moves are accepted or rejected based upon the energy difference between the new and old local minimum. The BH approach can be also viewed as a generalization of the "Monte Carlo plus energy minimization" procedure of Li and Scheraga.[51] The Monte Carlo part of the BH algorithm is introduced in order to allow the system to hop from one plateau to another at a thermal energy $k_B T^*$ measured in units of the binding energy of the K–Cs or Rb–Cs dimer. The hopping probability depends highly on the choice of the "temperature" T^* and on the reduced-energy difference between the plateaus of the two consecutive steps. In the present work the Monte Carlo simulation has been per-

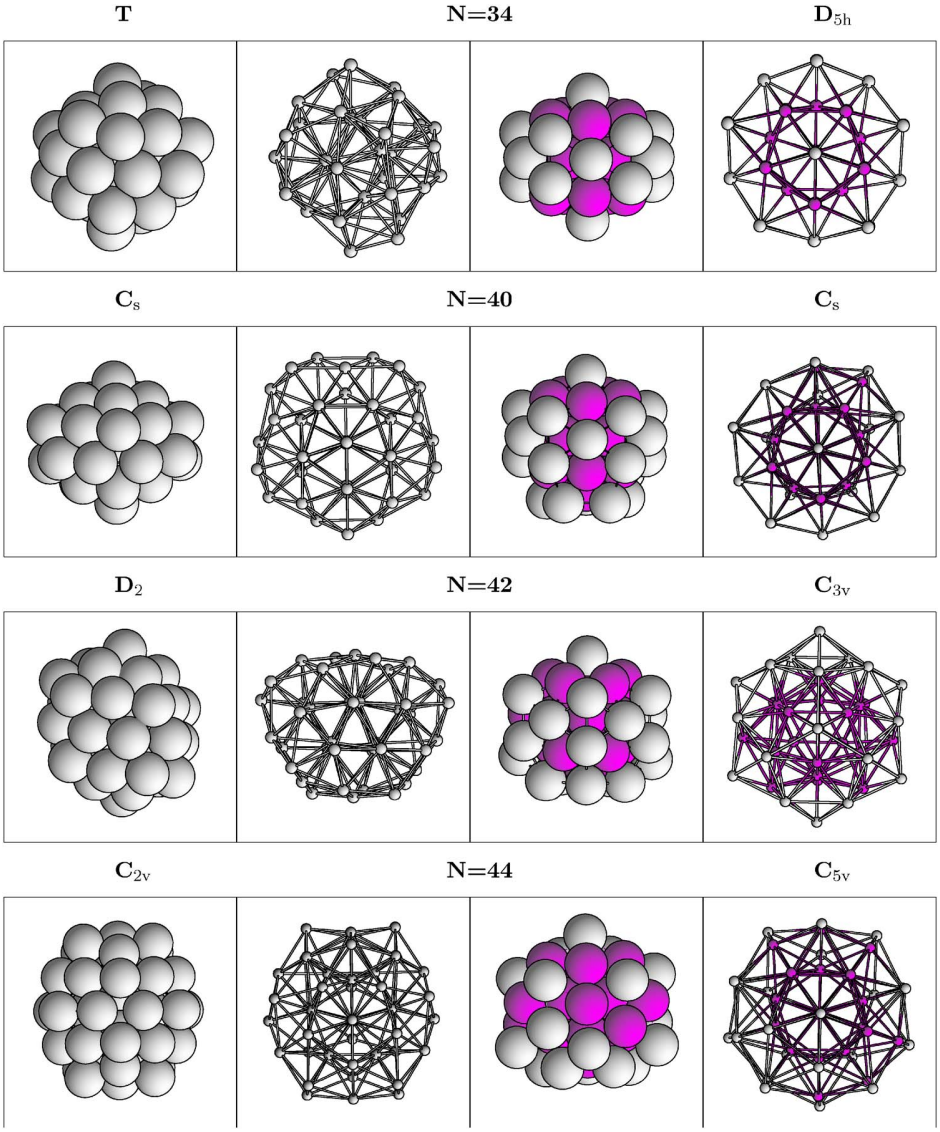

FIG. 2. (Color online) Different structures for which the pure K_N, Rb_N, and Cs_N clusters have the same structures as is the case for the $(KCs)_{N/2}$ and $(RbCs)_{N/2}$ clusters. In each row, the two left panels show the structure of the pure clusters, and the two right panels that of the bimetallic cluster. The values of N are given above each row, as is the case for the symmetry group of the clusters (here, the symmetry of the bimetallic clusters does not take the difference of the elements into account.

formed at a *constant* reduced "temperature" of 0.8. We emphasize that our approach does not allow for a molecular-dynamics simulation at a given temperature, but only for an efficient identification of the structure of the global total-energy minimum.

The BH algorithm has successfully located all the lowest known minima for Lennard-Jones clusters with up to 110 atoms, including all the nonicosahedral structures (sizes of 38, 75–77, and 102–104), for the first time in unbiased searches.[50] In a recent study, Doye *et al.* have found the particularly stable structures for binary Lennard-Jones clusters with up to 100 atoms.[52] Further, the BH algorithm combined with a Gupta potential has been successfully applied to calculate the ground state structures of the pure alkali metal clusters Na, K, Rb, and Cs.[43] The present study is accordingly an extension of the last mentioned studies.

III. RESULTS

A. Energetic properties

In order to identify particularly stable clusters we consider the stability function,

$$E_{\mathrm{stab}} = E_{\mathrm{tot}}(N+2) + E_{\mathrm{tot}}(N-2) - 2E_{\mathrm{tot}}(N). \quad (5)$$

E_{stab} is shown in Fig. 1 for binary K–Cs and Rb–Cs clusters and for pure K, Rb, and Cs clusters. Maxima of E_{stab} indicate particularly stable (magic) clusters. We observe that for smaller cluster sizes, up to $N=36$, the stability functions for pure and for bimetallic clusters possess the same maxima. From $N \geqslant 38$, however, the stability function of the bimetallic nanoalloys shows a complete different behavior compared to that of the pure clusters. For example, the sizes $N=44$ and 48 are magic for binary K–Cs and Rb–Cs clusters, but not for the monometallic ones.

The high stability for most of the magic K–Cs and Rb–Cs binary clusters is strongly correlated with drastic changes in structure towards a higher symmetry, compared to their monometallic counterparts. Some of the particular stable binary clusters are presented in Figs. 2 and 3. Here, the size $N=34$ is a magic one for pure as well as for binary clusters, but it displays a different symmetry in the two cases. For the pure cluster it has a T symmetry, whereas for the bimetallic cluster the heteroatomic interactions lead to the formation of a fivefold so-called "pancake" and to an

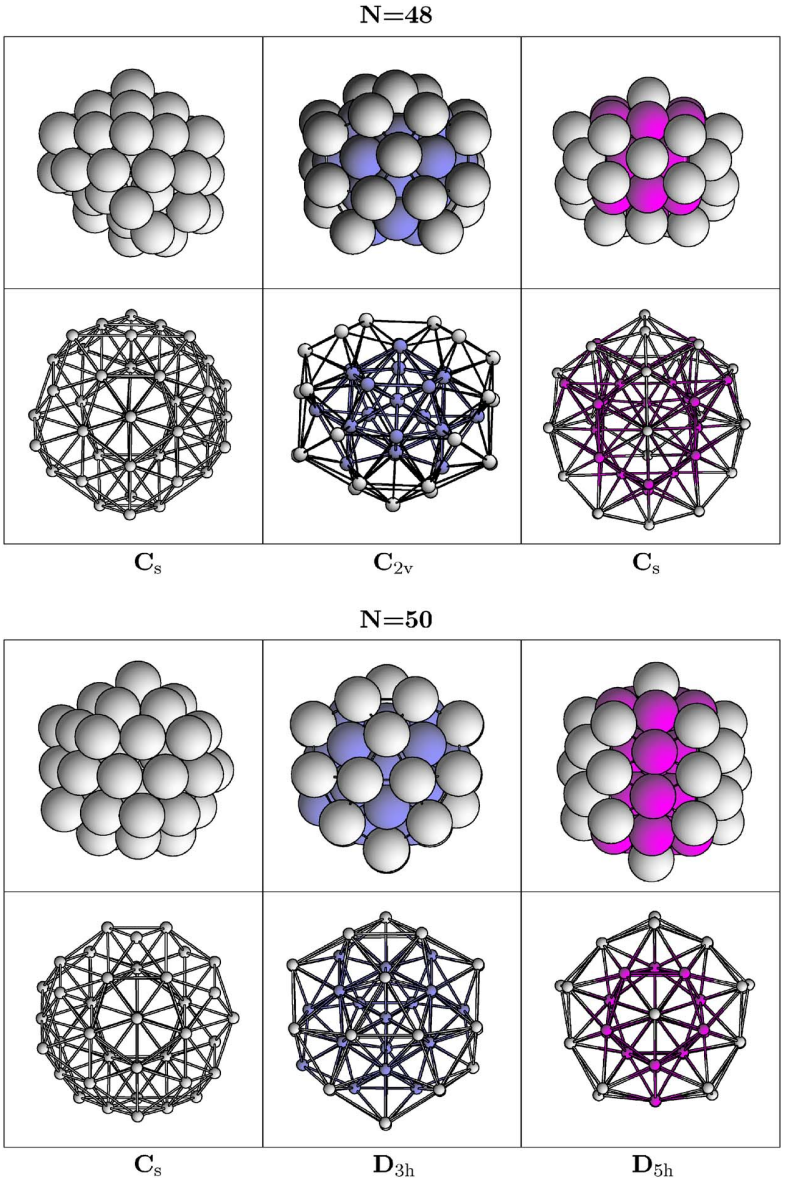

FIG. 3. (Color online) As in Fig. 2, but for clusters for which $(KCs)_{N/2}$ and $(RbCs)_{N/2}$ have different structures. For each N, the two left panels show the structure of the pure cluster, the middle ones that of $(KCs)_{N/2}$ and the right ones that of $(RbCs)_{N/2}$. Moreover, the symmetry groups are here given below the representations of the clusters.

increase in symmetry to D_{5h} (notice that the symmetries we are reporting do not distinguish between atom types).

The pancake structural element can be seen, e.g., in Fig. 2 in the left presentation for $(KCs)_{17}$ and $(RbCs)_{17}$ as the 32-atomic structure that is obtained by removing the top and bottom atoms. Equivalently, for $(KCs)_{20}$ and $(RbCs)_{20}$, the top atom and the seven bottom atoms shall be removed in order to arrive at the pancake motif.

The 34-atom fivefold pancake was labelled *magic pIh*[7] in Ref. 16 since it consists of seven interpenetrating icosahedra. The Rb–Cs ground state structure of the size $N=50$, which does not appear in the stability function as a particularly stable structure, is also interesting because it is formed by two interpenetrating fivefold pancakes, also in this case leading to D_{5h} symmetry. Binary clusters of the sizes $N=40$, 42, 44, and 48 shown in Figs. 2 and 3 belong to the same structural family and are obtained by capping the fivefold pancake. Exceptions are K–Cs clusters of the sizes $N=48$ and 50, which do not result from the 34-atom pancake but still possess an icosahedral core.

The structural motif of the fivefold pancake has been found also for Ag–Cu, Ag–Ni, Au–Cu, and Au–Ni systems for which a large size mismatch exists, but not for Ag–Pd and Pt–Pd clusters where the size mismatch is below 5%.[16] Rossi *et al.* explained the occurrence of such magic pIh binary clusters with the decrease in internal strain when the inner atoms of a pure pIh cluster are substituted by smaller ones. Besides, if the large atoms have a strong tendency towards segregation then core-shell pIh clusters will be favored. In K–Cs and Rb–Cs systems, the K and Rb atoms are 16% and 9% smaller than Cs atoms, respectively, which explains why the alkali binary clusters show the same structural motif as reported for binary transition metal clusters.

By further analyzing of the stability function, it is found that the K–Cs and Rb–Cs clusters of the sizes $N=28$ and 38, which show minima in the stability function, possess lower symmetry than their monometallic counterparts (see Fig. 4). For $N=28$ there is a reduction from T to C_s symmetry and for $N=38$ from O_h to C_1 symmetry.

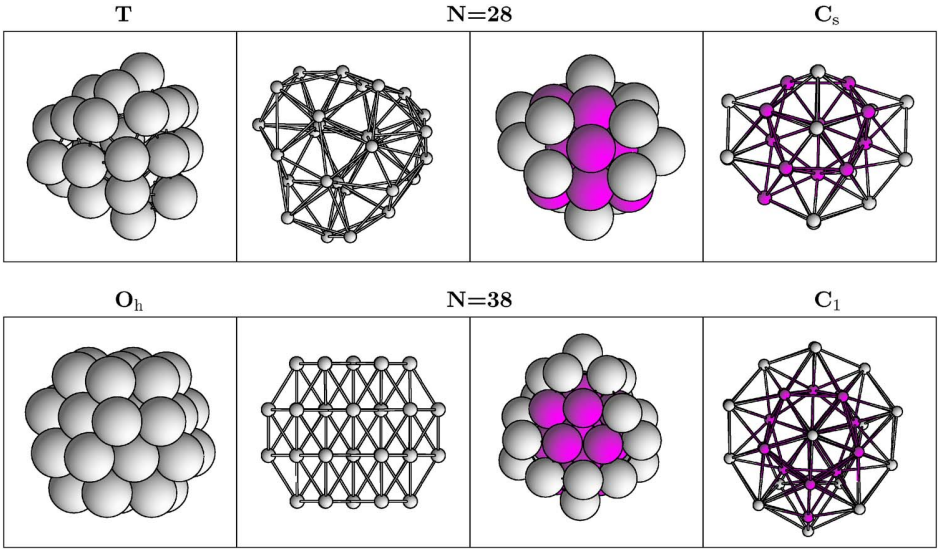

FIG. 4. (Color online) As in Fig. 2, but for other values of *N*.

B. Structural properties

In order to quantify structural differences and similarities between bimetallic clusters and pure clusters of the same size of *N* atoms we use the concept of similarity functions introduced by us in previous studies.[53,54] For each atom we define its radial distance,

$$r_n = |\mathbf{R}_n - \mathbf{R}_0|, \tag{6}$$

with

$$\mathbf{R}_0 = \frac{1}{N}\sum_{i=1}^{N} \mathbf{R}_i. \tag{7}$$

These are sorted in increasing order. Simultaneously, for each of the pure clusters, we calculate and sort the radial distances $\{r_n'\}$ for this, too. Subsequently, from

$$q = \left[\frac{1}{N}\sum_{n=1}^{N}\left(\frac{r_n}{d_0} - \frac{r_n'}{d_0'}\right)^2\right]^{1/2}, \tag{8}$$

we define a similarity function,

$$S_1 = \frac{1}{1+q}, \tag{9}$$

which approaches 1 (0) if the A_nB_n cluster is very similar to (different from) the pure cluster. In order to identify structural similarities, independent of scaling, we have scaled the radial distances in Eq. (8) with the bond lengths of the diatomic systems, d_0 and d_0'. The same procedure is applied to quantify whether the pure cluster consisting of *N* A atoms is structural related to that consisting of *N* B atoms.

The similarity functions are shown in Fig. 5 as functions of *N*. From the figure it can be seen that pure K and Cs clusters have essentially the same structures except for the sizes $N=16$, 24, and 30. Comparing pure Rb and Cs clusters, the geometries differ for $N=16$ and 24.

At next we will compare the pure clusters with the binary ones. Comparing K–Cs to K clusters and Rb–Cs to Rb clusters, it can be seen that there is a structural agreement between the bimetallic and the pure clusters below the size $N=26$. Accordingly, when comparing both types of binary clusters to pure Cs clusters there will be structural differ-

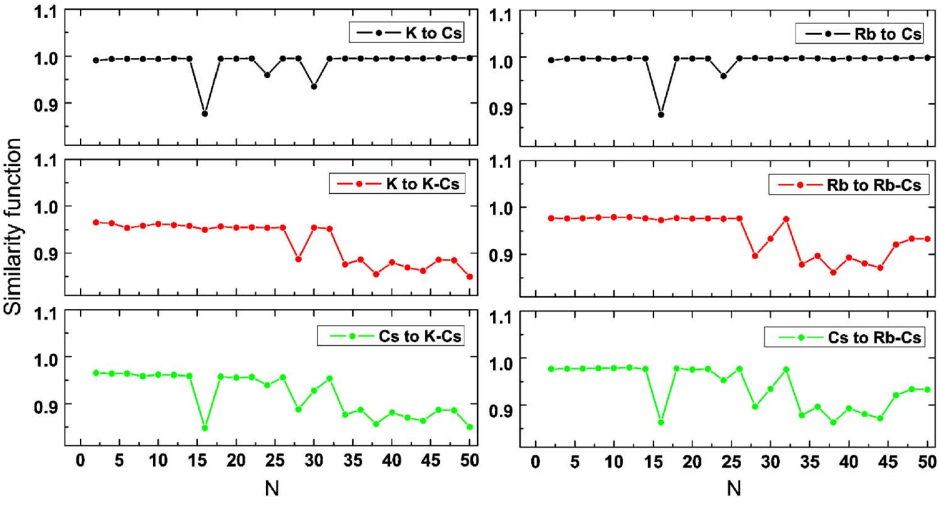

FIG. 5. (Color online) The similarity function S_1 vs the total number of atoms *N*. In the left panels we compare the structures of pure K to those of pure Cs clusters (top), of pure K to those of the bimetallic K–Cs clusters (middle), and of pure Cs to those of K–Cs clusters (bottom). The panels to the right show the same comparison, but for Rb and Rb–Cs clusters.

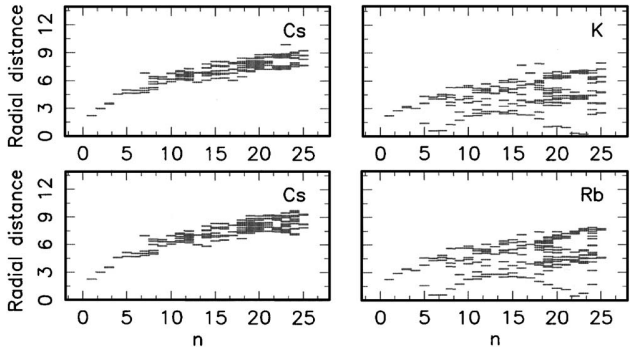

FIG. 6. The radial distances (in Å) for (top) Cs and K atoms in K–Cs clusters, and for (bottom) Cs and Rb atoms in Rb–Cs clusters as a function of the number of the corresponding type of atoms, $n=N/2$. In each panel a small horizontal line for a given value of n indicates that at least one atom of the corresponding type has that distance to the center of the cluster.

ences for exactly these cluster sizes (16 and 24) for which the pure clusters K and Cs (or Rb and Cs) differ from each other.

For $N=28$ and from $N=34$ upwards a drop in the similarity functions indicates the formation of new structures, different from those of the pure K, Rb, and Cs clusters. This size range covers the sizes for which the pure and bimetallic clusters show different particular stabilities as discussed above. The binary cluster with 28 atoms is an incomplete fivefold pancake for both K–Cs and Rb–Cs (Fig. 4) and, thus, it belongs also to the family of pIh structures.

In order to study the possibility of a segregation in the nanoalloys we consider the radial distances of the K and Cs (Rb and Cs) atoms separately, as shown Fig. 6. It is clear that the Cs atoms segregate preferentially to the surface in both types of bimetallic clusters. Accordingly, the K and Rb atoms are primarily located in the core. This is consistent with the differences in the surface energy[55] for Cs, Rb, and K, i.e., 95, 117, and 145 erg cm^{-2}, respectively, as well as in the atomic radii, i.e., 2.72, 2.50, and 2.35 Å, respectively.

An interesting issue is, thus, if the same segregation behavior will be observed for larger clusters. For this purpose we considered equiatomic K–Cs and Rb–Cs bimetallic clusters with $N=2n$ atoms constructed in the following way. For $N=100$ we construct an initial structure by optimizing that of the Cs_N cluster, whereas for $N=1036$ we take a spherical cutout of the fcc crystal structure of Cs with the center of the sphere at a nearest-neighbor bond. Subsequently, we replaced n of the Cs atoms with K or Rb atoms resulting in a core-shell structure with Cs atoms in the shell and K or Rb atoms in the core, core-shell structures with Cs atoms in the core and K or Rb atoms in the shell (notice that for these core-shell structures, the separation into a core and a shell is not perfect), a completely segregated, layered structure, and, finally, a completely mixed alloy (see Fig. 7). Each of these structures was relaxed to its closest total-energy minimum structure.

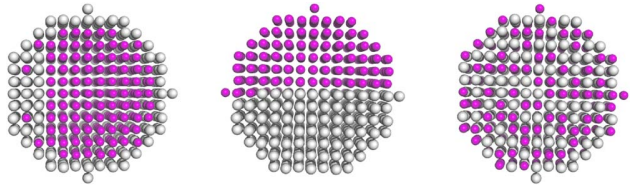

FIG. 7. (Color online) A cross-section of (from left to right) the core-shell, the layered, and the completely mixed structures for the cluster size $N=1036$.

The resulting binding energies are analyzed in Table I. For both K–Cs and Rb–Cs systems, the core-shell structure with Cs atoms in the shell possesses the highest binding energy. Thus, our results suggest that, both for K–Cs and Rb–Cs clusters, segregation will take place, leading to the formation of core-shell structures. On the other hand, the small differences in the binding energies suggest that at not very high temperatures, entropy effects will lead to a preference of the totally mixed alloys. The segregation-to-mixing transition could be confirmed or refuted by molecular-dynamics simulation on these systems at different temperatures in future studies.

Theoretical and experimental studies show that, while surface segregation is present for K–Cs alloys, it does not occur in Rb–Cs alloys.[40] The reason is the larger atomic-size mismatch in K–Cs compared to Rb–Cs. Moreover, the heats of formation for Rb–Cs are negative suggesting the existence of a mixed alloy instead of phase separation.[41]

In the preceding subsection we identified the pancake structural motif as a fundamental building block for the bimetallic clusters. This could imply that the clusters have very similar structures, independent of n, i.e., that the structures can be considered as being built up by adding KCs or RbCs atom pairs to a central core. In order to quantify this suggestion we consider two additional similarity functions.

For the cluster $(ACs)_n$ we first consider the $(ACs)_{n-1}$ cluster. Moreover, for the $(ACs)_n$ cluster we consider at first all those different n^2 parts that can be considered by removing one A and one Cs atom. We then construct

$$q=\left\{\frac{1}{2n-2}\sum_{i=1}^{n-1}\left[(r_{A,i}-r'_{A,i})^2+(r_{Cs,i}-r'_{Cs,i})^2\right]\right\}^{1/2}, \quad (10)$$

with the sorted, unprimed and primed radial distances being for the fragment of the $(ACs)_n$ cluster and for the $(ACs)_{n-1}$ cluster, respectively. From the smallest of those n^2 values we define a similarity function,

$$S_2=\frac{1}{1+q/u_l}, \quad (11)$$

with $u_l=1$ Å.

Alternatively, we consider all the $n(2n-1)$ possible $(2n-2)$-atomic fragments of the $(ACs)_n$ cluster without distinguishing between atom type. Also here, we sort and compare the radial distances of this system with those of the $(ACs)_{n-1}$ cluster, leading to

$$q=\left[\frac{1}{2n-2}\sum_{i=1}^{2n-2}(r_i-r'_i)^2\right]^{1/2}, \quad (12)$$

with a notation equivalent to that above. From the smallest value of q we define a similarity function,

TABLE I. Binding energy in eV/atom for $(ACs)_n$ clusters with A being K or Rb. $N=2n$ is the total number of atoms.

A	N	Core(A)-shell(Cs)	Core(Cs)-shell(A)	Layered	Mixed
K	100	0.713	0.681	0.702	0.699
	1036	0.80	0.773	0.792	0.785
Rb	100	0.680	0.665	0.673	0.672
	1036	0.761	0.749	0.757	0.755

$$S_3 = \frac{1}{1+q/u_l}. \tag{13}$$

The results are shown in Fig. 8, where we also show a similarity function similar to S_3 but for the monoatomic clusters. It is remarkable that there are very few features that are specific for the atom types, i.e., the curves are essentially identical for all systems considered here. Moreover, comparing the top and bottom panels, the bimetallic clusters seem to show a much more regular growth behavior than is the case for the monoatomic ones. Finally, for the bimetallic clusters, S_3 is in general larger than S_2, which may be ascribed to two effects. At first, by not distinguishing between atom type, it is easier to make two clusters look identical. But at second, the segregation behavior that we have seen in Fig. 7 means that, upon growth, one atom type has to be substituted by the other, so that the former remains localized to the surface region.

IV. CONCLUSIONS

In this work we have studied the structural and energetic properties of $(KCs)_n$ and $(RbCs)_n$ bimetallic clusters with $N=2n$ up to 50 atoms. The homo- and heteroatomic interactions in the bimetallic clusters have been modeled using the Gupta potential. The global geometry optimization has been performed using the basin-hopping algorithm.

We have found that K–Cs and Rb–Cs bimetallic cluster structures with $N<26$ atoms tend to have geometries similar to those of pure K and Rb clusters, respectively. On the other hand, for the size $N=28$ and for the size range $N=34-50$ the introduction of K and Rb substitutions in a Cs cluster results in new structures, different from those of the pure elements. In the size range from $N\geqslant 38$, the binary and pure clusters show not only structural differences, but they also display different magic numbers.

Most of the magic bimetallic structures are highly symmetric. They belong to the family of pIh structures obtained by capping the fivefold pancake. Such geometries have not been reported for any of the investigated alkali bimetallic clusters (Na–Li, Na–K, Na–Cs) so far. Moreover, tendency to phase separation (shell-like segregation) is predicted for both K–Cs and Rb–Cs clusters with up to 1000 atoms. These results for Rb–Cs clusters are in contrast to those of theoretical and experimental studies on bulk Rb–Cs, which have found that surface segregation in the alloy system is not present. Finally, the bimetallic clusters show a much more regular growth behavior than is the case for the monoatomic ones.

In conclusion, alkali metal K–Cs and Rb–Cs binary clusters are also suitable for building up magic core-shell pIh structures, already reported for binary transition metal clusters.

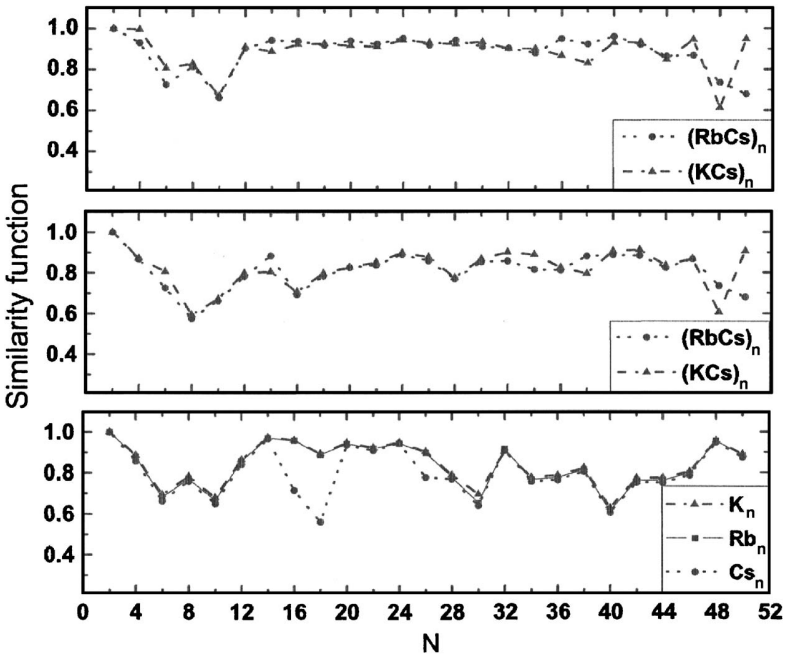

FIG. 8. The similarity functions S_2 (middle panel) and S_3 (top panel) for (dashed lines) $(KCs)_n$ and (dotted lines) $(RbCs)_n$ clusters as a function of $N=2n$. The lowest panel shows a similarity function similar to S_3 but for monatomic clusters of K (dashed lines), Rb (solid lines), and Cs (dotted lines) atoms.

ACKNOWLEDGMENTS

This work was supported by the DFG through Project No. Sp 439/24-1.

[1] S. Koutsopoulos, K. M. Eriksen, and R. Fehrman, J. Catal. **238**, 270 (2006).
[2] S. Devarajan, P. Bera, and S. Sampath, J. Colloid Interface Sci. **290**, 117 (2005).
[3] J. V. Barth, G. Costantini, and K. Kern, Nature (London) **437**, 671 (2005).
[4] C. N. R. Rao, G. U. Kulkarni, and P. J. Thomas, Chem. Soc. Rev. **29**, 27 (2000).
[5] M. Gaudry, E. Cottancin, M. Pellarin, J. Lerme, L. Arnaud, J. R. Huntzinger, J. L. Vialle, M. Broyer, J. L. Rousset, M. Treilleux, and P. Melinon, Phys. Rev. B **67**, 155409 (2003).
[6] S. Xiao, W. Hu, W. Luo, Y. Wu, X. Li, and H. Deng, Eur. Phys. J. B **54**, 479 (2006).
[7] A. Aguado, L. E. Gonzalez, and J. M. Lopez, J. Phys. Chem. B **108**, 11722 (2004).
[8] C. Mottet, G. Rossi, F. Balleto, and R. Ferrando, Phys. Rev. Lett. **95**, 035501 (2005).
[9] A. Christensen, P. Stoltze, and J. K. Nørskov, J. Phys.: Condens. Matter **7**, 1047 (1995).
[10] Y. Shimizu, K. S. Ikeda, and S. Sawada, Phys. Rev. B **64**, 075412 (2001).
[11] H. B. Liu, U. Pal, R. Perez, and J. A. Ascencio, J. Phys. Chem. **110**, 5191 (2006).
[12] Z. Li, J. P. Wilcoxon, F. Yin, Y. Chen, R. E. Palmer, and R. L. Johnston, Faraday Discuss. **138**, 363 (2008).
[13] M. Polak and L. Rubinovich, Phys. Rev. B **75**, 045415 (2007).
[14] M. Springborg, in *Specialist Periodical Reports: Chemical Modelling, Applications and Theory*, edited by A. Hinchliffe (Royal Society of Chemistry, London, 2006), Vol. 4, p. 249.
[15] S. Darby, T. V. Mortimer-Jones, R. L. Johnston, and C. Roberts, J. Chem. Phys. **116**, 1536 (2002).
[16] G. Rossi, A. Rapallo, C. Mottet, A. Fortunelli, F. Baletto, and R. Ferrando, Phys. Rev. Lett. **93**, 105503 (2004).
[17] A. Rapallo, G. Rossi, R. Ferrando, A. Fortunelli, B. C. Curley, L. D. Lloyd, G. M. Tarbuck, and R. L. Johnston, J. Chem. Phys. **122**, 194308 (2005).
[18] G. Rossi, R. Ferrando, A. Rapallo, A. Fortunelli, B. C. Curley, L. D. Lloyd, and R. L. Johnston, J. Chem. Phys. **122**, 194309 (2005).
[19] T. Van Hoof and M. Hou, Phys. Rev. B **72**, 115434 (2005).
[20] G. Barcaro, A. Fortunelli, G. Rossi, F. Nita, and R. Ferrando, J. Phys. Chem. B **110**, 23197 (2006).
[21] L. O. Paz-Borbón, R. L. Johnston, G. Barcaro, and A. Fortunelli, J. Phys. Chem. C **111**, 2936 (2007).
[22] D. Ferrer, A. Torres-Castro, X. Gao, S. Sepulveda-Guzman, U. Ortiz-Mendez, and M. José-Yacamán, Nano Lett. **7**, 1701 (2007).
[23] M. C. Fromen, J. Morrilo, M. J. Casanove, and P. Lecante, Europhys. Lett. **73**, 885 (2006).
[24] T. Van Hoof and M. Hou, Eur. Phys. J. D **29**, 33 (2004).
[25] D. Cheng, W. Wang, and S. Huang, J. Phys. Chem. B **110**, 16193 (2006).
[26] F. Baletto, C. Mottet, and R. Ferrando, Phys. Rev. Lett. **90**, 135504 (2003).
[27] L. D. Lloyd, R. L. Johnston, S. Salhi, and N. T. Wilson, J. Mater. Chem. **14**, 1691 (2004).
[28] J. Jellinek and E. B. Krissinel, Chem. Phys. Lett. **258**, 283 (1996).
[29] J. M. Montejano-Carrizales, M. P. Iñiguez, and J. A. Alonso, Phys. Rev. B **49**, 16649 (1994).
[30] C. Rey, J. García-Rodeja, and L. J. Gallego, Phys. Rev. B **54**, 2942 (1996).
[31] M. J. López, P. A. Marcos, and J. A. Alonso, J. Chem. Phys. **104**, 1056 (1996).
[32] P. J. Hsu and S. K. Lai, J. Chem. Phys. **124**, 044711 (2006).
[33] R. A. Lordeiro, F. F. Guimares, J. C. Belchoir, and R. L. Johnston, Int. J. Quantum Chem. **95**, 112 (2003).
[34] M. S. Bailey, N. T. Wilson, C. Roberts, and R. L. Johnston, Eur. Phys. J. D **25**, 41 (2003).
[35] A. Mañanes, M. P. Iñiguez, M. J. López, and J. A. Alonso, Phys. Rev. B **42**, 5000 (1990).
[36] M. J. López, M. P. Iñiguez, and J. A. Alonso, Phys. Rev. B **41**, 5636 (1990).
[37] A. Bol, G. Martín, J. M. López, and J. A. Alonso, Z. Phys. D: At., Mol. Clusters **28**, 311 (1993).
[38] M. D. Deshpande, D. G. Kanhere, I. Vasiliev, and R. M. Martin, Phys. Rev. A **65**, 033202 (2002).
[39] M. D. Deshpande, D. G. Kanhere, P. V. Panat, I. Vasiliev, and R. M. Martin, Phys. Rev. A **65**, 053204 (2002).
[40] H. Bogdanów and K. F. Wojciechowski, J. Phys. D **29**, 1310 (1996).
[41] R. Hultgren, P. D. Desai, D. T. Hawkins, M. Gleiser, and K. K. Kelley, *Selected Values of the Thermodynamic Properties of Binary Alloys* (American Society for Metals, Metals Park, OH, 1973).
[42] R. P. Gupta, Phys. Rev. B **23**, 6265 (1981).
[43] S. K. Lai, P. J. Hsu, K. L. Wu, W. K. Liu, and M. Iwamatsu, J. Chem. Phys. **117**, 10715 (2002).
[44] Y. Li, E. Blaisten-Barojas, and D. A. Papaconstantopoulos, Phys. Rev. B **57**, 15519 (1998).
[45] J. R. Christman, Phys. Rev. **153**, 225 (1967).
[46] F. Cleri and V. Rosato, Phys. Rev. B **48**, 22 (1993).
[47] J. P. K. Doye and D. J. Wales, Phys. Rev. Lett. **80**, 1357 (1998).
[48] D. J. Wales, *Energy Landscapes* (Cambridge University Press, Cambridge, 2003).
[49] D. J. Wales and H. A. Scheraga, Science **285**, 1368 (1999).
[50] D. J. Wales and J. P. K. Doye, J. Phys. Chem. A **101**, 5111 (1997).
[51] Z. Li and H. A. Scheraga, Proc. Natl. Acad. Sci. U.S.A. **84**, 6611 (1987).
[52] J. P. K. Doye and L. Meyer, Phys. Rev. Lett. **95**, 063401 (2005).
[53] V. G. Grigoryan and M. Springborg, Phys. Rev. B **70**, 205415 (2004).
[54] V. G. Grigoryan, D. Alamanova, and M. Springborg, Phys. Rev. B **73**, 115415 (2006).
[55] A. Kiejna and K. F. Wojciechowski, J. Phys. C **16**, 6883 (1983).

Eur. Phys. J. D (2007)
DOI: 10.1140/epjd/e2007-00167-8

THE EUROPEAN PHYSICAL JOURNAL D

Deposition of Ni_{13} and Cu_{13} clusters on Ni(111) and Cu(111) surfaces

E. Kasabova[a], D. Alamanova[b], M. Springborg[c], and V.G. Grigoryan[d]

Physical and Theoretical Chemistry, University of Saarland, 66123 Saarbrücken, Germany

Received 30 January 2007 / Received in final form 28 March 2007
Published online 23 May 2007 –

Abstract. The soft deposition of Ni_{13} and Cu_{13} clusters on Ni(111) and Cu(111) surfaces is studied by means of constant-energy molecular-dynamics simulations. The atomic interactions are described by the Embedded Atom Method. It is shown that the shape of the nickel clusters deposited on Cu(111) surfaces remains rather intact, while the copper clusters impacting on Ni(111) surfaces collapse forming double and triple layered products. Furthermore, it is found that for an impact energy of 0.5 eV/atom the structures of all investigated clusters show the lowest similarity to the original structures, except for the case of nickel clusters deposited on a Cu(111) surface. Finally, it is demonstrated that when cluster and substrate are of different materials, it is possible to control whether the deposition results in largely intact clusters on the substrate or in a spreading of the clusters. This separation into *hard* and *soft* clusters can be related to the relative cohesive energy of the crystalline materials.

PACS. 61.46.+w Nanoscale materials – 36.40.-c Atomic and molecular clusters – 68.65.-k Low-dimensional, mesoscopic, and nanoscale systems: structure and nonelectronic properties – 31.15.Ct Semi-empirical and empirical calculations (differential overlap, Huckel, PPP methods, etc.)

1 Introduction

Due to the numerous applications in the nanoindustry, nanodevices, catalysis, etc. [1–3] the deposition of transition and noble metal nanoparticles on diverse substrates has attracted considerable attention among experimentalists and theoreticians over the past decades. Various experimental techniques [4–6] have been developed in order to deposit accurately even very small metal clusters without damaging the surface and keeping the clusters as identifiable entities. Successful growth of monolayers and cluster islands has been achieved with controlled aggregation following atom vapor deposition. Through the use of scanning tunneling microscopy [7,8] it has become possible to deposit and move clusters on the surface. One of the most recent experimental techniques is the Low Energy Cluster Beam Deposition (LECBD) [4] that uses only moderate energies of deposition. With this technique, the surface structure remains largely intact in contrast to experimental methods where the substrate is bombarded with high-energy clusters resulting in thin films formed by the cluster atoms. In that case, the clusters have so large kinetic energies that they melt upon the deposition, lose their initial structures and spread out on the surface, that in turn may suffer from the radiation damage.

Unfortunately, even in the latest experimental set-ups it is not possible to determine the geometry of small or medium-sized clusters, neither in gas phase nor deposited on a substrate. Here, theory can be used in supplementing the experimental studies. However, since theoretical studies of cluster deposition processes on a substrate is computationally extremely demanding when the studies shall consider realistic systems and when attempting to use first-principles methods, semiempirical methods provide a useful alternative for this kind of simulations. In combination with molecular-dynamics (MD) simulations, these methods are very attractive for studying the temporal evolution of the systems of interest. Therefore, several studies of cluster deposition processes for higher impact energy have been reported [9–11]. However, the formation and growth of cluster islands through low-impact-energy deposition have hardly been studied.

The purpose of the present study is to simulate the experimental conditions of the LECBD experiment and, thereby, obtain further details of the cluster deposition that can not be derived in the experiment directly. We shall use the Embedded Atom Method (EAM) in its original version proposed by Daw, Baskes, and Foiles (DBF) [12–14] in describing the interatomic interactions. In a previous study [15] we demonstrated that these semi-empirical potentials are accurate for most metals. Very

[a] e-mail: elli@springborg.pc.uni-sb.de
[b] e-mail: deni@springborg.pc.uni-sb.de
[c] e-mail: m.springborg@mx.uni-saarland.de
[d] e-mail: vg.grigoryan@mx.uni-saarland.de

recently [16], we have studied the soft deposition of copper clusters on the Cu(111) surface using another version of the EAM, proposed by Voter and Chen [17,18] (VC). We considered different impact energies as well as orientations and sizes of the clusters. For the sake of comparison we shall here include results from that study. As a natural extension we shall here study what happens when the cluster and the substrate are of different metals. Accordingly, we shall study the deposition of copper and nickel clusters on copper and nickel substrates. We shall concentrate on the Cu_{13} and Ni_{13} clusters which are particularly stable according to previous studies [15,19,20].

The advantage of the EAM is that it is possible to study larger systems over longer time scales than what is possible with more accurate methods. Nevertheless, the EAM is approximate and, e.g., quantum effects of electrons and of vibrations are only very indirectly included. This means that the details of our conclusions may be altered when using more accurate methods, although we do not believe that our general conclusions will change. Finally, by studying Cu and Ni systems we are considering materials for which the EAM has been found to be particularly precise. Lacking experimental studies on those systems we, therefore, hope also that our work will serve as a motivation for studying those.

The paper is organized as follows. The computational details are described in Section 2 and the main results are presented in Section 3. Finally, we conclude in Section 4.

2 Computational methods

2.1 The embedded-atom method

The interactions between the atoms of the magic Ni_{13}, Cu_{13} clusters and of the surfaces are described through the EAM in the version of Daw, Baskes, and Foiles (DBF) [12–14]. Then the total energy of the system is split into a sum of atomic energies,

$$E_{\rm tot} = \sum_{i=1}^{N} E_i, \tag{1}$$

with E_i consisting of two parts, i.e., the embedding energy (which is obtained by considering the ith atom as an impurity embedded into the host provided by the rest of the atoms), and pair interactions with all other atoms. Accordingly,

$$E_i = F_i(\rho_i^h) + \frac{1}{2} \sum_{j=1,(j\neq i)}^{N} \phi_{ij}(r_{ij}) \tag{2}$$

where ρ_i^h is the local electron density at site i, F_i is the embedding energy, and ϕ_{ij} is a short-ranged potential between atoms i and j separated by distance r_{ij}.

The local density at site i is assumed being a superposition of atomic electron densities,

$$\rho_i^h = \sum_{j=1,(j\neq i)}^{N} \rho_j^a(r_{ij}), \tag{3}$$

where $\rho_j^a(r_{ij})$ is the spherically averaged atomic electron density provided by atom j at the distance r_{ij}.

The EAM has been successfully applied to many bulk and low-symmetric transition-metal systems such as defects, surface structures and segregation [21]. Furthermore, in our previous studies [15,19,20,22–24] we have tested its accuracy for nickel, copper, and gold clusters and showed that it describes very well the properties of most of those systems, with gold clusters being a possible exception.

In the present study we have studied deposition of a Ni_{13} cluster on the Ni(111) and the Cu(111) surface as well as deposition of a Cu_{13} cluster on the Ni(111) surface. We include our results on the deposition of a Cu_{13} cluster on the Cu(111) surface from our recent study [16]. In that study we did not use the DBF but the VC version of the EAM.

2.2 Molecular-dynamics simulation

Our computational approach is similar to that of our previous work on the deposition of copper clusters on a copper surface [16]. We model the (111) surfaces of the *fcc* copper and nickel crystals using a periodic slab of seven atomic layers and with a dimension of $10a_0 \times 10a_0$ with $a_0 = 3.62$ Å (3.52 Å) being the lattice constant for copper (nickel) for the periodically repeated unit. Periodic boundary conditions are applied parallel to the surface.

Before the deposition process is initiated we orient the icosahedral Cu_{13} and Ni_{13} clusters relative to the surface so that the S_6 symmetry axis of the cluster is perpendicular to the surface.

The equations of motion of the microcanonical (NVE) ensemble are integrated by using the Velocity Verlet algorithm. The time step is set to 2 fs and the total integration time is 50 ps. We consider impact energies of $E_0 = 0.0, 0.1, 0.3, 0.5, 0.7$, and 0.9 eV/atom, which is the range for Low Energy Cluster Beam Deposition experiments.

Both clusters and substrates are initially relaxed to equilibrium at 0 K. Subsequently, the clusters are located near the surface. Then the cluster atoms are given the initial velocity in a direction perpendicular to the substrate, whereas the substrate remains cold. At the end of the simulation the clusters and surfaces are cooled down by means of simulated annealing for a period of 5 ps.

3 Results and discussion

Limiting the summation in equation (1) to the 13 atoms of the cluster, we can introduce a total energy of the cluster. This corresponds to splitting the energy of the interaction between cluster and substrate into two equally large halfparts that each is attributed to one of the subsystems. In particularly the variation of the total energy of the cluster with deposition parameters (like impact energy and geometry) can be used in analysing the outcome of the

Table 1. The relative total energy (in eV) of the clusters after the collision with the surface as a function of the impact energy in eV/atom. The total energies of the initial, isolated structures obtained with the EAM are shown for comparison (denoted 'EAM'). 'A/B' denotes the A_{13} cluster deposited on the B(111) surface. Notice that for the Cu/Cu simulation we use the VC potential, whereas we for the others use the DBF potential. Thereby, the isolated Cu clusters have slightly different total energies.

Impact energy	Ni/Ni	Cu/Cu	Cu/Ni	Ni/Cu
0	−47.14	−36.66	−37.64	−48.46
0.1	−47.10	−37.67	−37.60	−48.46
0.3	−47.52	−37.67	−37.51	−48.46
0.5	−47.88	−37.79	−37.79	−48.43
0.7	−47.79	−36.80	−37.76	−48.46
0.9	−47.61	−36.96	−37.77	−47.61
EAM	−44.87	−33.50	−34.37	−44.87

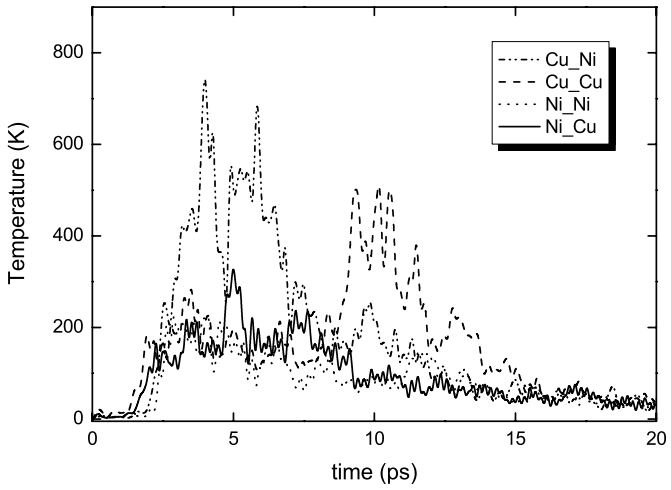

Fig. 1. The internal temperatures of Cu_{13} deposited on Ni(111), Cu_{13} deposited on Cu(111), Ni_{13} deposited on Ni(111), and Ni_{13} deposited on Cu(111) at an impact energy of 0.0 eV/atom as functions of the time. A_B marks the A cluster deposited on the B substrate.

deposition. Table 1 shows this quantity for all different impact energies and cluster/substrate combinations.

In all cases, the attractive interactions between substrate and cluster lead to a lowering of the total energy of the cluster when being deposited on the substrate. For clusters deposited on the Ni(111) surfaces the most stable structures are obtained at impact energies of 0.5 eV/atom. This result is consistent with our previous findings for Cu-Cu interactions described with another version of the EAM potential [16]. On the other hand, a nickel cluster deposited on a Cu(111) surface keeps its structure intact up to impact energies of 0.9 eV/atom, where the compact shape is distorted by the removal of a single atom from the cluster and substitution of this by a copper atom from the surface.

In Figure 1 we show the evolution of the internal temperature of the clusters as a function of time in the case that the depositions are driven only by attractive forces, i.e., for an impact energy of $E_0 = 0.0$ eV/atom. The internal temperature is defined as follows. We define the position of the center of mass of the cluster,

$$\boldsymbol{R}_0 = \frac{1}{N}\sum_i \boldsymbol{R}_i, \tag{4}$$

with $N = 13$ being the number of atoms in the cluster and $\boldsymbol{R}_i$ their positions. Subsequently,

$$\frac{3}{2}NkT = \frac{1}{2}m\sum_{i=1}^{N}\left[|\dot{\boldsymbol{R}}_i|^2 - |\dot{\boldsymbol{R}}_0|^2\right], \tag{5}$$

with m being the mass of a cluster atom and the dots represent time derivatives, defines the internal temperature. As seen in Figure 1, the clusters with the highest internal temperatures are the copper ones, independently of the substrate, whereas the nickel clusters have much lower internal temperatures. Since the higher internal temperatures imply that the atoms are more mobile, this finding can be explained through the lower binding energies of the Cu clusters than of the Ni clusters (cf. the lowest row in Tab. 1).

Moreover, when the copper cluster is deposited on the nickel substrate it obtains a rather high internal temperature during the first 2–3 ps of the simulation and after some further 5 ps the temperature drops again. On the other hand, when the same cluster is deposited on the copper substrate, the internal temperature does not reach as high an absolute value (notice, that in this case the simulations were initiated at a larger distance between cluster and substrate, so that at the beginning the cluster was moving as a whole towards the substrate and first after some 5 ps the structure of the cluster starts changing structure leading to an increase in the internal temperature). Again, the higher mobility of copper atoms (lower binding energy of the crystal) than of nickel atoms makes it easier for the copper substrate to absorb the impact energy from the collision process, leading to a more soft landing of the clusters. In particular for the deposition of Cu_{13} on Cu, initially most of the impact energy is absorbed by the substrate that deforms so much that the cluster partly enters the surface. First then the cluster experiences larger structural changes, indicated by the late decrease in the inner temperature for this system.

Furthermore, due to the larger cohesive energy and smaller lattice constant of nickel, it is favourable for a deposited copper cluster to spread out on the surface instead of staying intact. That this occurs is seen in Figure 2. The deposition of Cu_{13} on Cu(111) at negligible attractive forces results in the formation of a distorted icosahedron, cf. Figure 3, and the cluster atoms are not spread on the surface. Here, the maximal internal temperature of 500 K is not sufficient to break the cluster bonds. According to our previous results [16] the minimal impact energy needed to disturb significantly this cluster is at least 0.5 eV/atom.

Further information on the resulting cluster structures due to the deposition can be obtained by looking at the

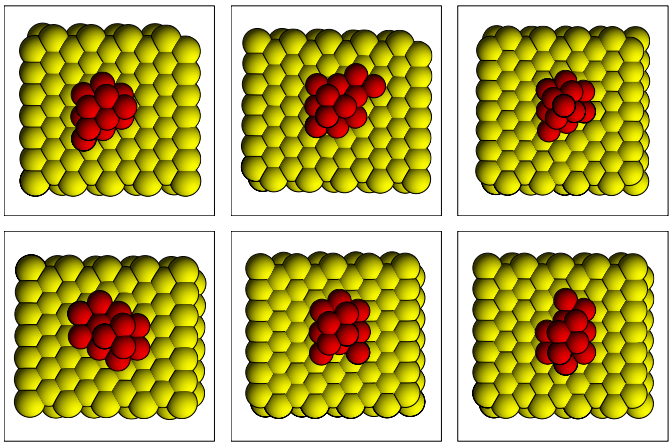

Fig. 2. (Color online) The final products of Cu_{13} clusters with different deposition energies after deposition on the Ni surface. The impact energies are (top, left) 0.0, (top, middle) 0.1, (top, right) 0.3, (bottom, left) 0.5, (bottom, middle) 0.7, and (bottom, right) 0.9 eV/atom.

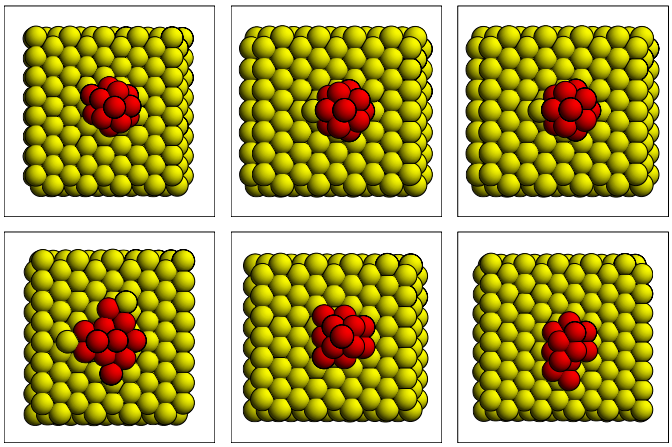

Fig. 3. (Color online) The final products of Cu_{13} clusters with different deposition energies after deposition on the Cu surface. The presentation is as in Figure 2.

Table 2. The height of the cluster (in Å) after the collision with the surface as a function of the impact energy in eV/atom. A/B labels the A cluster deposited on the B surface.

	Ni/Ni	Cu/Cu	Cu/Ni	Ni/Cu
0	5.741	5.365	4.135	5.364
0.1	5.822	5.295	3.955	5.377
0.3	5.301	5.349	5.742	5.295
0.5	3.905	3.609	3.954	5.254
0.7	5.134	5.564	4.014	5.157
0.9	5.693	4.042	4.006	5.289

height of the clusters measured as the positions of the atoms above the first plane of substrate atoms without the deposited cluster. This parameter is given in Table 2 as a function of the deposition energy. It can be seen that at a deposition energy of 0.5 eV/atom there is a minimum in the cluster height, except for the Ni_{13} cluster deposited on Cu(111) that has a minimum for an impact energy of

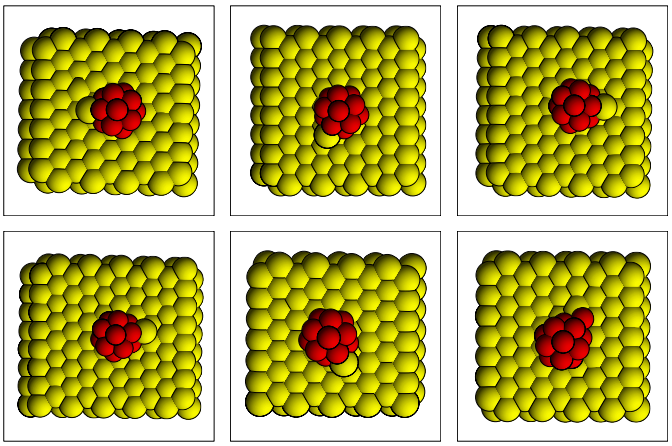

Fig. 4. (Color online) The final products of Ni_{13} clusters with different deposition energies after deposition on the Cu surface. The presentation is as in Figure 2.

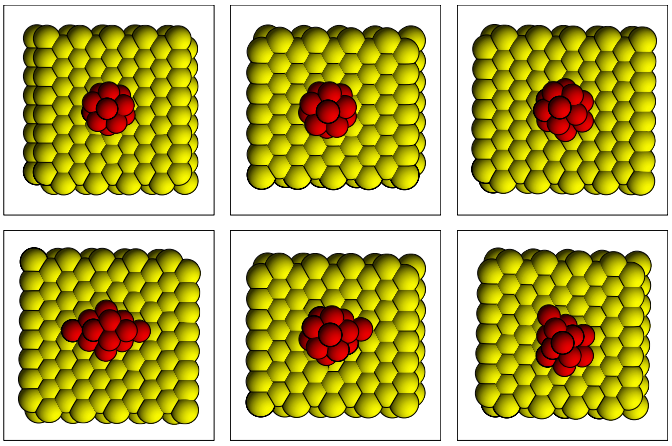

Fig. 5. (Color online) The final products of Ni_{13} clusters with different deposition energies after deposition on the Ni surface. The presentation is as in Figure 2.

0.7 eV/atom. Again, the stronger interatomic bonds for Ni than for Cu may explain this shift to higher impact energies.

When simply viewing the final products of the depositions, Figures 2, 3, 4, and 5, it is immediately seen that the shape of the Ni_{13} icosahedron deposited on a Cu(111) surface remains very well kept for all impact energies (see Fig. 4). On the other hand, the Cu_{13} icosahedron spreads out on the Ni(111) surface forming double layers for all impact energies except for a deposition energy of 0.3 eV/atom, where the final structure is a symmetrical pyramid (see Fig. 2). Also this finding is due to the fact that Ni-Ni bonds are much stronger than Cu-Cu bonds (nickel possesses a higher cohesive energy of 4.45 eV than copper (3.51 eV) [25]).

As Figures 3 and 5 show, the final products of deposition of Ni_{13} and Cu_{13} clusters on surfaces of the same atom type, are very similar for the lowest impact energies. However, while at a higher deposition energy of 0.5 eV/atom, the Cu_{13} cluster spreads out on the Ni(111) surface forming a slightly deformed monolayer, the Ni_{13} cluster forms

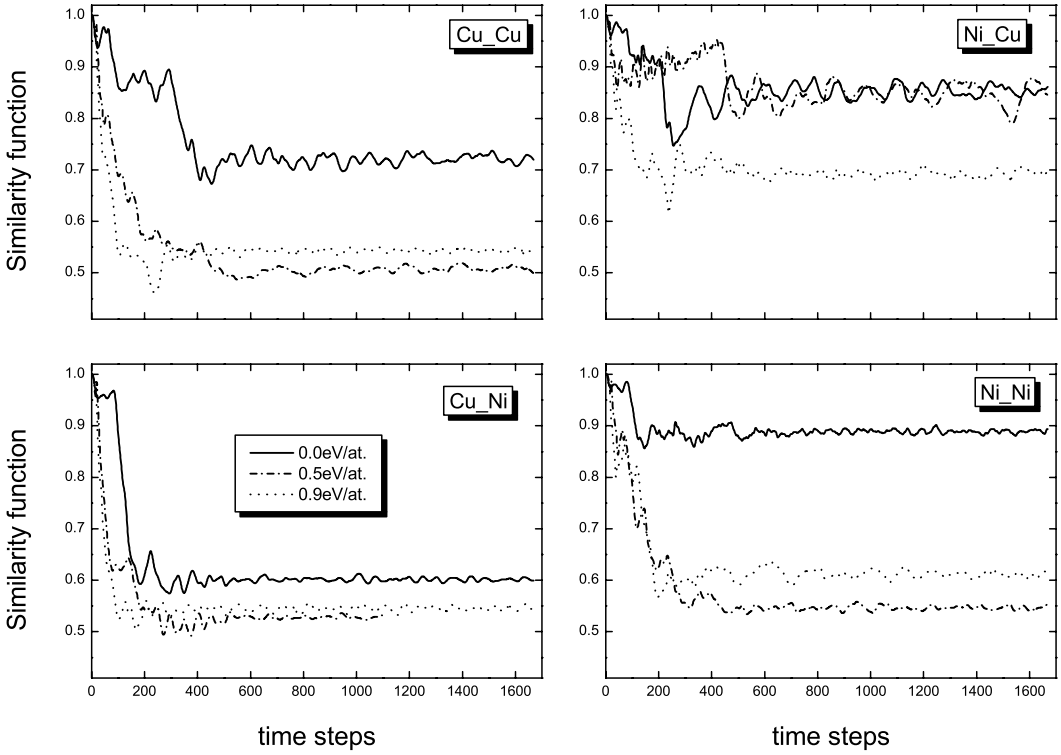

Fig. 6. The evolution of the similarity functions with time for the simulations with cluster energies of 0.0, 0.5, and 0.9 eV/atom. A_B marks the A cluster deposited on the B substrate.

only a double layer on the Cu(111) surface. For an impact energy of 0.7 eV/atom the Ni_{13} cluster remains relatively intact, with one atom substituted by a surface atom. At the same impact energy, the Cu_{13} cluster forms a symmetrical pyramid. A similar pyramid appears first at an impact energy of 0.9 eV/atom for the Ni_{13} cluster, whereas at this energy the Cu_{13} cluster collapses forming a double layer. All these results allow us to coin the nickel and copper clusters as being *hard* and *soft*, respectively.

The concept of *hard* and *soft* clusters can be further quantified through the evolution of the cluster shape with the simulation time. In order to compare the structures of the deposited products with their initial structures we use the so-called similarity functions introduced by us in previous studies [19,20]. For each atom we define its radial distance

$$r_n = |\boldsymbol{R}_n - \boldsymbol{R}_0|. \tag{6}$$

These are sorted in increasing order. At any time in the simulation we compare these with the sorted radial distances for the initial structure, $\{r'_n\}$. From

$$q = \left[\frac{1}{N}\sum_{n=1}^{N}(r_n - r'_n)^2\right]^{1/2}, \tag{7}$$

the similarity function is defined as

$$S = \frac{1}{1 + q/u_l} \tag{8}$$

($u_l = 1$ Å), which approaches 1 if the cluster has changed structure very little.

The results are shown in Figure 6. The similarity function for nickel deposited on a copper surface stays at a higher value than the one for copper deposited on a nickel surface. This supports the consensus of *hard* nickel and *soft* copper clusters. In contrast to these results, the nickel cluster readily spreads on its homoatomic surface, producing a symmetric bilayered structure at an impact energy of 0.5 eV/atom, as indicated by the low values seen in Figure 6. It can also be seen in the figure that when depositing a cluster on a surface of the same type of atoms the separation into hard and soft clusters becomes less relevant (see also Figs. 3 and 5).

A further relevant question is whether the substrate dictates the structure of the deposited cluster, i.e., to which extent the deposition can be classified as being epitaxial. To this purpose we use an 'index of epitaxy', I, [16] defined through

$$I = \frac{1}{1 + q/u_l^2}, \tag{9}$$

with

$$q = \sum_{i}^{N} |\boldsymbol{R}_i - \boldsymbol{R}_c|^2 \tag{10}$$

where $|\boldsymbol{R}_i - \boldsymbol{R}_c|$ is the distance between the position of the ith atom of the cluster and the closest-lying fictitious atom in the infinite ideal crystal formed by the substrate (notice that thereby I can also become close to 1 even when the cluster and the substrate are far apart). When I reaches 1, perfect epitaxy is obtained.

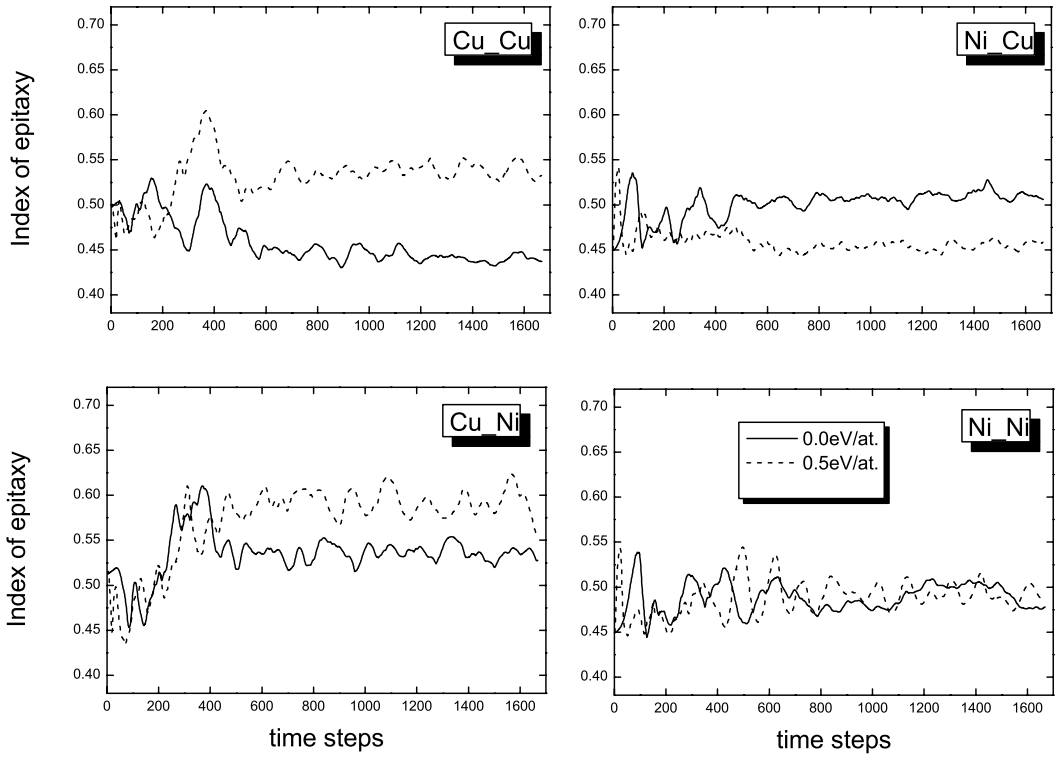

Fig. 7. The evolution of the index of epitaxy with time for the simulations with cluster impact energies of 0.0 and 0.9 eV/atom. A_B marks the A cluster deposited on the B substrate.

In agreement with our previous study [16], there is no direct relationship between the impact energy and the value of I. In Figure 7 we show I for impact energies of 0.0 and 0.5 eV/atom. In all cases I is well below 1 which implies that the interatomic forces within the clusters are sufficiently strong to keep the cluster fairly intact and prevent epitaxial spreading on the surface. It is again seen that the nickel clusters are *harder* than the copper clusters, since I stays roughly constant. A similar behaviour is observed also for the highest impact energy of 0.9 eV/atom, which is not shown here. On the other hand, the *softer* copper clusters show an increasing index of epitaxy, which reflects the spreading of these cluster on the Ni(111) and Cu(111) surfaces. The highest indices of epitaxy are obtained for the combination Cu_{13} deposited on Ni(111). In this case, the cluster forms double layers for all impact energies, except for $E_0 = 0.3$ eV/atom, where a symmetric pyramid is obtained (see also Fig. 2).

4 Conclusions

In the present work we have studied the structural rearrangements of nickel and copper clusters softly deposited on Ni(111) and Cu(111) surfaces. We have used constant-energy molecular-dynamics simulations with impact energies being typical of the Low Energy Cluster Beam Deposition experiment. The main point of this study was to investigate the differences in the structural and energetic properties of the final products when comparing depositions with homoatomic and heteroatomic interactions. According to our findings we conclude that in the case of heteroatomic interactions the cohesive energy of the bulk element is a crucial factor influencing the shape of the final structures. Thus, the deposition of Cu_{13} on a Ni(111) surface results in an overall spreading of the cluster due to the lower cohesive energy of copper, whereas the deposition of the nickel cluster on a Cu(111) surface leads to relatively small changes of the initial structure.

This may be the most interesting outcome of our study, i.e., that when clusters of one type of metal are deposited on another type of metal, it is possible to distinguish between *hard* and *soft* clusters, depending on whether the cohesive energy of the cluster material is larger or smaller than that of the substrate material. Then, *soft* clusters tend to spread on the substrate even at modest impact energies, whereas *hard* clusters largely remain intact also at slightly higher impact energies.

Moreover, it turned out that a deposition energy of 0.5 eV/atom could be favorable for the production of monolayers in the case of Cu_{13} cluster deposited on Cu(111) and Ni(111) surfaces, and the formation of double layers in the case of Ni_{13} cluster deposited on Ni(111).

Finally, we add that our study not at all aims at being exhaustive. We have only considered two types of cluster and substrate metals, only one cluster size and substrate surface, and only one impact geometry. As we have found in our recent study [16], varying the cluster size and impact geometry may very easily change details of the outcome of the deposition. Furthermore, in some preliminary

studies we also found that by changing the approximate method used in describing the interatomic interactions (specifically, we considered the DBF potential instead of the VC potential for the Cu on Cu deposition), slightly different results will be found. Nevertheless, we are convinced that our main conclusions remain valid, also when taking such extensions into account.

This work was supported by the SFB 277 of the University of Saarland and by the German Research Council (DFG) through project Sp439/14-1.

References

1. U. Heiz, W.-D. Schneider, J. Phys. D: Appl. Phys. **33**, R85 (2000)
2. P. Jensen et al., in *Nanoclusters and Nanocrystals*, edited by H.S. Nalwa (American Science Publishers, 2003), Chapt. 4
3. R.E. Palmer, S. Pratontep, H.-G. Boyen, Nature Materials **2**, 443 (2003)
4. P. Melinon et al., Int. J. Mod. Phys. B **9**, 339 (1995)
5. T. Takagi, I. Yamada, A. Sasaki, J. Vac. Sci. Technol. **12**, 1128 (1975)
6. T. Takagi, *Ionized-Cluster Beam Deposition and Epitaxy* (Materials Science and Process Technology Series, Noyes Publications, 1989)
7. K. Bromann, C. Félix, H. Brune, W. Harbich, R. Monot, J. Buttet, K. Kern, Science **274**, 956 (1996)
8. X. Hu, P. von Blanckenhagen, Appl. Phys. A **68**, 137 (1999)
9. L. Rongwu, P. Zhengying, H. Yukun, Phys. Rev. B **53**, 4156 (1996)
10. M. Hou, R.W. Lee, Z.Y. Pan, Nucl. Instr. Meth. B **115**, 536 (1996)
11. S.J. Carroll, S.G. Hall, R.E. Palmer, Phys. Rev. Lett. **81**, 3715 (1998)
12. M.S. Daw, M.I. Baskes, Phys. Rev. Lett. **50**, 1285 (1983)
13. M.S. Daw, M.I. Baskes, Phys. Rev. B **29**, 6443 (1984)
14. S.M. Foiles, M.I. Baskes, M.S. Daw, Phys. Rev. B **33**, 7983 (1986)
15. V.G. Grigoryan, D. Alamanova, M. Springborg, Eur. Phys. J. D **34**, 187 (2005)
16. D. Alamanova, V.G. Grigoryan, M. Springborg, unpublished
17. A.F. Voter, in *Intermetallic Compounds*, edited by J.H. Westbrook, R.L. Fleisch (Wiley, New York, 1994), Vol. 1
18. A.F. Voter, S.P. Chen, Proc. Mat. Res. Soc. **82**, 175 (1987)
19. V.G. Grigoryan, M. Springborg, Phys. Rev. B **70**, 205415 (2004).
20. V.G. Grigoryan, D. Alamanova, M. Springborg, Phys. Rev. B **73**, 115415 (2006)
21. M.S. Daw, S.M. Foiles, M.I. Baskes, Mat. Sci. Rep. **9**, 251 (1993)
22. D. Alamanova, Y. Dong, H. ur-Rehman, M. Springborg, V.G. Grigoryan, Comput. Lett. **1**, 319 (2005)
23. D. Alamanova, V.G. Grigoryan, M. Springborg, Z. Phys. Chem. **220**, 811 (2006)
24. V.G. Grigoryan, M. Springborg, Chem. Phys. Lett. **375**, 219 (2003)
25. C. Kittel, *Introduction to Solid State Physics*, 8th edn. (Wiley, New York, 2005)

Structures and stability of Ag clusters on Ag(111) and Ni(111) surfaces

Elisaveta Hristova*, Valeri G. Grigoryan, Michael Springborg

Physical and Theoretical Chemistry, University of Saarland, 66123 Saarbrücken, Germany

Abstract

The lowest-energy structures of small Ag_N clusters with N=2-20, which are adsorbed on Ag(111) and Ni(111) surfaces, are determined using a combination of the embedded-atom method and the basin-hopping algorithm. We have found that Ag cluster structures which correspond to magic sizes with $N < 18$ tend to have similar geometries on both surfaces. On the other hand, the geometries of the Ag clusters for the non-magic sizes in the same size range differ for the different surfaces. From N=18 upwards a reversal of the magic numbers for the Ag/Ni(111) system compared to the Ag/Ag(111) system takes place. Finally, due to the large size mismatch it is energetically unfavorable for Ag to form a pseudomorphic monolayer structures on Ni(111) and there is considerable strain produced at the interface. The effect of this strain and the increased adatom-substrate interactions will give rise to disordered and elongated structures of the adsorbed Ag clusters.

Key words: Adatoms, Growth, Surface structure, morphology, roughness,

*Corresponding author

Email addresses: elli@springborg.pc.uni-sb.de (Elisaveta Hristova), vg.grigoryan@mx.uni-saarland.de (Valeri G. Grigoryan), m.springborg@mx.uni-saarland.de (Michael Springborg)

1. Introduction

The preparation of individual nanostructures or thin films on solid surfaces becomes more and more important during the last years because of their technological importance in the field of catalysis and microelectronics. The latter application is due to the novel magnetic and electronic effects that result from low dimensional structures. Moreover, the creation of bimetallic surfaces by hetero-epitaxial metal growth offers the potential to grow artificially structured materials with novel physical and chemical properties. Beside the importance for nanotechnological applications, the geometrical structures of clusters adsorbed on single-crystal surfaces reflect fundamental aspects of adatom-adatom and adatom-substrate interactions and afford insights into the initial stages of crystal growth modes and nucleation processes. Systematic studies of the changes of the structural properties of clusters on surfaces as a function of cluster size lead to detailed understanding of such processes.

Thus, one fundamental question that has to be answered is what is the initial stage of thin film formation and crystal growth of the investigated metals: do the clusters develop chains parallel to the substrate or do they form islands, and what is the dominant geometry of these islands. Zhuang *et al.* [1, 2, 3] have performed global optimization on a series of adatom-surfaces systems: Ag/Ag(111), Ni/Ni(111), Cu/Cu(111), and Au/Au(111) with selected sizes up to N=52 atoms using a genetic algorithm combined with embedded-atom method. They found close-packed islands of hexagonal

shape with maximum number of nearest-neighbor bonds, which was in good accordance with observations in scanning tunneling microscopy (STM) experiments [4]. Also for Ir/Ir(111) and Ni/Au(111) compact islands are found to be preferred, as observed in STM and field ion microscopy (FIM) experiments [5, 6]. Linear chains are predicted e.g. for Pt_N clusters (N=3 and 5) on Pt (001) surface by semiempirical calculations [7], also for small Pt_N (N=1-7) and Pd_N (N=1-17) clusters on Ag(110) surface by photoemission study [8], and for Pt and Ir clusters on W(110) by FIM study [9].

Alternatively, the deposited cluster may alloy into the first or the first several layers. For example, Ni adatoms can replace Ag atoms in the first surface layer of a Ag(111) surface under the formation of a surface alloy [10, 11], although Ag and Ni show no tendency for alloying in the bulk. The reason is the strong tendency of Ag atoms for surface segregation. In contrast to Ni/Ag(111), latest STM experiments show that Ag atoms deposited on a Ni(111) surface aggregate in complex islands of two monolayer thickness and do not show any diffusion processes at the Ag/Ni interface [12]. Unfortunately, experiments can not provide information on the exact structure of the Ag islands and additional theoretical investigations are needed.

To our knowledge there are no theoretical studies which determine the geometry and energetics of Ag clusters interacting with a Ni surface. However, such investigations could provide important information on the initial stages of Ag thin film formation on Ni surfaces. Further, the Ag–Ni system presents a large lattice mismatch (the lattice constant of Ag is 16 % larger than this of Ni) and a large difference in the cohesive energies (-2.96 eV for Ag and -4.44 eV for Ni) [13, 14]. Thus, it would be interesting to know how

the system releases the strain induced by the size mismatch and what is the influence of the large difference in the cohesive energies on the most stable equilibrium structures of the adsorbed Ag clusters. Therefore the detailed structural evolution of Ag clusters on a Ni(111) surface will be in the focus of the present work.

Our aim is, accordingly, to determine and analyze the ground state structures of Ag_N clusters adsorbed on a Ni(111) surface with N=2-20 in an unbiased study and to compare them with those of Ag_N clusters on a Ag(111) surface investigated in the same study. Further, we shall explore whether those values of N that for the Ag clusters on the Ni(111) surface correspond to particularly stable structures also do so for Ag clusters on the Ag(111) surface.

The lowest-energy structures of Ag_N clusters with N=2-20 adsorbed on a Ag(111) and a Ni(111) surface have been determined using a basin-hopping algorithm combined with the embedded-atom method. The paper is organized as follows. In Sec. 2 we briefly outline the embedded-atom method and the basin-hopping algorithm. The main results are presented in Sec. 3, and a brief summary is offered in Sec. 4.

2. Computational methods

2.1. The Embedded-Atom Method (EAM)

The homoatomic and heteroatomic interactions Ag–Ag, Ni–Ni, and Ag–Ni between the atoms in the Ag/Ag(111) and Ag/Ni(111) systems are mimicked by the EAM in the version of Daw, Baskes and Foiles (DBF) [15, 16, 17]. The main idea of the EAM is to split the total energy of the system into a

sum of atomic energies,

$$E_{\rm tot} = \sum_{i}^{N} E_i, \tag{1}$$

with E_i consisting of two parts, i.e., an embedding energy (which is obtained by considering the ith atom as an impurity embedded into the host provided by the rest of the atoms) and a pair-potential interaction with all other atoms. Accordingly,

$$E_i = F_i(\rho_i^h) + \frac{1}{2}\sum_{j\neq i} \phi_{ij}(r_{ij}), \tag{2}$$

where ρ_i^h is the local electron density at site i, F_i is the embedding energy, and ϕ_{ij} is a short-ranged potential between atoms i and j separated by distance r_{ij}.

The local density at site i is assumed being a superposition of atomic electron densities,

$$\rho_i^h = \sum_{j\,(\neq i)} \rho_i^a(r_{ij}), \tag{3}$$

where $\rho_i^a(r_{ij})$ is the spherically averaged atomic electron density provided by atom j at the distance r_{ij}.

In accord with Ref. [17] the A-B/B-A heterointeraction can be approximated in the EAM by the geometric mean of the pair interaction for the individual species: $\phi_{AB}(r) = \sqrt{\phi_{AA}(r)\cdot\phi_{BB}(r)}$. Daw, Baskes and Foiles determined the embedding functions for the Ag–Ni system empirically by fitting to experimental data of bulk sublimation energy, elastic constant and the heat of solution of binary alloys [17]. The values for ρ_i^a, F_i and ϕ_{ij} are available in numerical form for Ni and Ag [18]. The validity of the embedding functions for the Ag–Ni system has been tested by computing a wide range

of properties as e.g. the segregation energy of substitutional impurities to the (100) surface [17].

The EAM has been successfully applied to many *bulk* and low-symmetric problems in transition metals such as defects, surface structures and segregation [19]. Furthermore, in our previous works [20, 21, 22, 23] (those include also the discussions with the available experiments) we have found that this approach provides accurate information on pure nickel and silver clusters, which is our main reason for choosing this potential for studying the structures of Ag clusters on Ag(111) and Ni(111) surfaces.

2.2. The Basin-Hopping Algorithm (BH)

To find the lowest energy structures of the Ag/Ag(111) and Ag/Ni(111) systems we use the BH method [24, 25, 26, 27]. The basic idea of the BH method is to transform the complex energy landscape as a function of $\vec{X} \equiv (\vec{R}_1, \vec{R}_2, \ldots, \vec{R}_N)$ (with $\vec{R}_i$ being the position of the ith atom) to a new reduced energy landscape, which consists of plateaus of energy minima only

$$\tilde{E}(\vec{X}) = \min\{E(\vec{X})\}, \tag{4}$$

where $\min\{...\}$ represents a local energy minimization process with $\vec{X}$ as initial structure. Perturbations in the algorithm are introduced by changing slightly the latest set of coordinates and carrying out a gradient-based optimization from the resulting geometry. Moves are accepted or rejected based upon the energy difference between the new and old local minimum. Thus, the difference from the standard Monte Carlo algorithm is that the energy should be minimized with respect to the local minimum before the Metropolis acceptance rule is applied. The BH approach can be also viewed

as a generalization of the "Monte Carlo plus energy minimization" procedure of Li and Scheraga [28]. The Monte Carlo part of the BH algorithm is introduced in order to allow the system to hop from one plateau to another at a thermal energy $k_B T^*$. The hopping probability depends highly on the choice of the "temperature" T^* and on the reduced-energy difference between the plateaus of the two consecutive steps. In this study the Monte Carlo simulation has been performed at a *constant* reduced "temperature" of 0.8.

In the present modified version of the BH algorithm we start with randomly generated cluster structures which are initially placed at a distance of $a_1/2$ above the relaxed Ag(111) and $a_2/2$ above the relaxed Ni(111) surface, where a_1=4.09 Å is the bulk lattice constant of Ag and a_2=3.52 Å this of Ni. Then we disturb randomly the coordinates of the cluster separately from those of the surface and carry out a gradient-based optimization on the "cluster+surface" system. Afterwards the Metropolis acceptance rule is applied using the old and new local minima of the "cluster+surface". For the next step the cluster atoms that belong to the latest set "cluster+surface" coordinates are disturbed randomly again. This procedure is repeated until the lowest total energy of the "cluster+surface" system is found. Thus, in contrast to the optimization procedure of Ref. [1] in which relaxation is carried out only for the cluster, we relax the whole atoms including those of the surface after each disturbance of the coordinates.

2.3. Surface model

Before starting the optimization, first of all non-relaxed Ni(111) and Ag(111) surface slabs were generated, using the equilibrium lattice constants

a_1 and a_2 of both Ni and Ag bulk obtained from the EAM potential. To find out how large the slab should be to mimic the surface behavior we carried out a series of relaxations of slabs in which the number of layers (in z-direction) and the number of hexagonal shells (in x-y direction) increase. Then we evaluated the difference in the surface energy between a slab with L layers and a slab with (L-1) layers. Thereby the surface energy is defined as follows

$$E_{SURF}(L) = 0.5 \cdot (E_{tot}^{L} - L \cdot E^{BULK}) \tag{5}$$

with

$$E^{BULK}(L) = 0.5 \cdot (E_{tot}^{L+2} - E_{tot}^{L}). \tag{6}$$

For the surface energy and for the binding energy of a cluster with the maximum number of N=20 atoms, we applied a convergence criterion of 0.1 meV to decide for which combination of layers and shells the slab will represent bulk properties. Thereby the convergence will be automatically fulfilled for smaller clusters. For the further calculations we used a Ni(111) slab consisting of 9 shells and 11 layers and a Ag(111) slab consisting of 10 shells and 15 layers.

3. Results and discussion

First of all we will investigate if Ag clusters adsorbed on a Ag(111) surface possess the same particular stable structures as Ag clusters adsorbed on a Ni(111) surface. In order to identify particularly stable clusters we consider the stability function

$$E_{\mathrm{stab}} = E_{\mathrm{tot}}(N+1) + E_{\mathrm{tot}}(N-1) - 2E_{\mathrm{tot}}(N). \tag{7}$$

E_{stab} is shown in Fig. 1 (bottom) for Ag clusters on a Ag(111) and a Ni(111) surface separately. Maxima of E_{stab} indicate particularly stable (magic) clusters. The magic sizes N=7, 10, 12, 14, 16, and 19 found for the Ag/Ag(111) system are in good agreement with those of Ref. [1]. Further, we observe that for cluster sizes, up to N=12, the stability function for both homo- and heteroatomic systems possess the same maxima and minima. In the size range $13 \leq N \leq 17$, the stability functions of Ag clusters on Ni(111) surface shows the same peaks, but they are less pronounced compared to that of Ag clusters on Ag(111) surface. Surprisingly, for N=18 and 19 there is a reversal of the maxima in both stability functions. While N=19 is magic size for Ag clusters adsorbed on a surface consisting of Ag atoms, it is non-magic size for Ag clusters adsorbed on a surface consisting of Ni atoms. For the last case a new magic size appears, at N=18.

At next we want to find out if the clusters which are especially stable on both surfaces possess the same structures and if the difference in the magic numbers for homo- and heteroatomic system corresponds to different geometries. In order to quantify structural differences and similarities between two Ag clusters of the same size of N atoms placed on different surfaces we use the concept of similarity functions introduced by us in previous studies [20, 22]. For each atom in a Ag cluster adsorbed on a Ag(111) surface we define its radial distance

$$r_n = |\vec{R}_n - \vec{R}_0| \tag{8}$$

with

$$\vec{R}_0 = \frac{1}{N} \sum_{i=1}^{N} \vec{R}_i. \tag{9}$$

These are sorted in increasing order. Simultaneously, for each atom in the

Ag cluster on Ni(111) we calculate and sort the radial distances, $\{r'_n\}$, for this, too. Subsequently, from

$$q = \left[\frac{1}{N} \sum_{n=1}^{N} (r_n - r_{n'})^2 \right]^{1/2}, \tag{10}$$

we define a similarity function,

$$S_1 = \frac{1}{1 + q/u_l} \tag{11}$$

($u_l = 1$ Å), which approaches 1 (0) if the Ag cluster on the Ag(111) surface is very similar to (different from) the Ag cluster on the Ni(111) surface. The similarity function S_1 is shown in Fig. 1 (top) as a function of the cluster size N. From this figure it can be seen that Ag clusters have the same structures for all magic sizes up to N=16, on both the Ag and the Ni surface. In contrast, the non-magic clusters of the sizes N=6, 9, 11, and 13 possess different geometries on the different surfaces. In the size range N=17-20 the difference in the cluster geometries corresponds to the reversal of the magic numbers of the Ag clusters on the homo- and heteroatomic surfaces described above. Some of the structures which are different on the Ag(111) and the Ni(111) surface are shown in Fig. 2. (The similarity function S_2 in Fig. 1 will be discussed later in this work.)

To explain the appearance of different lowest-energy structures and magic numbers in the heteroatomic system we plot the number of nearest-neighbor bonds (NN) in Fig. 3 (left side) and the number of nearest substrate atoms (SA) (right side) in dependence of cluster size. From the plot and from Fig. 2 it is visible that the ground-state structure of Ag_{19} on Ni(111), for example, does not possess the geometry which maximizes the number of NN bonds in

contrast to Ag_{19} on Ag(111). The first one is elongated and has more nearest substrate atoms. This indicates that the adatom-substrate interaction in the case of the Ag/Ni(111) system dominates over the adatom-adatom interaction and can compensate the loss in binding energy caused by the NN bond breaking (Ag–Ni interaction is stronger than Ag–Ag interaction [29]). However, as compact structures are preferred (at least in the investigated size range), Ag_{19} adsorbed on Ni(111) loses its special stability compared to its neighbors Ag_{18} and Ag_{20} and instead Ag_{18}, which possesses a more compact structure, becomes more stable. For lower sizes the influence from the adatom-substrate interactions is obviously not strong enough to change the predominance of the NN adatom-adatom interactions and therefore the same structures of magic clusters appear on the different surfaces.

An interesting question is also if cluster growth is a regular one, i.e. if the structure of a Ag_N cluster can be considered as being built up by adding a Ag atom to the structure of Ag_{N-1} cluster. In order to quantify this suggestion we consider the similarity function S_2. We calculate and sort all interatomic distances d_i, $i = 1, 2, \cdots, \frac{N(N-1)}{2}$. Subsequently we consider each of the N fragments of the N-cluster that can be obtained by removing one of the atoms and keeping the rest at their positions. For each of those we also calculate and sort all interatomic distances d'_i, and calculate, subsequently,

$$q = \Big[\frac{2}{N(N-1)} \sum_{i=1}^{N(N-1)/2} (d_i - d'_i)^2\Big]^{1/2}. \qquad (12)$$

Among the N different values of q we choose the smallest one, $q_{\min}$ and

calculate the similarity function

$$S_2 = \frac{1}{1 + q_{\min}/u_l} \tag{13}$$

($u_l = 1$Å) which approaches 1 if the Ag_N cluster is very similar to the Ag_{N-1} cluster plus an extra atom. The results for Ag clusters on both Ag and Ni surfaces are shown in Fig. 1 (middle row). In contrast to the Ag/Ag(111) system, on the Ni(111) surface we observe a regular growth of the cluster monolayer up to N=11, due to the presence of the hexagon as growth motif. In the size range N=12-20 the cluster growth becomes irregular one for both surfaces and we can not find a dominant structural growth motif.

In order to study the influence of the underlying substrate on the adsorbed cluster structure we used the so-called 'Index of epitaxy', I, introduced by us in a previous study [30]. This parameter enables us to quantify whether the structure of the adsorbed cluster is dictated by the underlying substrate, i.e., to which extent the adsorption or growth process of the clusters can be classified as being epitaxic. It is described with the following formula:

$$\begin{aligned} q &= \sum_{i}^{N} |\vec{R}_i - \vec{R}_c|^2 \\ I &= \frac{1}{1 + q/u_l^2}, \end{aligned} \tag{14}$$

where $|\vec{R}_i - \vec{R}_c|$ is the distance between the positions of the ith atom and the closest-lying fictitious atom in the infinite ideal crystal. In this case we generated very large (more than 20000 atoms) ideal Ag(111) and Ni(111) crystals using the lattice constants of the metals. When I reaches 1, a perfect epitaxy is obtained. In Fig. 4 we show the results for the index of epitaxy

for Ag clusters adsorbed on a Ag(111) surface and for Ag clusters adsorbed on a Ni(111) surface. In the case when the underlying substrate consists of Ag atoms I is near to 1, which indicates perfect epitaxial growth. All Ag adatoms are adsorbed at the normal fcc sites (see Fig. 5), i.e. they occupy equivalent sites with respect to the substrate lattice. In contrast, when the underlying substrate consists of Ni atoms I decreases with cluster size and possesses a minimum of I=0.47 at N=14. Fig. 5 shows examples for the difference in the epitaxy for clusters of the same size on different surfaces. As we can see all the Ag adatoms sit in inequivalent sites, i.e. they are neither located all at fcc sites, nor at hcp sites. Instead most of them are placed at intermediate sites as e.g. at bridge sites between two Ni atoms. This lost of the three fold symmetry in the heteroatomic system compared to the Ag/Ag(111) system leads to more irregular structures for Ag clusters adsorbed on a Ni(111) surface.

To get a better understanding of the atomic structure of also larger clusters on Ni(111) we take a cut out from a Ag monolayer of the ideal Ag(111) crystal to obtain nearly close-packed structures of N=50 and 100 atoms and let them relax on a Ag(111) and a Ni(111) surface to their most stable equilibrium positions. The results are presented in Fig. 6. Here, it becomes visible that when the cluster size increases to N=100 the Ag atoms start to occupy also top sites (on Ni atoms) beside bridge sites. Further, we observe some kind of waving of the Ag atom rows in x-y direction, so that Ag cluster atoms propagate to one additional substrate row than expected from the homoatomic case. See for example the structures of the cluster size N=50 shown in Fig. 6: the Ag atoms on Ag(111) are laying between 10 rows of

substrate atoms, whereas on the Ni substrate they cover 11 rows of substrate atoms. This effect becomes stronger with increasing cluster size. It is due to the fact that Ag atoms try to keep the adatom-adatom distances as near as possible to those of the pure Ag cluster (the Ag–Ag dimer bond length (2.44 Å) is larger than the Ni–Ni dimer bond length (2.12 Å) and the lattice constant of Ag is 16 % larger than this of Ni). By introducing the distortion described above, some of the strain in the heteroatomic system due to the mismatch is released, and the structure becomes more stable.

4. Conclusions

In this work we have studied the structural and energetic properties of Ag_N clusters on a Ag(111) and a Ni(111) surface with N up to 20 atoms. The homo- and heteroatomic interactions in the cluster-surface systems have been modeled using the EAM and the global geometry optimization has been performed using the BH algorithm. For both Ag/Ag(111) and Ag/Ni(111) systems the tendency to form close-packed structures with maximum number of nearest-neighbor bonds, except for Ag_{19} on Ni(111), is common. Further, the magic sizes up to N=17 and the corresponding structures are the same for the homo- and heteroatomic system. In contrast, the geometries of the Ag clusters for the non-magic sizes in the same size range differ for the different surfaces. From N=18 upwards a reversal of the magic numbers for the Ag/Ni(111) system compared to the Ag/Ag(111) system takes place, due to the stronger influence of the adatom-substrate interactions compared to the adatom-adatom interactions in Ag_{19}. The increase in adatom-substrate interactions for Ag clusters on Ni(111) results in a higher number of nearest substrate atoms and in the preference of elongated structures. Finally, for the Ag/Ni(111) system the index of epitaxy is decreasing with increasing cluster size because of the large mismatch of dimer bond lengths and lattice constants between Ag and Ni.

References

[1] J. Zhuang, T. Kojima, W. Zhang, L. Liu, L. Zhao, Y. Li, Phys. Rev. B 65 (2002) 045411.

[2] Z. Sun, Q. Liu, Y. Li, J. Zhuang, Chin. Phys. Lett. 21 (2004) 1604.

[3] P. Zhang, Y. Xie, X. Ning, J. Zhuang, Nanotechnology 19 (2008) 255704.

[4] M. Giesen, C. Steimer, H. Ibach, Surf. Sci. 471 (2001) 80.

[5] S. C. Wang, G. Ehrlich, Surf. Sci. 239 (1990) 301.

[6] D. D. Chambliss, R. J. Wilson, S. Chiang, Phys. Rev. Lett. 66 (1991) 1721.

[7] A. F. Wright, M. S. Daw, C. Y. Fong, Phys. Rev. B 42 (1990) 9409.

[8] H.-V. Roy, P. Fayet, F. Patthey, W.-D. Schneider, Phys. Rev. B 49 (1994) 5611.

[9] D. R. Tice, D. W. Basset, Thin Solid Films 20 (1974) S37.

[10] J.-M. Roussel, A. Saúl, G. Tréglia, Phys. Rev. B 55 (1997) 10931.

[11] B. Aufray, H. Giordano, B. Legrand, G. Tréglia, Surf. Sci. 307-309 (1994) 531.

[12] C. Chambon, A. Coati, Y. Garreau, Surf. Sci. 602 (2008) 2363.

[13] C. Kittel, Introduction to Solid State Physics, seventh ed., John Wiley and Sons, 1995.

[14] V. Rosato, M. Guillope, B. Legrand, Phil. Mag. A 59 (1989) 321.

[15] M. S. Daw, M. I. Baskes, Phys. Rev. Lett. 50 (1983) 1285.

[16] M. S. Daw, M. I. Baskes, Phys. Rev. B 29 (1984) 6443.

[17] S. M. Foiles, M. I. Baskes, M. S. Daw, Phys. Rev. B 33 (1986) 7983.

[18] http://enpub.fulton.asu.edu/cms/potentials/main/main.htm

[19] M. S. Daw, S. M. Foiles, M. I. Baskes, Mat. Sci. Rep. 9 (1993) 251.

[20] V. G. Grigoryan, M. Springborg, Chem. Phys. Lett. 375 (2003) 219.

[21] V. G. Grigoryan, D. Alamanova, M. Springborg, Eur. Phys. J. D 34 (2005) 187.

[22] V. G. Grigoryan, M. Springborg, Phys. Rev. B 70 (2004) 205415.

[23] D. Alamanova, V. G. Grigoryan, M. Springborg, J. Phys. Chem. C 111 (2007) 12577.

[24] J. P. K. Doye, D. J. Wales, Phys. Rev. Lett. 80 (1998) 1357.

[25] D. J. Wales, Energy Landscapes, Cambridge University Press, Cambridge, 2003.

[26] D. J. Wales, H. A. Scheraga, Science 285 (1999) 1368.

[27] D. J. Wales, J. P. K. Doye, J. Phys. Chem. A 101 (1997) 5111.

[28] Z. Li, H. A. Scheraga, Proc. Natl. Acad. Sci. U.S.A. 84 (1987) 6611.

[29] A. Rapallo, G. Rossi, R. Ferrando, A. Fortunelli, B. C. Curley, L. D. Lloyd, G. M. Tarbuck, R. L. Johnston, J. Chem. Phys. 122 (2005) 194308.

[30] D. Alamanova, V. G. Grigoryan, M. Springborg, Surf. Sci. 602 (2008) 1413.

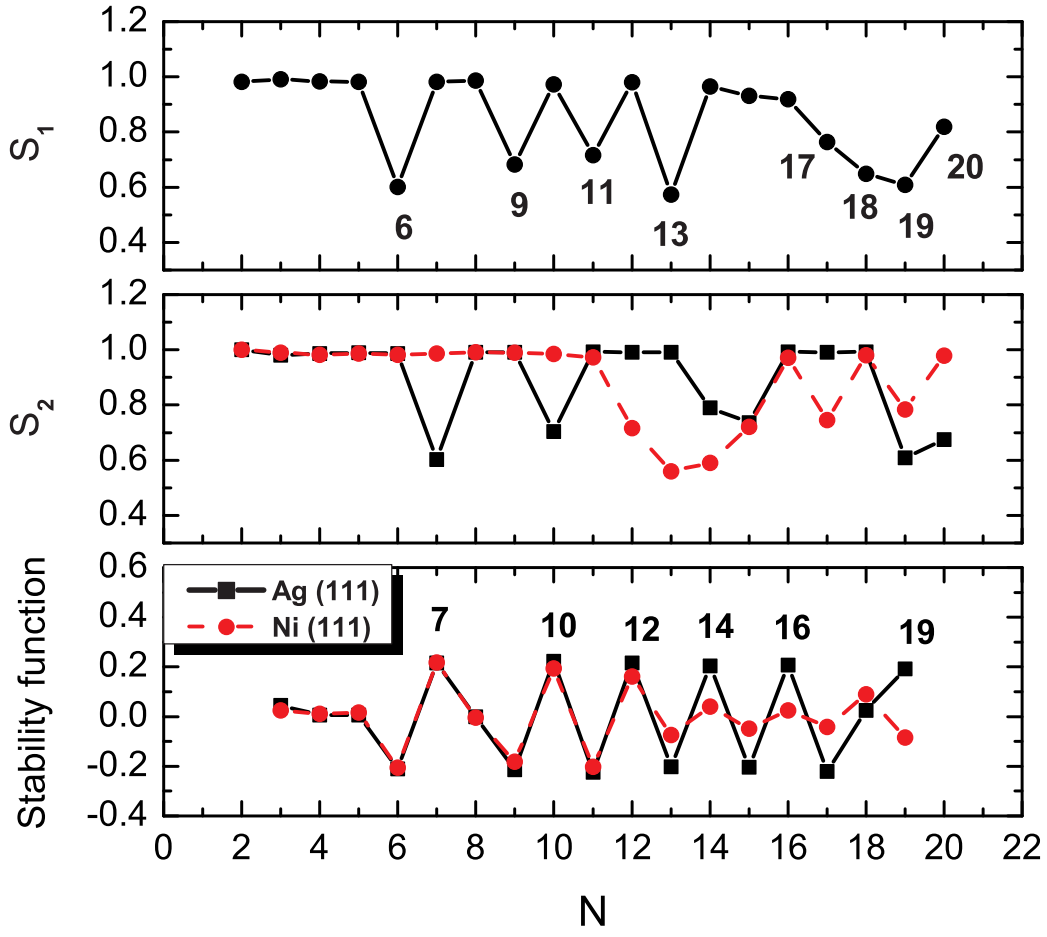

Figure 1: The similarity functions S_1 and S_2 (top and middle row) in dependence of the cluster size N. The third row shows the stability functions of Ag clusters on Ag(111) and of Ag clusters on Ni(111) surface.

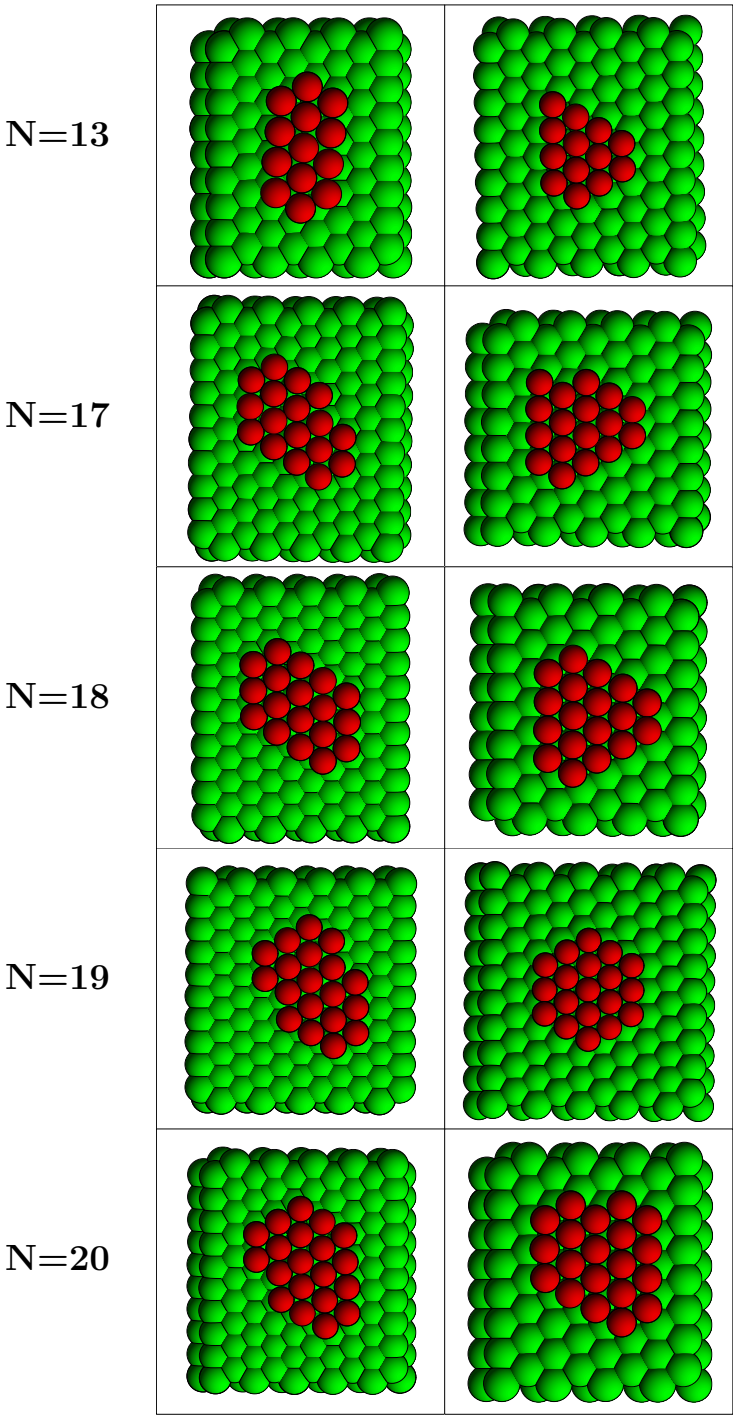

Figure 2: The lowest-energy structures of Ag clusters on a Ni(111) (left column) and on a Ag(111) (right column) surface.

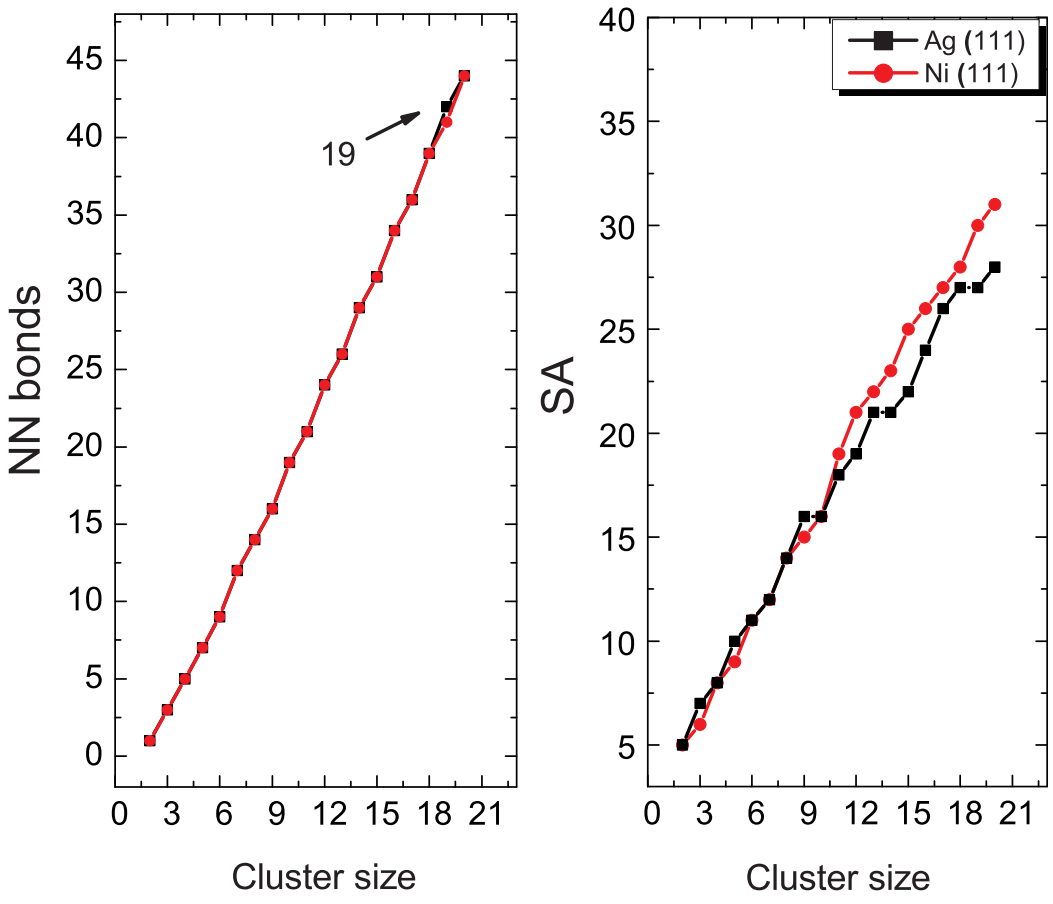

Figure 3: The number of nearest-neighbor (NN) bonds (left side) and the number of nearest substrate atoms (SA) (right side) in dependence of cluster size separately for Ag clusters on Ag(111) surface (square) and for Ag clusters on Ni(111) surface (circle).

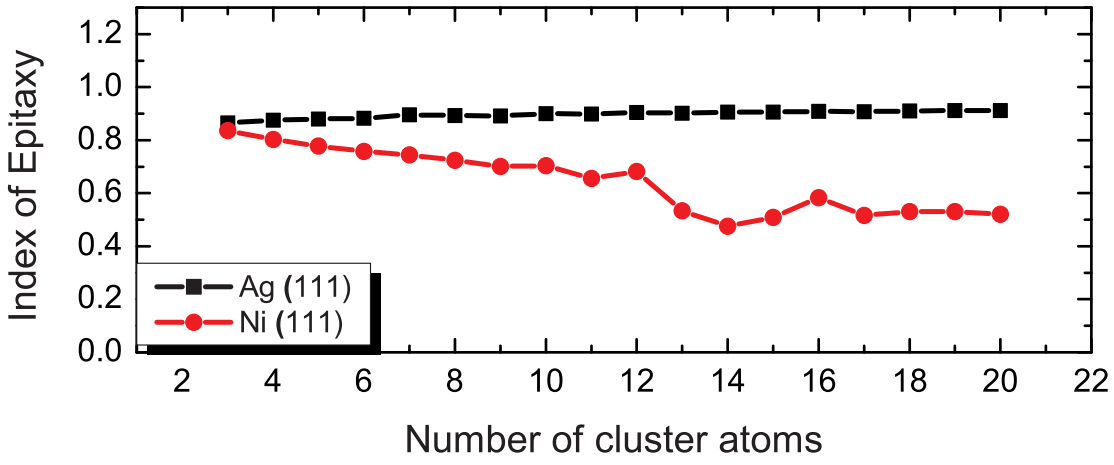

Figure 4: The evolution of the index of epitaxy with cluster size separately for Ag clusters on Ag(111) surface (square) and for Ag clusters on Ni(111) surface (circle).

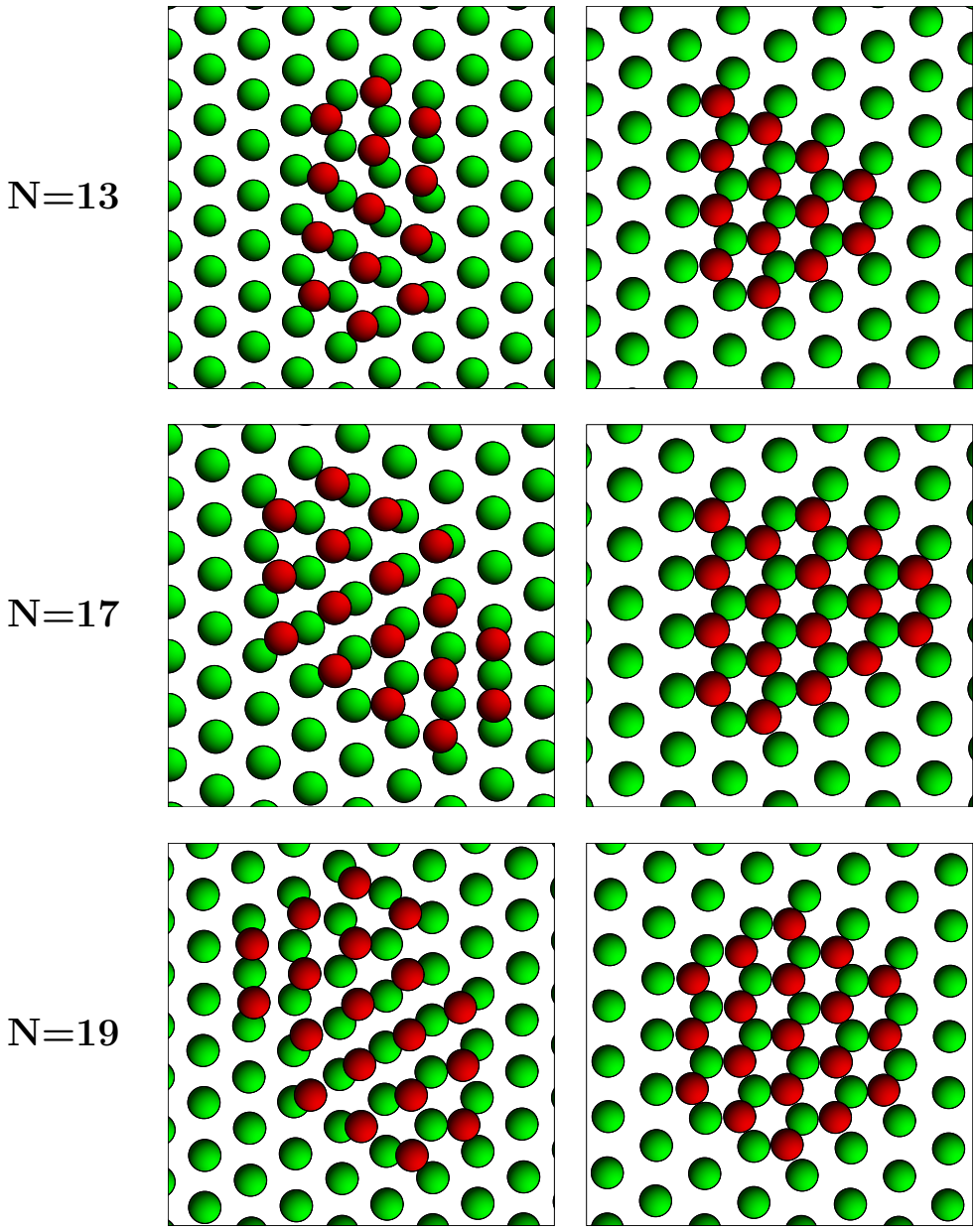

Figure 5: The lowest-energy structures of Ag clusters on a Ni(111) (left column) and a Ag(111) (right column) surface.

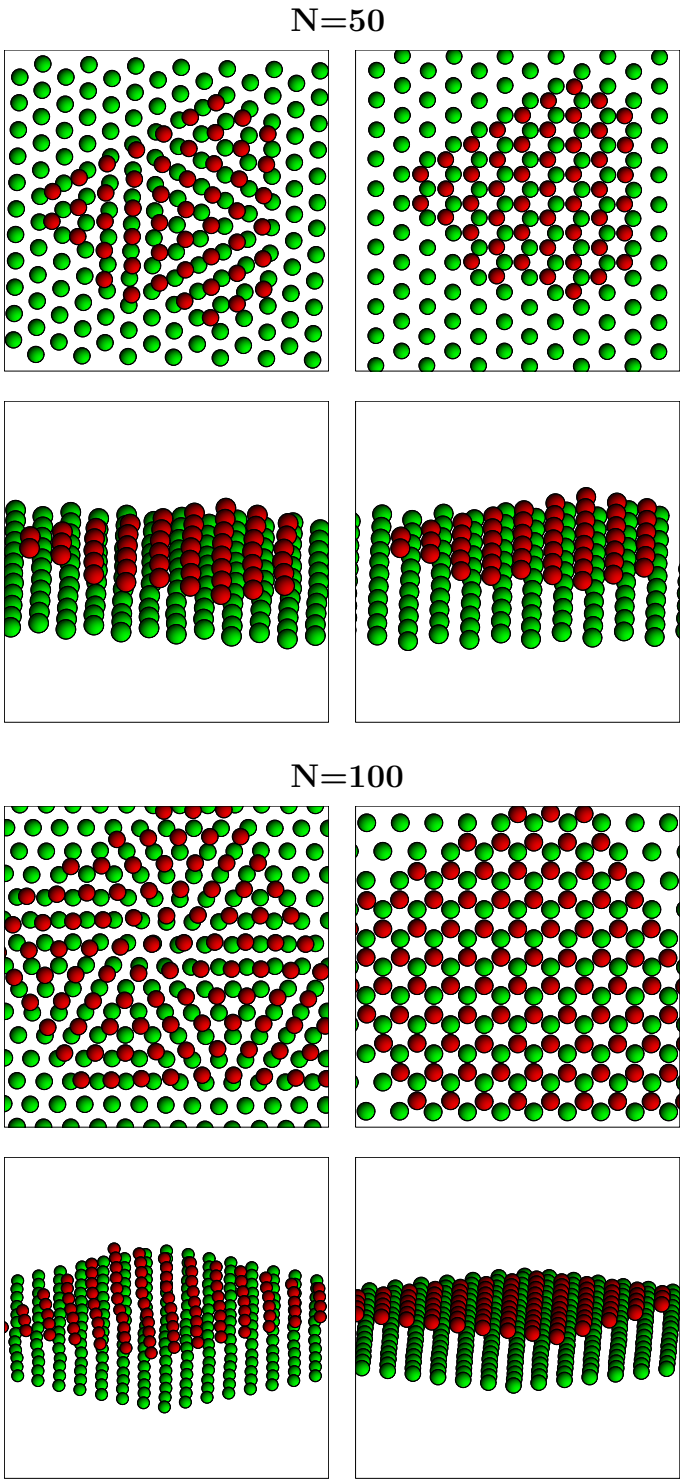

Figure 6: The relaxed structures of Ag_{50} and Ag_{100} clusters on a Ni(111) (left side) and a Ag(111) (right side) surface.